Computational Evaluation of Thermohydarulic Performance of Mixed Refrigerants with Nano Particles for Industrial Refrigeration Systems

Dissertation—I

Submitted in partial fulfillment of the requirement for the award of degree of

Master of Technology

in

Mechanical Engineering

by

Seepana Praveenkumar

Regd. No: 11501856

Under the guidance of

Dr. Raja Sekhar Dondapati

U.ID: 17715

DEPARTMENT OF MECHANICAL ENGINEERING

LOVELY PROFESSIONAL UNIVERSITY

PUNJAB

2016-2017

CERTIFICATE

I hereby certify that the work being presented in the dissertation entitled "***Computational Evaluation of ThermoHydarulic Performance of Mixed Refrigerants with Nano Particles for Industrial Refrigeration Systems"*** in partial fulfilment of the requirement of the award of the Degree of master of technology and submitted to the Department of Mechanical Engineering of Lovely Professional University, Phagwara, is an authentic record of my own work carried out under the supervision of Dr. Raja Sekhar Dondapati, Associate Professor Department of Mechanical Engineering, Lovely Professional University. The matter embodied in this dissertation has not been submitted in part or full to any other University or Institute for the award of any degree.

Date:

Name: Seepana Praveenkumar

Registration No: 11501856

This is to certify that the above statement made by the candidate is correct to the best of my knowledge.

Date: Name: Dr. Raja Sekhar Dondapati

UID: 17715

COD: Sudhanshu Dogra

The external viva-voce examination of the student was held successfully on

Signature of Examiner Signature Examiner

DECLARATION

I, Seepana Praveenkumar, student of **Master of Technology (Mechanical Engineering)** under School of **Mechanical Engineering** of Lovely Professional University, Punjab, hereby declare that all the information furnished in this dissertation reports based on my own intensive research and is genuine. This dissertation does to the best of my knowledge, contain part of my work which has been submitted for the award of my degree either of this university without proper citation.

Seepana Praveenkumar
Registration No.11501856

Date:

ACKNOWLEDGMENT

First and the foremost I offer my sincerest gratitude to my supervisor, **Dr. Raja Sekhar Dondapati**, Assistant Professor, School of Mechanical Engineering, Lovely Professional University, Punjab and **Mrs. Preeti Rao Usurumarti,** P.V.K.Institute of Technology, Ananthapur, Andhra Pradesh who has supported me throughout my thesis with their patience, knowledge, valuable advice, uninterrupted active supervision and constant encouragement. I attribute the level of my Master's degree to their encouragement and effort without them this thesis, too, would not have been completed or written.

I am thankful to **Mr. Gurpreet Singh Phull**, (HOS) and **Mr. Sudhanshu Dogra** (HOD) School of Mechanical Engineering, Lovely Professional University, Punjab.

I would like to thank all the staff members of School of Mechanical engineering who have been very patient and co-operative with me.

I am thankful to **Mr. Gaurav Vyas**, **Mr. Mahidar Duggal** and **Ajay Kumar Sharma** Assistant Professor, School of Mechanical Engineering, Lovely Professional University, Punjab who continuously motivated, clearing concepts and encouraged me to do this research work.

I would also like to extend my gratitude to my seniors Mr. Abhinav Kumar, Mr. Jeswanth Ravula, Mr. Mohit Kalisa, Mr. Syed Mahaboob Idris, Mr. Venkata Ramana Uppada, Mr. Gadekula Rajesh Kumar, and all my M.Tech Friends who always encouraged and supported me in this thesis work.

I would like to thank **Lovely Professional University** for giving me opportunity to use their resources and work in such a challenging environment. I am grateful to the individuals whom contributed their valuable time towards my thesis.

Last but not the least, I express my sincere gratitude to my parents and brother who have always supported me throughout all my studies at university and encouraged me with their best wishes.

Seepana Praveenkumar-11501856

Table of Contents

1 Introduction 1
1.1 Vapour compression refrigeration system 1
1.2 Major Components of VCRS 1
1.2.1 Evaporator 2
1.2.2 Compressor 2
1.2.3 Condenser 3
1.2.4 Expansion valve 3
1.3 Role of refrigerants in the VCRS 4
1.4 Nano-refrigerants 4
1.5 Preparation of Nano refrigerants 5
1.6 Classification of Nanoparticles 5
2 Scope of the Study 7
3 Objectives of the Study 8
4 Review of Literature 9
5 Research Methodology 23
6 Expected Outcomes 25
7 Complete Work Plan with Timeline 26
8 Results and Discussions 27
8.1 Effect of Thermophysical properties of a mixed refrigerant 27
8.2 CFD Analysis of Mixed Refrigerant at Different Inlet Temperature 37
8.3 Thermophysical Properties of Mixed refrigerant with addition of CuO Nano-Particle at pressure 3MPa 48
8.4 CFD Analysis of Mixed Refrigerant with addition of CuO Nano-article at Pressure 3MPa 60
9 Summary and Conclusions 72
References 73

List of Figures

Figure 1 Vapour Compression Refrigeration Cycle 1
Figure 2 Evaporator 2
Figure 3 Compressor 3
Figure 4 Condenser 3
Figure 5 Expansion Valve 4
Figure 6 TiO2 Nanoparticles [2] 4
Figure 7 ZnO Nanoparticles [3] 5
Figure 8 Classification of Nanoparticles 6
Figure 9: Proposed work with timeline 26
Figure 10 density as a function of temperature at pressure 3MPa 27
Figure 11 Viscosity as a function of Temperature at 3MPa 28
Figure 12 Thermal conductivity as a function of Temperature at 3MPa 28
Figure 13 Specific heat as a function of Temperature at 3MPa 29
Figure 14 Density as a function of temperature at 4MPa 29
Figure 15 Viscosity as a function of Temperature at 4MPa 30
Figure 16 Thermal Conductivity as a function of Temperature at 4MPa 30
Figure 17 Specific heat as a function of Temperature at 4MPa 31
Figure 18 Density as a function of Temperature at 5MPa 31
Figure 19 Viscosity as a function of Temperature at 5MPa 32
Figure 20 Thermal conductivity w.r.t temperature 32
Figure 21 Specific Heat as a function of Temperature at 5MPa 33
Figure 22 Density as a function of temperature at 6MPa 33
Figure 23 Viscosity as a function of Temperature at 6MPa 34
Figure 24 Thermal conductivity as a function of Temperature at 6MPa 34
Figure 25 specific heat as a function of Temperature at 6MPa 35
Figure 26 Density as a function of Temperature at 7MPa 35
Figure 27 viscosity as a function of temperature at 7MPa 36
Figure 28 Thermal conductivity as a function of temperature at 7MPa 36
Figure 29 Specific Heat as a function of Temperature at 7MPa 37
Figure 30 Mesh analysis of compressor 38
Figure 31 represents stimulated results for mixed refrigerant 38

Figure 32 Pressure drop vs Mass flow rate at 300K 38
Figure 33 Pressure drop vs Mass flow rate at 310K 39
Figure 34 Pressure drop vs Mass flow rate at 320K 39
Figure 35 Pressure drop vs Mass flow rate at 330K 40
Figure 36 Heat transfer vs Mass flow rate at 300K 40
Figure 37 Heat transfer vs Mass flow rate at 310K 41
Figure 38 Heat transfer vs Mass flow rate at 320K 41
Figure 39 Heat transfer vs Mass flow rate at 330K 42
Figure 40 Reynold number vs Mass flow rate at 300K 42
Figure 41 Reynold number vs Mass flow rate at 310K 43
Figure 42 Reynold number vs Mass flow rate at 320K 43
Figure 43 Reynold number vs Mass flow rate at 330K 44
Figure 44Nusselt number vs Reynolds number at 300K 44
Figure 45 Nusselt number vs Reynolds number at 310K 45
Figure 46 Nusselt number vs Reynolds number at 320K 45
Figure 47 Nusselt number vs Reynolds number at 330K 46
Figure 48 Nusselt number vs Mass flow rate at 300K.....46
Figure 49 Nusselt number vs Mass flow rate at 310K.....47
Figure 50 Nusselt number vs Mass flow rate at 320K.....47
Figure 51 Nusselt number vs Mass flow rate at 330K.....48
Figure 52 Effective Thermal conductivity w.r.t Volume concentration of nanoparticles .48
Figure 53 Effective Thermal conductivities w.r.t Volume concentration of nanoparticles 49
Figure 54 Effective Thermal conductivities vs Volume concentration of nanoparticles...49
Figure 55 Effective Thermal conductivities vs Volume concentration of nanoparticles...50
Figure 56 Effective Thermal conductivities w.r.t Volume concentration of nanoparticles 50
Figure 57 Effective Thermal conductivities w.r.t volume concentration of nanoparticles 51
Figure 58 Effective viscosity w.r.t volume concentration of nanoparticles 51
Figure 59 Effective viscosity w.r.t volume concentration of nanoparticles. 52
Figure 60 Effective viscosity w.r.t volume concentration of nanoparticles. 53
Figure 61 Effective viscosity w.r.t volume concentration of nanoparticles. 53
Figure 62 Effective viscosity w.r.t volume concentration of nanoparticles. 54
Figure 63 Effective viscosity w.r.t volume concentration of nanoparticles. 54

Figure 64 Effective viscosity w.r.t volume concentration of nanoparticles. 55
Figure 65 Effective specific heat w.r.t volume concentration of nanoparticles.....55
Figure 66 Effective specific heat w.r.t volume concentration of nanoparticles.....56
Figure 67 Effective specific heat w.r.t volume concentration of nanoparticles.....56
Figure 68 Effective specific heat w.r.t volume concentration of nanoparticles.....57
Figure 69 Effective density w.r.t volume concentration of nanoparticles. 57
Figure 70 Effective density w.r.t volume concentration of nanoparticles. 58
Figure 71 Effective density w.r.t volume concentration of nanoparticles. 58
Figure 72 Effective density w.r.t volume concentration of nanoparticles. 59
Figure 73 Effective density w.r.t volume concentration of nanoparticles 59
Figure 74 Effective density w.r.t volume concentration of nanoparticles 60
Figure 75 Pressure Drop vs Mass flow rate CuO Nano-Particle at 300K 60
Figure 76 Pressure Drop vs Mass flow rate CuO Nano-Particle at 310K 61
Figure 77 Pressure Drop vs Mass flow rate CuO Nano-Particle at 320K 61
Figure 78 Pressure Drop vs Mass flow rate CuO Nano-Particle at 330K 62
Figure 79 Heat transfer rate vs Mass flow rate CuO Nano-Particle at 300K 62
Figure 80 Heat transfer rate vs Mass flow Rate CuO Nano-Particle at 310K 63
Figure 81 Heat transfer rate vs mass flow rate of CuO Nano-Particle at 320K.....63
Figure 82 Heat transfer rate vs Mass flow rate CuO Nano-Particle at 330K 64
Figure 83 Reynolds Number vs Mass flow rate CuO Nano-Particle at 300K 65
Figure 84 Reynolds Number vs Mass flow rate CuO Nano-Particle at 310K 65
Figure 85 Reynolds Number vs Mass flow rate CuO Nano-Particle at 320K 66
Figure 86 Reynolds Number vs Mass flow rate CuO Nano-Particle at 330K 66
Figure 87 Nusselt Number vs Mass flow rate CuO Nano-Particle at 300K 67
Figure 88 Nusselt Number vs Mass flow rate CuO Nano-Particle at 310K 67
Figure 89 Nusselt Number vs Mass flow rate CuO Nano-Particle at 320K 68
Figure 90 Nusselt Number vs Mass flow rate CuO Nano-Particle at 330K 68
Figure 91 Nusselt Number vs Reynolds number rate CuO Nano-Particle at 300K.....69
Figure 92 Nusselt Number vs Reynolds number rate CuO Nano-Particle at 310K.....70
Figure 93 Nusselt Number vs Reynolds number rate CuO Nano-Particle at 320K.....70
Figure 94 Nusselt Number vs Reynolds number rate CuO Nano-Particle at 300K.....71

ABSTRACT

The concept of Nano fluid has emerged during the past decade due to superior thermophysical properties of Nano fluids as compared to those of conventional fluids. A refrigerant that is based on Nano fluids is called as Nano refrigerant that shows improvement in thermophysical properties such as thermal conductivity, density, viscosity and specific heat. In present research work, effective thermal conductivity has been calculated by using experimental correlations that are available in the literature. Volume concentration of 1% (0.01) to 5% (0.05) is considered for the present work. The study is carried out by choosing the mixed refrigerant propane and ISO-butane with different compositions with the addition of Nano particles such as Copper Oxide (CuO). The analyses are carried out for temperature range of 300-350K and a pressure range of 3MPa to 7MPa. The results show that there is a decrease in thermal conductivity, density, viscosity with respect to temperature. However, the specific heat is found to be increasing with increases in temperature.

Hence, it is evident that the heat transfer enhances due to the introduction of Nano refrigerants in the industrial refrigeration systems.

1 Introduction

The job of refrigeration plant is to cool articles, and maintain them ambient temperature. Refrigeration can be defined as the process remove heat. The oldest and most well-known among refrigerants are ice, water and air. In the beginning the sole purpose to conserve food [1] . Basic principle refrigeration is if you were to place a hot cup of coffee on a table and leave if for a while, the heat in the coffee is transferred would be transferred into the materials in contact with the coffee i.e. the cup, the table and the surrounding air. As the heat is transferred the coffee in time cools. Using the same principle, removing heat from a product and transferring heat to the outside air.

1.1 Vapour compression refrigeration system

Vapour compression refrigeration system is mainly used in refrigerants and air-conditioning systems. In VCRS System working fluid known as a refrigerant, undergoes phase change during the evaporation process at low temperatures to produce a cooling effect. A wide variety of refrigerants are used in the VCRS systems in an important application and capacities. Vapour compression refrigeration system is an important application being where various refrigerants are used for cooling purposes. In vapour compression refrigeration system, where refrigerant undergoes phase changes, is used to produce a cooling effect.

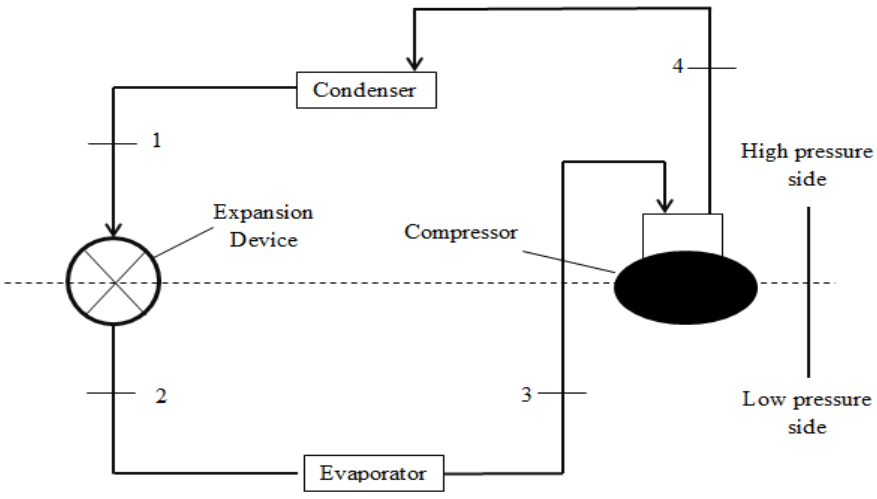

Figure 1 Vapour Compression Refrigeration Cycle

1.2 Major Components of VCRS

A simple VCRS system consists of following four main components.

- Evaporator
- Compressor
- Condenser
- Expansion valve

1.2.1 Evaporator

In above Figure 2 Vapour compression refrigeration system process 1-2 shows heat absorption process in the evaporator at constant pressure. In evaporator, low temperature, low pressure liquid refrigerants absorb the latent heat of vaporization is converted into vapour form.

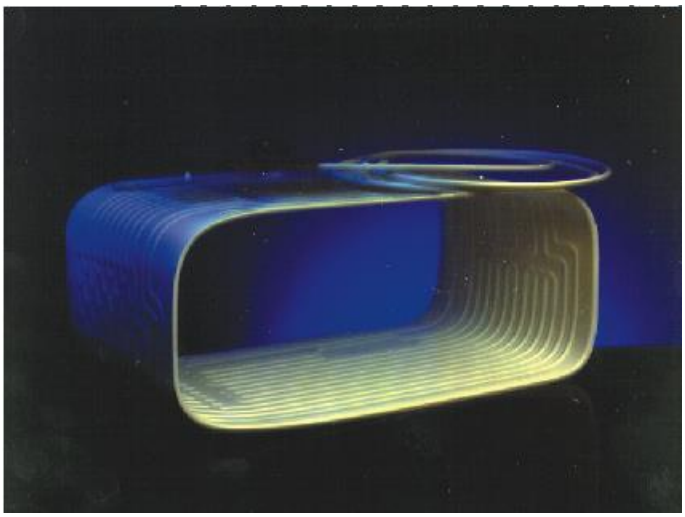

Figure 2 Evaporator

1.2.2 Compressor

In Figure 3 Vapour compression refrigeration system process 2-3 shows the isentropic compression of saturated vapour refrigerant in the compressor. Pressure and temperature of the refrigeration system increase by reducing its volume. The compression process external work supplies from the surrounding.

Figure 3 Compressor

1.2.3 Condenser

In the Figure 4 above process 3-4 shows the isobaric heat rejection process while refrigerants flows into the condenser tubing. In the condensation process refrigerant undergoes phase changes from gases to a liquid state by rejecting latent heat of condensation to the surroundings. Superheated refrigerant flows into the condenser to dissipate heat to the environment.

Figure 4 Condenser

1.2.4 Expansion valve

In the Figure 5 above process shows the irreversible adiabatic expansion of saturated refrigerants through the expansion valve. In the expansion process pressure and temperature of refrigerants reduces.

Figure 5 Expansion Valve

1.3 Role of refrigerants in the VCRS

Thermal properties of refrigerants play an important role in cooling. Conventional refrigerants such as R-290 and R-600a are used in this research as a mixed refrigerants and composition of refrigerants is calculated by the addition of Nano-particles.

1.4 Nano-refrigerants

In the past few decades, advancements in the Nanotechnology led to a new generation of refrigerants were called Nan-refrigerants. Nano-refrigerants are a relatively new class of fluids which consists of base Nano sized particles called Nanoparticles. The Nanoparticles used in Nano refrigerant are typically made of metals, metal oxides, carbides or carbon nanotubes. Novel properties of Nano refrigerants make them potentially useful in many applications like domestic and commercial refrigerators, storage of food and meat and air conditioning etc.

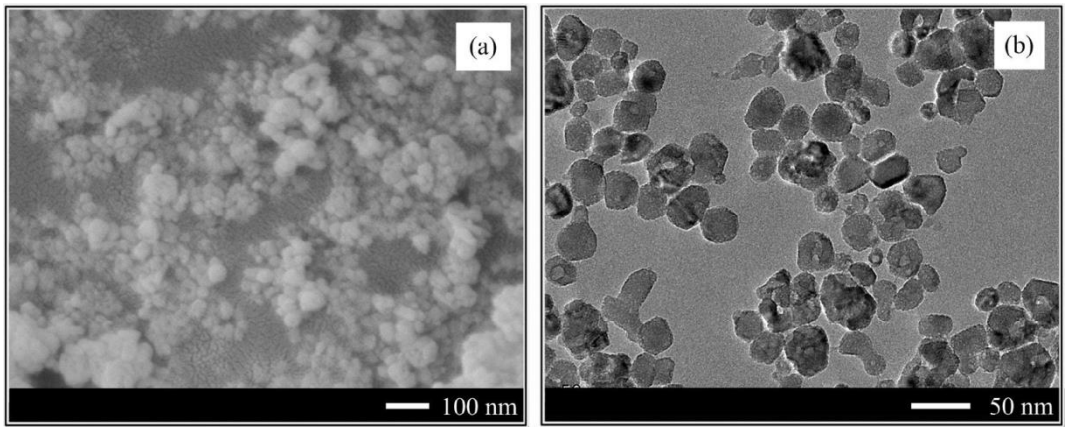

Figure 6 TiO2 Nanoparticles [2]

World scenario in the refrigeration field is to use such kind of refrigerants which provide a safer environment and better thermal performances. A lot of work is pending in this region to find such refrigerants. In this research mixed refrigerants are used Propane R290 and R600a in the condenser of vapour compression refrigeration system.

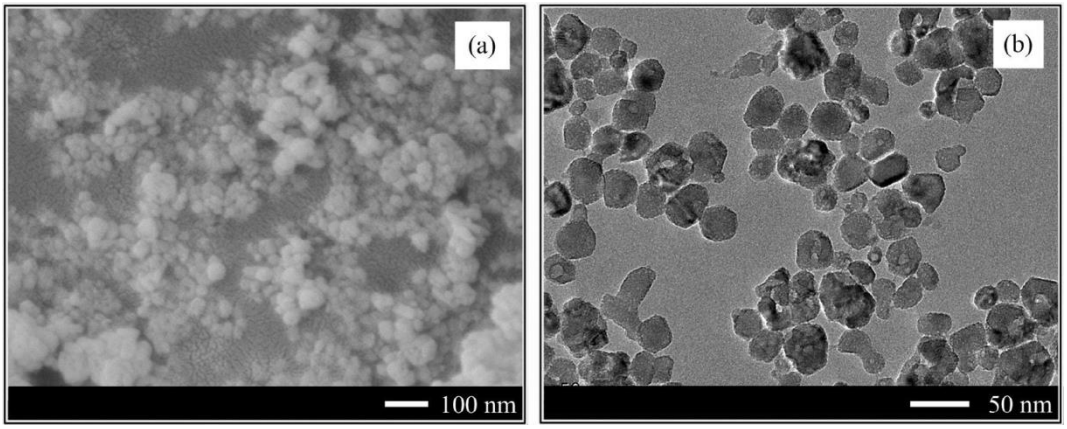

Figure 7 ZnO Nanoparticles [3]

In this research work Al_2O_3 (Polycrystalline, Sapphire), TiO_2, CuO, ZnO Nanoparticles is used for the investigation of various thermo-physical properties of refrigeration's mentioned. Fig.2 and fig. 3 shows TiO_2 and ZnO of 2µm and the 100µm size of the Nanoparticles

1.5 Preparation of Nano refrigerants

Nano-refrigerants with concentration 1% to 5% of above mentioned Nanoparticles Al_2O_3 (Polycrystalline, Sapphire), TiO_2, CuO, ZnO are prepared for the analyses. The Nano refrigerant mixture is prepared with the aid of magnetic stirrer for two hours. This mixture is further vibrated with the help of Ultrasonic Homogenizer for one hour to separate the Nanoparticles completely. Complete separation of Nanoparticles is required to prevent clogging or settling down of Nanoparticles.

1.6 Classification of Nanoparticles

Nanotechnology has emerged as science which uses particles to change the various characteristics of a material medium. These particles are of atomic and molecular order. Particles are generally classified with respect to their diameters

Nanoparticles are regarded as ultrafine particles. Course and fine particles are generally not used in heat transfer application as the problem of fouling, sedimentation, erosion and higher pressure drop occurs. So ultrafine particles or Nano particles are the ultimate solution to the problems caused by the coarse and fine particles. Nano particles can be metallic oxides, carbides and carbon Nano tubes.

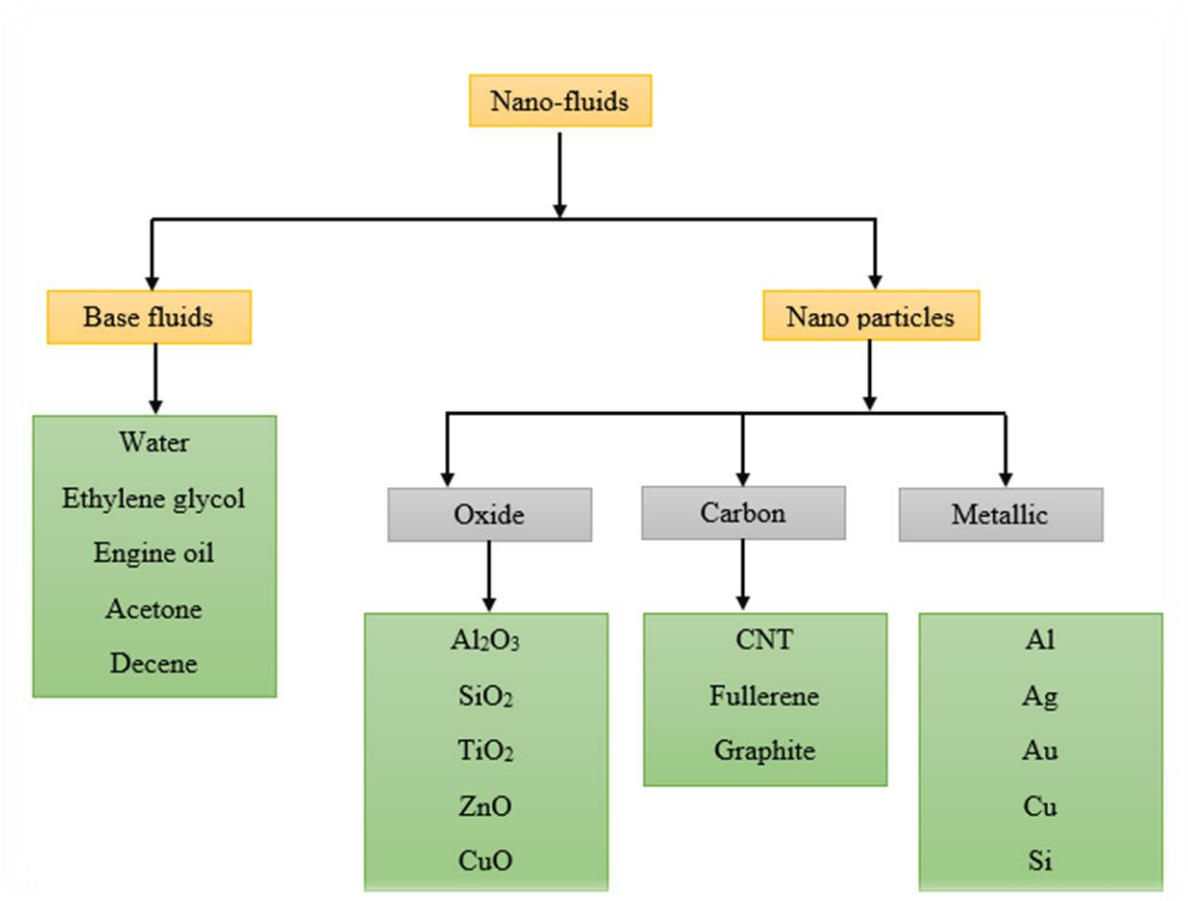

Figure 8 Classification of Nanoparticles

2 Scope of the Study

The scope of the research is as follows

a) The scope of the study is to find out the new refrigerants and Nano particles mixture can enhance the thermo physical properties such as
    - Thermal conductivity
    - Viscosity
    - Density
    - Specific heat
b) The significant changes in these properties in the refrigerants will make them more effective and to be used in
    - Domestic refrigeration system
    - Industrial refrigeration system
    - Air condition system
    - Storage of perishable products such as fish, meat, insulin, milk etc.;
    - Water chiller system
    - Heat exchanger system
    - Diesel generators for the purpose of coolant
c) The comparison of Nano refrigerants will lead to a conclusion of the feasibility and Woking of these refrigerants at different pressure range and temperature.
d) This study elaborates the various thermo physical properties of Nano refrigerants which can compare the performance of different Nano refrigerants.

3 Objectives of the Study

The main objectives of the research as follows

- To estimate the Thermal conductivity of mixed refrigerants at different temperatures and pressure.
- To estimate the Viscosity of mixed refrigerants at different temperatures and pressure.
- To estimate the Density of mixed refrigerants at different temperatures and pressure.
- To estimate the Specific heat of Nano refrigerants at different temperatures and pressure.
- To estimate the Effective Thermal conductivity of Nano refrigerants at different temperatures and pressure.
- To estimate the Effective Viscosity of Nano refrigerants at different temperatures and pressure.
- To estimate the Effective Density of Nano refrigerants at different temperatures and pressure.
- To estimate the Effective Specific heat of Nano refrigerants at different temperatures and pressure.
- To estimate the pressure drop computationally for a mixed refrigerant at different inlet temperatures (300-330K) with and without addition of Nano-particle at different compositions pressure at 3MPa
- To estimate the heat transfer rate computationally for a mixed refrigerant at different inlet temperatures (300-330K) with and without addition of Nano-particle at different compositions pressure at 3MPa
- To estimate the heat transfer rate computationally for a mixed refrigerant at different inlet temperatures (300-330K) with and without addition of Nano-particle at different compositions pressure at 3MPa
- To estimate Reynolds number rate computationally for a mixed refrigerant at different inlet temperatures (300-350K) with and without addition of Nano-particle at different compositions pressure at 3MPa
- To estimate Nusselt number rate computationally for a mixed refrigerant at different inlet temperatures (300-350K) with and without addition of Nano-particle at different compositions pressure at 3MPa

4 Review of Literature

Abdolbaqi et al., 2016 [4]. In this study, Nano fluids have been prepared by dispersing TiO2 Nanoparticles in different base fluids such as 20:80% and 30:70% by volume of Bio Glycol (BG)/water (W) mixtures. Thermal conductivity and viscosity experiments have 20 been conducted in temperatures between 30 °C and 80 °C and in volume concentrations between 0.5% and 2.0%. Results show that thermal conductivity of Nano fluids increases with the increase of volume concentrations and temperatures. Viscosity of Nano fluid increases with the increase of volume concentrations, but decreases with increase of temperatures.

Abdolbaqi et al., 2016 [5]. Study, Nano fluids has been prepared by dispersing SiO2 Nanoparticles in different base fluids such as 20:80% and 30:70% by volume of Bio Glycol (BG)/water (W) mixtures. Show that thermal conductivity of Nano fluids increases with the increase of volume concentrations and temperatures. Similarly, viscosity of Nano fluid increases with the increase of volume concentrations, but decreases with increase of temperatures.

Noreen Sher Akbar et al., 2016 [6]. The current investigation is carried out to analyse the effects of variable viscosity and thermal conductivity of CNT Nano fluid flow driven by cilia induced movement through a circular cylindrical tube. Analytical solutions for velocity, temperature and pressure gradient and stream function are obtained. The analytical results are numerically simulated by using the Mathematical Software and plotted the graphs for velocity profile, temperature profile, pressure gradient and streamlines to better discussion and visualization.

Chiam et al., 2016 [7]. The present study reports the analysis on thermal conductivity and dynamic viscosity for Al2O3 Nanoparticle dispersed in a different volume ratio of water (W) and ethylene glycol (EG) mixture. The Nano fluids have better enhancement as the percentage of ethylene glycol increases. Meanwhile, the average dynamic viscosity enhanced up to 50% since 60:40 (W: EG). The enhancement of viscosity of Nano fluids decreased with the increment percentage of ethylene glycol.

Babita et al., 2016 [8]. The main focus of this study is to review the work carried out by various researchers in the last two decades and to summarize the preparation and analytical techniques used for preparation of stable Nano fluids. Long term stability of Nano fluid is one of the basic requirements for its better utilization in heat transfer applications. Preparation of a long term stable Nano fluid is one of the main technical challenges.

Kanjirakat Anoopet al., 2016. [9].The effect of high-pressure on the rheological characteristics of alumina-silicone oil Nano fluids at room temperature is investigated in this paper. An increase in, the pressure is observed to have an equal effect on the base fluid and on the Nano

fluids, which results in an average pressure viscosity coefficient for both to be approximately 0.015 mm2/N.

Ali Aminian et al., 2016 [10]. This work presents a neuromorphic model for predicting the thermal conductivity of Nano fluids, which takes into consideration the effects of size, volume fraction, temperature, and thermal Conductivity of Nanoparticles as well as the properties of base fluids. The presented model is found to correctly predict the trends observed in the experimental data for different combinations of Nano particles-base fluids with varying concentrations. Twenty six different types of Nano fluids are used to assess the effectiveness of the proposed neuromorphic model.

Coumaressin et al., 2016 [11]. In this experiment the effect of using CuO-R134a in the Vapour compression system on the evaporating heat transfer coefficient was investigated by CFD, heat transfer analysis using the FLUENT software. By addition of Nanoparticles to the refrigerant results in improvements in the Thermo physical properties and heat transfer characteristics of the refrigerant, thereby improving the performance of the refrigeration system.

Azmi et al., 2016 [12]. This paper introduces the historical background about the development of water based, ethylene glycol (EG) based and EG: Water mixture Nano fluids for the past 20 years. The determination of the forced convection heat transfer and pressure drop was reviewed for Nano fluid flow in a tube. The experimental and numerical heat transfers of Nano fluids were presented.

Anushree et al., 2016 [13]. In this paper, the long term stability of three water based metal oxide Nano fluids: α-Al2O3, TiO2 and γ-Al2O3 Nano fluids- has been investigated. As a result, Nano fluids have been used in certain engineering applications such as in automotive, transportation, cooling of electronics components, solar, and nuclear reactor coolant.

R. Deepak Selvakumar et al., 2016 [14]. In this work, a simple model to predict the thermal conductivity of Nano fluids based on particle size distribution and multi-level homogenization has been proposed. This model considers the Brownian motion, inter facial layer formation and particle clustering. Particle clusters are characterized based on Particle Size Distribution (PSD) analysis and their thermal conductivity is calculated exclusively. Present model predictions are compared with experimental results from the literature and are found to match well. Contributions of aggregation.

Du et al., 2016 [15]. Optical properties of plasmonic Nano fluids containing gold Nanoparticles with different shapes, sizes, aspect ratios and concentrations are studied numerically. Show that the LSPR of gold Nano rods and Nano ellipsoids can be improved by tuning the aspect ratio.

Jan Rudolf Eggers et al., 2016 [16]. In the roughly two decades since the first publication until today, Nano fluids have found their way into various research fields. To-date published documents range from basic research to high-tech applications. This contribution aims at outlining current fields of research regarding Nano fluid research. It is shown that Nano fluid science pushes increasingly into the scientific world, providing plenty of new questions and challenges.

Tasawar Hayat et al., 2016 [17]. Mixed convection flow of magneto hydrodynamic (MHD) Nano fluid. Water based Nano fluid comprising silver and copper as nanoparticles is used. It is observed that velocity profiles for both Nano fluids show decreasing behaviour for Hartman number and angle of inclination. Temperature profile enhances for increasing temperature ratio parameter and radiation parameter in copper water Nano fluid.

Hosseini et al., 2016 [18]. This paper aims to overcome this problem through developing a Tammann-Tait like equation, in which the number of adjustable coefficients is reduced by introducing a nanoparticle concentration-dependent function to the original scheme. Introducing a nanoparticle concentration-dependent function to the original scheme. High pressure densities of some ethylene glycol, water, and ethylene glycol+water-based Nano fluids were predicted using new version of Tammann-Tait equation over the temperature range within 273–363 K and pressures up to 45MPa.

Raja et al., 2016 [19]. The review is made by considering different parameters which govern the Nano fluids characteristics, heat transfer performance and its application. Maximum effort is taken to account the contributions of different researchers available in open literature on different aspects of Nano fluids such as thermal conductivity, viscosity, experimental, numerical studies on heat transfer performances and applications of Nano fluids. The intention of this review is to provide an overview of the most recent studies on Nano fluid in the literatures. It will be very useful for the scientific community working on Nano fluid to update their knowhow about the Nano fluid.

Ningbo Zhao [20] et al., 2016 . This paper first summarizes the recent research on data-driven modelling of Nano fluids thermal physical properties based on artificial neural networks (ANN). Then, the potential applications of Nano fluids in automotive radiator are analysed. Given sufficient samples, ANN seems to be an effective approach to predicting the thermal- physical properties of Nano fluids. The overall heat transfer performance of automotive radiator can be enhanced by using Nano fluids even if there are some discrepancies in the percentage of enhancement and the optimum amount of nanoparticles; and there are many contradictory

results in the literatures about the influences of nanoparticle concentration on Nusselt number and pumping power.

Baojie Weiet al., 2016 [21]. Fabricate Nano fluids, which could increase the efficiency of thermal systems remarkably. This paper studied TiO2 nanoparticles dispersed in diathermic oil to form Nano fluids. In order to explore stability and transfer performance of TiO2 Nano fluids, the two-step method was introduced to prepare the Nano fluids up to volume fraction of 1%. Results showed that the thermal conductivity of Nano fluids increased with increasing volume fractions of TiO2 nanoparticles and increasing of temperature. Thermal conductivity enhancement ratio was a linear relationship with the volume fractions. Adding TiO2 nanoparticles to base fluids was helpful to enhance heat transfer heat system.

Hussein Togun et al., 2016 [22]. Effects of separation flow and Nano fluids on thermal performance for laminar range presented experimentally and numerically in this review. The results showed increase in Nusselt number with increase of Reynolds number, step height, and number of ribs.

Esteban A. Taborda et al., 2016 [23]. The nanoparticles of acidic silica were used to prepare a water-based Nano fluid at different concentrations in distilled water, and also with the addition of 2.0 wt% of a non-ionic surfactant. Experimental results indicate that increasing the concentration of nanoparticles in the mixture, up to 10,000 ppm, leads to a viscosity reduction of approximately 90% in comparison with the nanoparticle-free crude oil.

Suganthi [24] et al., 2016 . The unsteady state heat transfer performance of ZnO–PG–water Nano fluids revealed 16.5 % increase in heat transfer rate for 2 vol % Nano fluids under constant heat flux conditions. These results summarily indicate that ZnO–PG– water Nano fluids perform better than PG–water mixture for solar energy collection and discharging of solar thermal energy storage.

Satnam Singh et al., 2016 [25]. The present paper investigate the performance of the Nano refrigerant in vapour compression cycle and the challenges of using Nano refrigerants in vapour compression cycle. The conventional refrigerants have major role in global warming and depletion of the ozone layer. Therefore, there is need to improve the performance of vapour compression refrigeration system with the help of using suitable refrigerant.

Nor AzwadiCheSidik et al., 2016 [26]. In this work, the ethylene glycol-based TiO2 (EG/TiO2) Nano fluids were prepared by dispersing TiO2 nanoparticles into the base fluid of EG via ultra-sonication. The rheological behaviour of EG/TiO2 Nano fluids over 25–45◦C and particle weight concentration of 0–35 wt% were investigated. It was found that the steady state shear viscosity of the Nano fluids was remarkably enhanced compared with the base fluid of EG.

Moreover, the Nano fluids showed a characteristic shear thinning behaviour particularly at particle Concentrations in excess of ∼5 wt%.

Ruiwen Shu et al., 2016 [27]. In this work, the ethylene glycol-based TiO2 (EG/TiO2) Nano fluids were prepared by dispersing TiO2 nanoparticles into the base fluid of EG via ultra-sonication. The rheological behaviour of EG/TiO2 Nano fluids over 25–45◦C and particle weight concentration of 0–35 wt% were investigated. It was found that the steady state shear viscosity of the Nano fluids was remarkably enhanced compared with the base fluid of EG. Moreover, the Nano fluids showed a characteristic shear thinning behaviour particularly at particle Concentrations in excess of ∼5 wt%.

Mohammad Sardarabadi et al., 2016 [28]. In this study, the use of metal-oxides/water Nano fluids as coolants in photovoltaic thermal units (PVT) is investigated experimentally and numerically. The t-statistic indicator is used to verify that the results of the numerical model are statistically significant. The electrical efficiency for the PVT system is calculated based on the measured temperature of the photovoltaic surface and the fluid outlet. The Both numerical and experimental results show that the TiO2/water and ZnO/water Nano fluids present a better performance in terms of the electrical efficiency compared to that of the Al2O3/water Nano fluids and deionized water. In terms of the thermal performance of the system, the ZnO/water Nano fluids is found to have the highest thermal efficiency compared to deionized water and the other two Nano fluids.

Bartosz Dawidowicz [29] et.al; the experimental stand and procedure for flow boiling investigations are described. Experimental data for pure R22, R134a, R407C and their mixtures with polyester oil FUCHS Reniso/Triton SEZ 32 in a tube with porous coating and smooth, stainless steel reference tube are presented. Mass fraction of oil was equal to 1% or 5%. During the tests inlet Vapour quality was set at 0 and outlet quality at 0.7. Mass velocity varied from about 250 to 500 kg/m^2s. The experiments have been conducted for average saturation temperature 0^{0C}. In the case of flow boiling of pure refrigerants, the application of a porous coating on inner Surface of a tube results in higher average heat transfer coefficient and simultaneously in lower pressure drop in comparison with the flow boiling in a smooth tube for the same mass velocity. Correlation equation for heat transfer coefficient calculation during the flow boiling of pure refrigerants inside a tube with porous coating has been proposed.

Mao-Yu Wen [30] et.al; Flow condensing experiments for refrigerant R-290, and R-600a mixed with the lubricating oil (EMKARATERL 32H) in serpentine small-diameter (2.46 mm) U-tubes are reported. The tests were run at the saturation temperature of 40^{0C}, vapor qualities of 0.41–

0.82, mass flux of 300–600 (kg/m^2s) and inlet oil concentrations from 0 to 5 mass% oil. It was found that the condensation heat-transfer coefficients increased as mass flux values, vapor quality and the number of tube bends increased, but it decreased as the oil concentration increased. In addition, the two-phase pressure drops increased with increases in mass flux values, the number of tube bends and the oil concentration.

Alberto Cavallini [31] et.al; The paper presents a comprehensive overview of the most recent research works on heat transfer (and pressure drop) with natural refrigerants in mini channels, aimed at proper design of heat transfer equipment. About boiling heat transfer, experimental HT results are mainly fitted by empirical correlations referring to the common mechanisms used in more conventional geometries (nucleate and convective boiling); evaporation heat transfer through thin liquid film around vapor plugs is at times considered. About shear dominated condensation heat transfer, suggested design tools again mostly refer to the extension of the semi-empirical correlations earlier established for conventional geometries. For CO2, heat transfer at supercritical conditions, such as in a gas cooler, is also treated. Finally the concept of the Penalty Factor is applied to shear condensation in mini channels to establish the heat transfer performance of the different working fluids, the superior effectiveness of Mini tubes over macro tubes, and the optimization of mini channel condensers.

A.S. Dalkilic [32]et.al; experimental setup, the horizontal test section was a 3.81 m long countercurrent flow double tube heat exchanger with refrigerant flowing in the inner smooth copper tube (8.01 mmi.d.) and cooling water flowing in the annulus (13.7 mm i.d.). Their test runs were performed at saturated condensing temperatures from 38.33 °C to 51.78 °C while the mass fluxes were between 119 and 617 kg $m^{-2}s^{-1}$ for the horizontal test section. Ten different void fraction models and correlations modified the separated flow model, as well as six different correlations of friction factors, in order to determine the best combination for the validation of the experimental pressure drop values. Carey's friction factor was found to be the most predictive. The refrigerant side total and frictional pressure drops were determined within ±30% using the above friction factor and the void fraction combinations of Carey, Baroczy, and Armand for R410a; and those of Carey, Speeding and Spence, and Rigot for R502 and R507a. The equivalent Reynolds number model was modified using the void fraction correlation of Rigot in order to determine the frictional condensation pressure drop and the two-phase friction factor. The effects of vapor quality and mass flux on the pressure drop are discussed in this paper. The importance of using the alternative void fraction and friction factor models and correlations for the separated flow model is also addressed.

Jianchang Huang [33] et.al; Plate heat exchangers (PHE's) are being used to an increasing extent as refrigerant evaporators but published information on their performance in this mode is rather limited. In this paper, two-phase heat transfer and pressure drop characteristics are presented for PHE's when used as refrigerant liquid over-feed evaporators. Laboratory experiments were carried out with three industrial PHE's having different chevron angle combinations, using refrigerant R134a and R507A. Measurements were made over ranges of mass flux, heat flux and corresponding outlet vapour qualities, and the effects of these parameters on the thermal and hydraulic performance of the evaporators were evaluated. Additional field test data of thermal performance were collected from ammonia and R12 water chillers, operating as thermosiphon evaporators. Based on all these data, empirical correlations are proposed for predicting the refrigerant boiling heat transfer coefficient and two-phase frictional pressure drop in PHE's.

Xiangchao Huang [34] et.al; Flow condensation pressure drop characteristics of R410A-oil mixture inside small diameter (5.0 mm and 4.0 mm O.D.) horizontal micro fin tubes were investigated experimentally covering nominal oil concentrations from 0% to 5%. The research results indicate that, comparing with the frictional pressure drop of pure R410A-oil, the frictional pressure drop of R410Aeoil mixture may decrease by maximum of 18% when the vapor quality is lower than 0.6, and increase by maximum of 13% when the vapor quality is higher than 0.6. A new frictional pressure drop correlation for R410A-oil mixture flow condensation inside micro fin tubes is developed based on the refrigerant oil mixture properties, and can agree with 94% of the experimental data within a deviation of _30% to + 30%.

GiovannA.Longo [35] et.al; this paper presents the heat transfer coefficients and pressure drop measured during HC- 600a, HC-290and HC-1270 saturated vapour condensation inside a brazed plate heat exchanger: the effects of refrigerant mass flux, saturation temperature (pressure) and fluid properties are investigated. The heat transfer coefficients show weak sensitivity to saturation temperature (pressure) and sensitivity to refrigerant mass flux and fluid properties .At transition point between gravity controlled and forced convection condensation has been found for a refrigerant mass flux around15–18kgm-^{2}s-^{1}. In the forced convection condensation region the heat transfer coefficients showa35–40% enhancement for a 60%increase of the refrigerant mass flux. The frictional pressure drop shows a linear dependence on the kinetic energy per unit volume of the refrigerant flow. HC-1270 shows heat transfer coefficients 5% higher than HC-600 a and10–15% higher than HC-290, together with frictional pressure drop20–25%lower than HC-290 and 50–66% lower than HC-600a.

Yang Zou [36] et.al; Refrigerant maldistribution among parallel microchannel tubes deteriorates the performance of microchannel heat exchanger because it creates unwanted superheated

region that has lower heat transfer. Besides phase separation in the header, the pressure drop in the header causes the pressure drop in the microchannel tube to be deferent between each tube, also resulting in ow rate maldistribution. This paper experimentally investigates the pressure drop of single-phase and two-phase ow in the vertical header of a multi-pass microchannel heat exchanger. The overall pressure drop in the header include four components: acceleration, gravitation, friction, and minor pressure drop due to microchannel tube protrusion. The gravitation and minor pressure drops are dominant for single-phase liquid ow and at low qualities of two-phase ow, whereas the acceleration and minor pressure drops are dominant for single-phase vapor ow and at high qualities of two-Phase ow. The model to predict the overall pressure drop in the header for single-phase and two-phase ow are proposed based on the experimental results.

S. M. Sami [37]et.al; Heat transfer characteristics of two-phase flow condensation and boiling of quatemary (four components) refrigerant mixtures, on air/refrigerant horizontal enhanced surface tubing are presented, discussed and compared to other refrigerants proposed as substitutes for CFC-502, such as R-507 and R-407B. Heat transfer characteristics, such as average heat transfer coefficients, as well as pressure drops of ternary azeotropic refrigerant mixtures, flow condensation and boiling inside enhanced surface tubing, were predicted. Experimental data showed that our proposed quatemary blend has a superior boiling heat transfer coefficient and higher pressure drop compared to CFC-502.

Rui Cao [38] et.al; The gaseous pVTx properties of trans-1,3,3,3-tetrafluoropropene (R1234ze(E)) + 2-methylpropane (R600a) mixtures were measured in temperatures from 280.15 to 330.15 K and corresponding pressures from 138 to 930 kPa and the compositions of R1234ze(E) from 0.65 to 0.90 mass fraction using the Burnett isothermal expansion method. The uncertainties of experimental device was estimated to be within ±10 mK for temperature, ±10 kPa for pressure, and ±0.001 mass fraction for composition and 0.5% for density. Meanwhile, the density and gas virial equation of state of the mixed refrigerants were fitted on the basis of the experimental pVTx property data. It provided thermophysical parameters for the further research on the performance of the mixed refrigerants as new alternative refrigerants.

C S Choudhari [39] et.al; Use of natural refrigerant R290 can play a vital role in fulfilling the objectives of the international protocols like Montreal and Kyoto. Because of environmental problems such as ozone depletion and global warming, R22 needs to be phased out on urgent basis. This paper analyzes the possibilities of R290 as a potential substitute to 22.Thermodynamic performance analysis of refrigerants R290 and R22 was carried out using standard vapour compression cycle, with evaporating temperature range of - 25°C to 10°C for

the condensing temperature of 45°C, based on analytical calculations. Refrigerant properties were obtained from REFPROP 9.0.Performance parameters like, discharge temperature, volumetric refrigerating capacity and required mass flow of refrigerant were found to be lower with R290 when compared to R22.Coefficient of performance with R290 is slightly lower than that of with R22.However, higher COP can be expected by especially designed system pertaining to the properties of R290.Overall, R290 can be a better substitute to R22 in real applications because of its excellent environmental and thermophysical properties.

Guogeng He, [40] et.al; A new refrigerant mixture composed of R290 and R32 is proposed by the present paper. With a mass ratio of m32/m290 = 68/32, the new refrigerant mixture is near azeotropic, zero ODP and low GWP, which will be a competitive R22 replacement in household air conditioners. An experimental apparatus has been designed and built to analyze the flow boiling performance of this new refrigerant mixture. Flow boiling heat transfer performances of the new refrigerant mixture inside different horizontal heat transfer tubes including 5 mm smooth and micro-fin tubes, 7 mm smooth and micro-fin tubes and 9.52 micro-fin tube, have been experimentally investigated. Variations of flow boiling heat transfer coefficient with mass flux under the condition of different evaporation temperature and different tube inner diameters were obtained. Comparison of flow boiling heat transfer coefficient of the new R32/R290 mixture with that of R410A has been carried out. Flow boiling heat transfer coefficient of the new R32/R290 mixture is 14.3–68.4% higher than that of R410A. The researching results of the present study will be of great help in evaporator design and optimization for R32/R290 refrigeration units.

Wang Zhang [41] et.al; currently, the most common refrigerants used in household split air conditioners are R22 and R410A. Due to environmental concerns, benign options such as R290 (propane) are under consideration as an alternative. However, R290 is flammable, which poses additional fire and explosion risks. The ignition source and location of the leak that may appear within the indoor and outdoor units were analyzed. A series of experiments were carried out to better understand the ignition hazard. The explosion characteristics associated with the indoor and outdoor units were studied whereby the overpressure arising from ignition of R290 was measured at different locations. According to the internal volume of indoor and outdoor units, the amount of R290 that should be deposited inside the indoor and the outdoor units is 7 g and 16 g respectively, to form a stoichiometric concentration. The explosion overpressure in the indoor and outdoor units is sufficiently low so as to not damage the air conditioner system. However, if R290 is ignited during the leak, the indoor or outdoor unit will be burned.

Qi Chen, Jianlin Yu [42] et.al; this study presents a modified vapor compression refrigeration cycle (MVRC) using zeotropic mixture R290/R600 for freezers. In the MVRC, an internal sub-cooler with additional bypass tube is introduced to enhance the overall system performance. Energetic and exergetic analysis methods are introduced to theoretically evaluate the system operating performance, and compared with the performance of the traditional vapor compression refrigeration cycle (TVRC). The results show that the MVRC Yields higher refrigeration coefficient of performance (COP), volumetric cooling capacity and exergy efficiency than the TVRC. Under the given condition, the COP, volumetric cooling capacity and exergy efficiency of MVRC could be improved by up to an average of 8.9%, 12.4% and 10.4%. Moreover, COP and exergy efficiency of MVRC increases with the rising bypass coefficient of the refrigerant. The performance characteristics of the proposed novel cycle demonstrate the potential advantages for application in freezer systems.

Zhao Yang [41] et.al; currently, the most common refrigerants used in household split air conditioners are R22 and R410A. Due to environmental concerns, benign options such as R290 (propane) are under consideration as an alternative. However, R290 is flammable, which poses additional fire and explosion risks. The ignition source and location of the leak that may appear within the indoor and outdoor units were analyzed. A series of experiments were carried out to better understand the ignition hazard. The explosion characteristics associated with the indoor and outdoor units were studied whereby the overpressure arising from ignition of R290 was measured at different locations. According to the internal volume of indoor and outdoor units, the amount of R290 that should be deposited inside the indoor and the outdoor units is 7 g and 16 g respectively, to form a stoichiometric concentration. The explosion overpressure in the indoor and outdoor units is sufficiently low so as to not damage the air conditioner system. However, if R290 is ignited during the leak, the indoor or outdoor unit will be burned.

Zhenhua Chen [43] et.al; The cold and warm startup characteristics of an R290 heat pump system and its rotary compressor were experimentally investigated under a low ambient temperature heating condition. These startup characteristics included the temperatures in the compressor shell and system and the pressures in the cylinder and system. The results showed that the minimum suction gauge pressure (-48 kPa) during a cold startup was lower than that during a warm startup (155 kPa) under a low ambient temperature heating condition. In addition, the time required for the R290 heat pump system to reach a steady pressure was much longer than that of a system using R410A as the refrigerant. Compared with that of the cooling condition, smaller amounts of liquid were generated in the cylinder at the beginnings of both the cold and warm startup processes under the low ambient temperature heating condition.

Tejaswi Saran Pilla [44]et.al; Mixed refrigerant systems are reported to be thermally efficient. However, the mechanical input required by the compressor is not investigated in the literature. Hence, in the present work, two refrigerants are chosen (R-290 and R-600a) to evaluate the mechanical performance of compressor of domestic refrigerators. The refrigeration cycle consists of four major processes. The isentropic compression in the compressor, isobaric heat rejection in the condenser, isenthalpic reduction in pressure and isobaric heat addition in the evaporator. The present work aims at investigation of mechanical performance of compressor with mixed refrigerants (R-290 and R-600a). The boiling point of the each of the refrigerant is different and hence the specific volume occupied by each is different. This in turn affects the work input required. Hence, the present work is aimed at evaluating the compressor performance with mixed refrigerants. The temperature distribution during the cycle operation process is estimated. This turn enables the effective design of the compressors for domestic refrigeration systems for effective operation.

Dong Lv [41] et.al; currently the most common refrigerants used in household split air conditioners are R22 and R410A. Due to environmental concerns, benign options such as R290 (propane) are under consideration as an alternative. However, R290 is flammable, which poses additional fire and explosion risks. The ignition source and location of the leak that may appear within the indoor and outdoor units were analyzed. A series of experiments were carried out to better understand the ignition hazard. The explosion characteristics associated with the indoor and outdoor units were studied whereby the overpressure arising from ignition of R290 was measured at different locations. According to the internal volume of indoor and outdoor units, the amount of R290 that should be deposited inside the indoor and the outdoor units is 7 g and 16 g respectively, to form a stoichiometric concentration. The explosion overpressure in the indoor and outdoor units is sufficiently low so as to not damage the air conditioner system. However, if R290 is ignited during the leak, the indoor or outdoor unit will be burned.

Yingxia Qi [38] et.al; The gaseous pVTx properties of trans-1,3,3,3-tetrafluoropropene (R1234ze(E)) + 2-methylpropane (R600a) mixtures were measured in temperatures from 280.15 to 330.15 K and corresponding pressures from 138 to 930 kPa and the compositions of 234ze(E) from 0.65 to 0.90 mass fraction using the Burnett isothermal expansion method. The ncertainties of experimental device was estimated to be within ±10 mK for temperature, ±10 kPa for pressure, and ±0.001 mass fraction for composition and 0.5% for density. Meanwhile, the density and gas virial equation of state of the mixed refrigerants were fitted on the basis of the experimental pVTx property data. It provided thermophysical parameters for the further research on the performance of the mixed refrigerants as new alternative refrigerants.

Houxue Huang [45] et.al; A key parameter in designing two-phase ow systems for the cooling of high heat ux electronics is the pressure drop in microchannel evaporators. As a result, an experimental study was performed to investigate the boiling pressure drop of refrigerants in two silicon multi-microchannel evaporators. Three types of refrigerants (R1233zd (E), R245fa and R236fa) were tested under three inlet sub-cooling and three nominal outlet saturation temperatures. The test section's backside base temperatures were measured by an infrared (IR) camera. A single-phase ow validation in terms of the inlet and outlet restriction pressure drops and the channel ow friction factor was carefully done before the boiling tests. The operating conditions for stable low boiling tests were: mass fluxes from 1250 to 2750 kg $m^{-2}s^{-1}$, heat fluxes from 20 to 64 W cm^{-2}. The resulted maximum vapor quality at the outlet manifold was 0.51. It is found that within the present test conditions

Di Yang [46] et.al; the heat transfer and flow characteristics of MWCNT-R141b Nano refrigerant with different mass fractions have been studied through experiments. Experimental results were compared with existing correlations. A two-step method was used to prepare the Nano refrigerants. Span-80 was used as surfactant with an average particle diameter of 20 nm. Transmittance method was used to evaluate the stability of Nano refrigerants. Results showed that the stability of MWCNT-R141b Nano refrigerant, which is the added dispersant, was good during the experiments. The 0.3 wt% MWCNT-R141b Nano refrigerants had optimal heat transfer enhancement effects compared with pure refrigerants. The maximum Nusselt number increased by 40%. The specific pressure drop of Nano refrigerant increased as the Reynolds number (Re) increased, and the specific pressure drop of the pure refrigerant was minimum, which is similar to R141b.

Rishuai Chen [38] et.al; The gaseous pVTx properties of trans-1,3,3,3-tetrafluoropropene (R1234ze(E)) + 2-methylpropane (R600a) mixtures were measured in temperatures from 280.15 to 330.15 K and corresponding pressures from 138 to 930 kPa and the compositions of R1234ze(E) from 0.65 to 0.90 mass fraction using the Burnett isothermal expansion method. The uncertainties of experimental device was estimated to be within ±10 mK for temperature, ±10 kPa for pressure, and ±0.001 mass fraction for composition and 0.5% for density. Meanwhile, the density and gas virial equation of state of the mixed refrigerants were fitted on the basis of the experimental pVTx property data. It provided thermophysical parameters for the further research on the performance of the mixed refrigerants as new alternative refrigerants.

S.B. Ingole [23] et.al; Jet impingement is exceedingly operational for numerous field applications including electronics cooling and process industry. Its implementation comfort makes it common for many applications. The paper deals with investigation of heat transfer

characteristics of a cooling flat surface. It is cooled by air jet impinged at an inclination of 15–75_ to target plate. For understanding variation in cooling performance, comprehensive experiments are performed with different configurations of inclined jets on hot surface. For simplicity in using air, it is recommended for verity of applications as cooling fluid. Air Inclined jet with Reynolds Number in the range of 2000 6 Re 6 20,000 is examined for the circular Inclined jet. The target to inclined jet perpendicular height (H) is varied from 0.5 6 H/D 6 6.8 for understanding effect of H on cooling performance of different locations on target plate. The investigation leads to equations for average Nusselt Number for inclined non-confined air jet for cooling applications.

Qiang Liu [47] et.al; Organic Rankine cycles (ORCs) are preferred to convert low temperature geothermal energy (<150^{0C}) to electricity. The working fluid selection and system parameters optimization are the main approaches to improve geothermal ORC systems performance. Zeotropic mixtures are showing promise as ORC working fluids due to the better match between the working fluid and the heat source/sink temperatures. This study optimizes the cooling water temperature rise as well as the evaporation and condensation pressures of isobutane/isopentane (R600a/R601a) mixtures for various mole fractions to maximize the net power output of a geothermal ORC for geothermal water temperatures of 110^{0C}, 130^{0C} and 150^{0C} and reinjection temperatures not less than 70^{0C}. Two mole fractions maximize the turbine power generation, while the maximum net power output occurs for R600a mole fractions from 0.7 to 0.9 due to the variation of the parasitic power consumed by the working fluid feed pump and the cooling water circulating pump. A geothermal ORC using R600a/R601 can generate 11%, 7% and 4% more power than an ORC using pure R600a for geothermal water inlet temperatures of 110^{0C}, 130^{0C} and 150^{0C}, respectively. Both the evaporator and condenser area per unit power output using R600a/R601a are higher than that using pure R600a or R601a due to the reduction in the heat transfer coefficient and the temperature difference between the mixture working fluid and the heat source/sink. The total heat transfer area per unit power output increases to a maximum at an R600a mole fraction of 0.5 and then decreases with increasing R600a mole fraction. The total heat transfer area can be reduced for the same power output with higher geothermal source temperatures. The turbine using R600a/R601a with higher R600a mole fractions is nearly the same size as a turbine using pure R600a.

Mao-Yu Wen [48] et.al; This investigation was undertaken in order to better understand the characteristics of sub-cooled flow boiling heat transfer and pressure drop of a hydrocarbon refrigerant R600a (ISO-butane) flowing in a circular pipe within dispersed-copper porous inserts. The test was conducted at a saturation temperature of 10^{0C}, vapour qualities were from

0.076 to 0.87, and there was shown to be a mass flux of 120e1100 kg/ m^2 s and a heat flux of 12e65 kW/m^2. The effects of Reynolds number and the sizes of inserts (the porosity, mean pore diameters and permeability) on the heat transfer and pressure drop of R-600a are presented. In addition, empirical correlations for estimating the boiling heat transfer coefficients and pressure drop for pure R-600a under these conditions have been proposed.

5 Research Methodology

Steps to be followed

- **Selection of a refrigerant mixture**
  - The very first step in this research work is the selection of different refrigerants which are currently used in the Vapour compression refrigeration system.
  - In this present research work mixed refrigerant Propane (R290) and ISO-butane (R600a) are selected that are used in the vapour compression refrigeration system.
- **Study of thermo-physical properties**
  - Thermo-physical properties like thermal conductivity, density, viscosity, and specific heat of propane and ISO-butane are studied. Different graph have been plotted with respect to temperature and graphs are shown in the succeeding chapter.
- **Selection of Nano-particles**
  - Thermal properties of metals and metal oxides are very good as compared to refrigerants. That's why Nano-particles Such as Al_2O_3 (Sapphire, Poly-crystalline), CuO, TiO_2, and ZnO are used in the research work.
- **Preparation of Nano-refrigerants**
  - Nano-refrigerants are prepared by adding Nano-particles in different refrigerants. Volume concentration of Nano-particle in the refrigerants varies from 1% to 5%.
- **Study on Nano-refrigerants**
  - Thermo-physical properties of Nano-refrigerants with respect different volume concentration of Nano-particles with addition of different correlations for effective Thermal Conductivity, Effective Density, Effective Specific Heat and Effective Specific Heat are investigated and the results are written in the succeeding chapter.
- **Effective Thermal Conductivity**

  Maxwell Correlation $$k_{effe} = \frac{k_p + 2k_f + 2\phi(k_p - k_f)}{k_p + 2k_f - \phi(k_p - k_f)}$$
- **Effective Viscosity**

  Drew and Passman $$\frac{\mu_{effe}}{\mu_f} = 1 + 2.5\phi$$
- **Effective Density:**

  Xuan Y, $$\rho_{nf} = (1-\phi)\rho_{Bf} + \varphi\rho_{np}$$

- **Effective Specific Heat**

Pak BC $$C_{pNF} = \frac{(1-\phi)(\rho C_p)_{BF} + \phi(\rho C_p)_{NP}}{(1-\phi)\rho_{BF} + \phi\rho_{NP}}$$

- **Computational evaluation of pressure drop**

- In the present research work, pressure drop is evaluated for compressor pipe and corrugated pipe in addition with respect to different mass flow rates at different temperatures varies from 300-330K for a mixed refrigerant at different compositions.

- **Computational evaluation of heat transfer rate**

- In the present research work, heat transfer rate is evaluated for compressor pipe and corrugated pipe in addition with respect to different mass flow rates at different temperatures varies from 300-330K for a mixed refrigerant at different compositions.

- **Computational evaluation of Reynolds number**

- In the present research work, Reynolds number is evaluated for compressor pipe and corrugated pipe in addition with respect to different mass flow rates at different temperatures varies from 300-330K for a mixed refrigerant at different compositions.

- **Computational evaluation of Nusselt number**

- In the present research work, Nusselt number is evaluated for compressor pipe and corrugated pipe in addition with respect to different mass flow rates at different temperatures varies from 300-330K for a mixed refrigerant at different compositions.

6 Expected Outcomes

In the present research work, a refrigerants mixture Propane and ISO-butane are used for the analysis to find thermo physical properties. In the present work thermo physical properties such as thermal conductivity, viscosity, density and specific heat are evaluated at pressure of 3MPa-7MPa and temperature of 300-350K

The following outcomes are as follows

- Density of a mixed refrigerant at different compositions may decreases with respect to temperature.
- Viscosity of a refrigerant mixture at different compositions may decreases with respect to temperature.
- Thermal conductivity of a refrigerant mixture at different compositions may decreases with increase in temperature.
- Specific Heat of a refrigerant mixture at different compositions may decreases with increase in temperature.
- Effective thermal conductivity of mixed refrigerant with addition of CuO Nano-particles may be increase at pressure 3MPa
- Effective viscosity of mixed refrigerant with addition of CuO Nano-particles may be increase at pressure 3MPa
- Effective density of mixed refrigerant with addition of CuO Nano-particles may be decreases at pressure 3MPa
- Effective specific heat of mixed refrigerant with addition of CuO Nano-particles may be decreases at pressure 3MPa
- Pressure drop of a mixed refrigerant with and without addition of CuO Nanoparticles may be increases exponentially at different inlet temperatures (300-330K) at pressure 3MPa
- Heat transfer rate of a mixed refrigerant with and without addition of CuO Nanoparticles may be increases linearly at different inlet temperatures (300-330K) at pressure 3MPa
- Reynolds number of a mixed refrigerant with and without addition of CuO Nanoparticles may be increases linearly at different inlet temperatures (300-330K) at pressure 3MPa
- Nusselt number of a mixed refrigerant with and without addition of CuO Nanoparticles may be increases linearly at different inlet temperatures (300-330K) at pressure 3MPa

7 Complete Work Plan with Timeline

The Project work commenced in January 2016 and was successfully completed by April 2017. Unparalleled dedication, work coupled with awe-inspiring mentorship was the corner stone of this project.

All the team members showed tremendous determination in achieving the desired results within the set time frame. The figure shows the complete work plan with timelines.

The figure below shows the various activities undertaken during the course of the project.

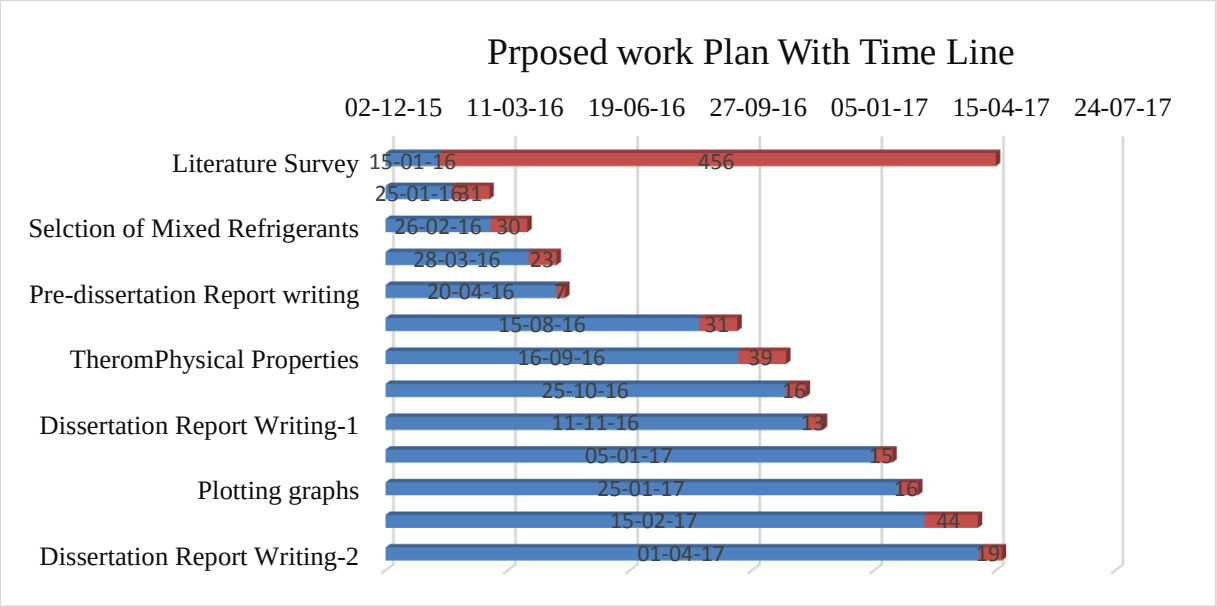

Figure 9: Proposed work with timeline

8 Results and Discussions

In the present research work density, Viscosity, Thermal conductivity, Specific heat, is calculated for a mixed refrigerant. The analysis is carried out on refrigerants for their thermo-physical properties and results are shown as below from 3MPa to 7MPa. In each case specific heat increases with increase in temperature and density, viscosity, thermal conductivity decreases with increase in temperature. Moreover, Effective Thermal conductivity, Effective Viscosity, Effective Specific heat and Effective Density is calculated computationally with addition of CuO Nano-particle composition at pressure 3MPa. It is also calculated Pressure Drop, Heat Transfer rate, Reynolds and Nusselt Number using CFD analysis for mixed refrigerant with and without addition of Nano-particle.

8.1 Effect of Thermophysical properties of a mixed refrigerant At pressure 3MPa

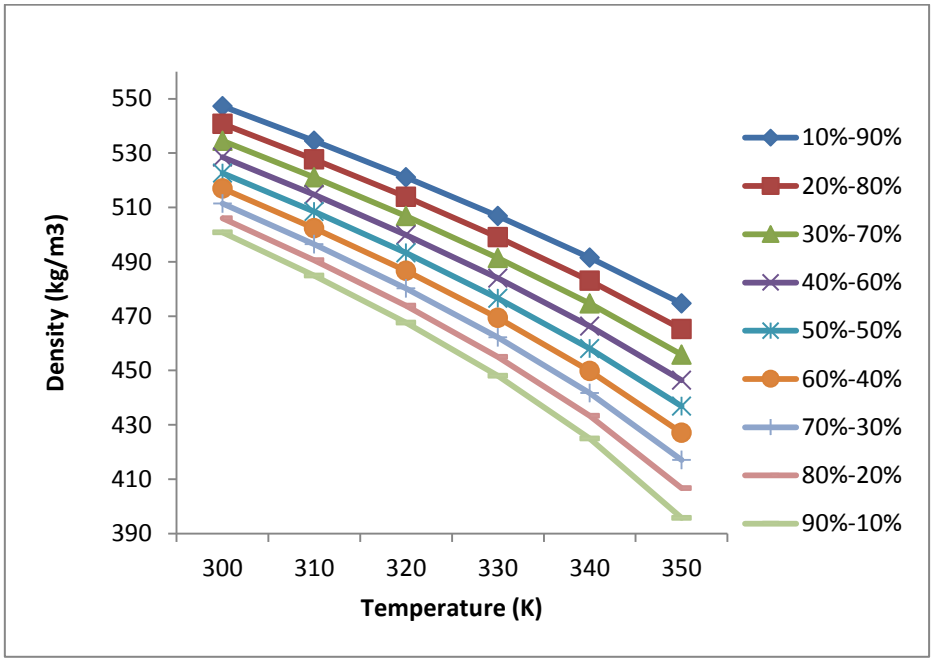

Figure 10 density as a function of temperature at pressure 3MPa

Figure 10 represents that density is a function of temperature at a pressure of 3MPa. Moreover, it is observed that as the temperature increase density decreases for a mixed refrigerant of all above 9 cases.

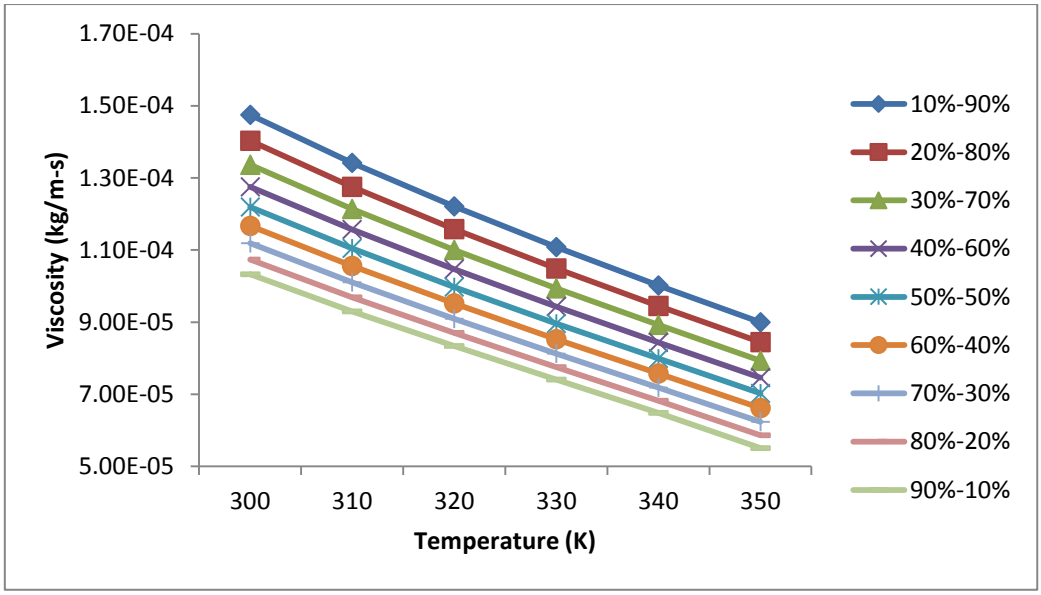

Figure 11 Viscosity as a function of Temperature at 3MPa

Figure 11 viscosity is a function of temperature at constant pressure 3MPa. It is observed that as the temperature increases viscosity decreases in a mixed refrigerant for all the above 9 cases.

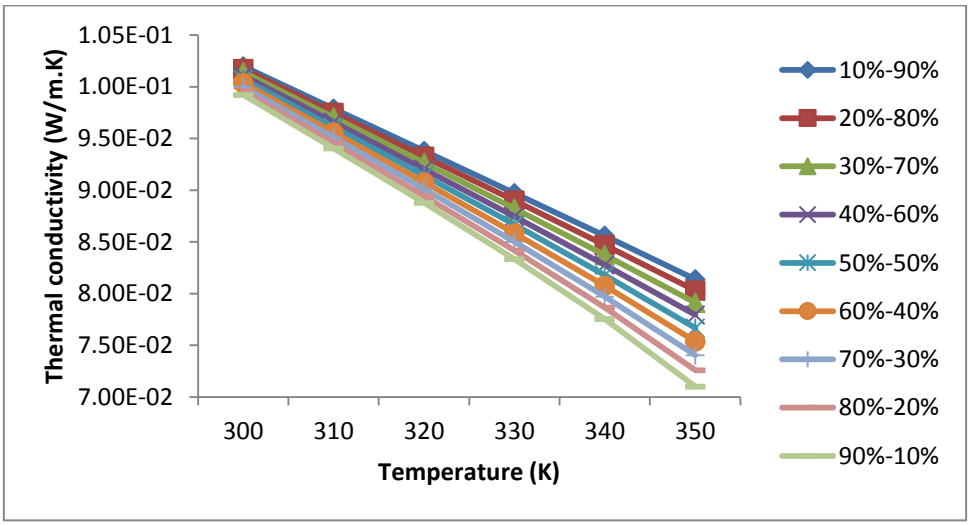

Figure 12 Thermal conductivity as a function of Temperature at 3MPa

Figure 12 represents that thermal conductivity as a function of temperature. Moreover, it is observed that as the thermal conductivity decreases with increase in temperature for a mixed refrigerant at different compositions.

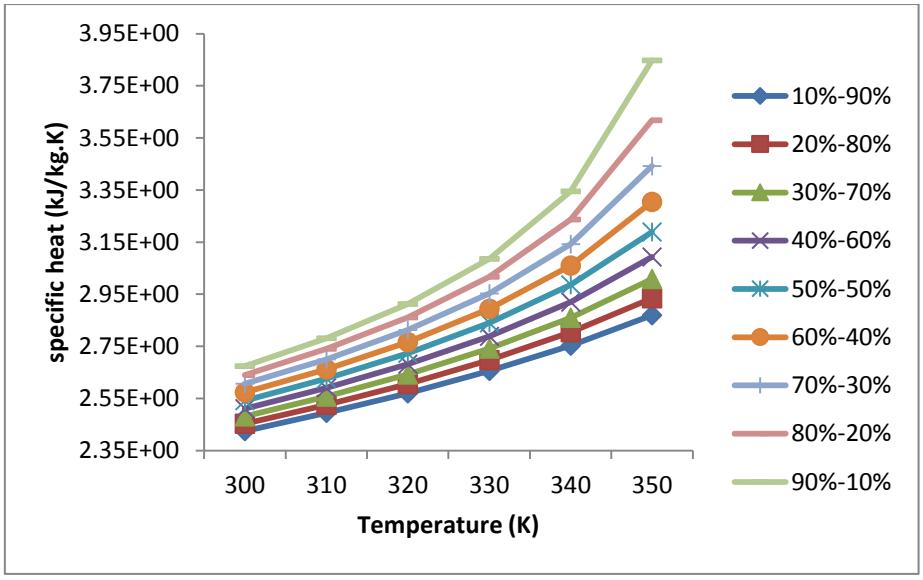

Figure 13 Specific heat as a function of Temperature at 3MPa

Figure 13 reveals that specific heat is a function of temperature at constant pressure 3MPa. Moreover, it is observed that as the specific heat increases with increase in temperature for a refrigerant mixture.

At Pressure 4MPa

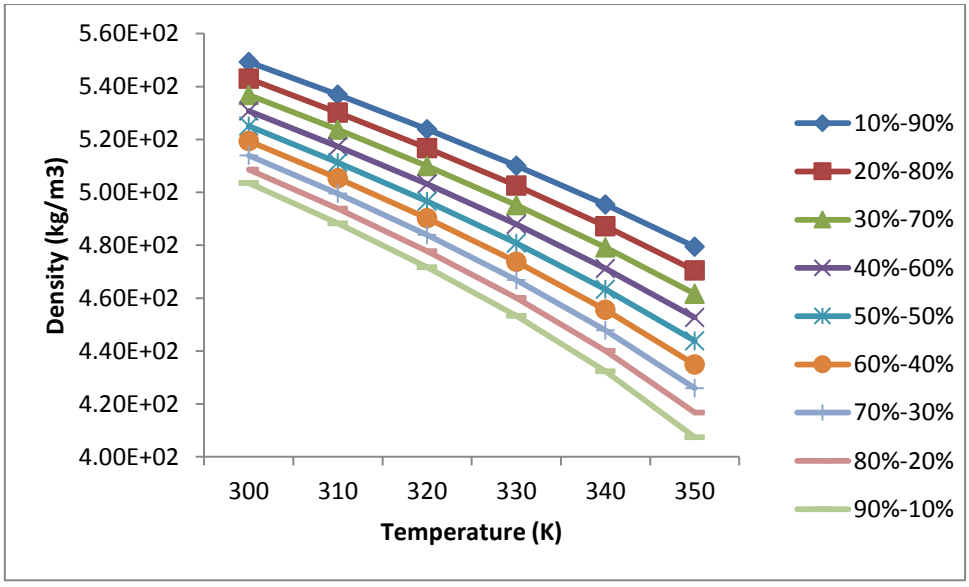

Figure 14 Density as a function of temperature at 4MPa

Figure 14 represents that density is a function of temperature at constant pressure 4MPa. It can be seen that as the temperature increases density decreases for a mixed refrigerant of all above 9 cases.

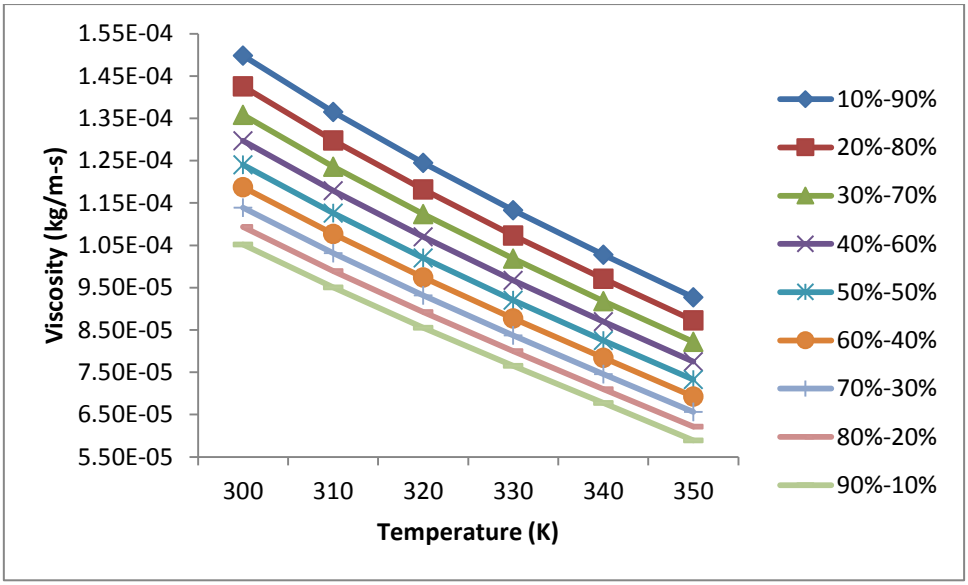

Figure 15 Viscosity as a function of Temperature at 4MPa

Figure 15 shows that viscosity is a function of temperature at constant pressure. It is also observed that as the viscosity decreases with increase in temperature for a mixed refrigerant at different composition.

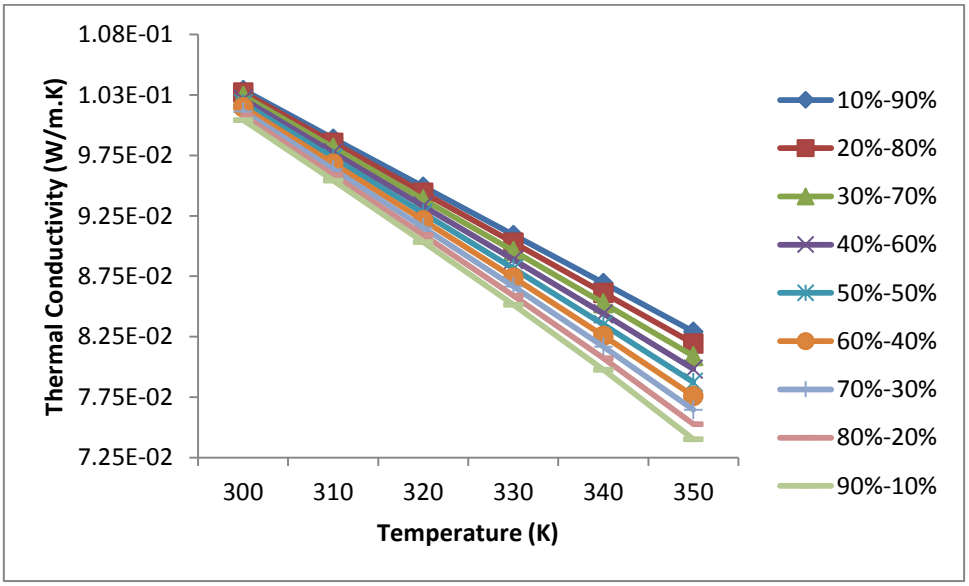

Figure 16 Thermal Conductivity as a function of Temperature at 4MPa

Figure 16 represents that thermal conductivity as a function of temperature at constant pressure 4MPa. Moreover, it is also observed that as the temperature increase from 300-350K thermal conductivity decreases for different compositions.

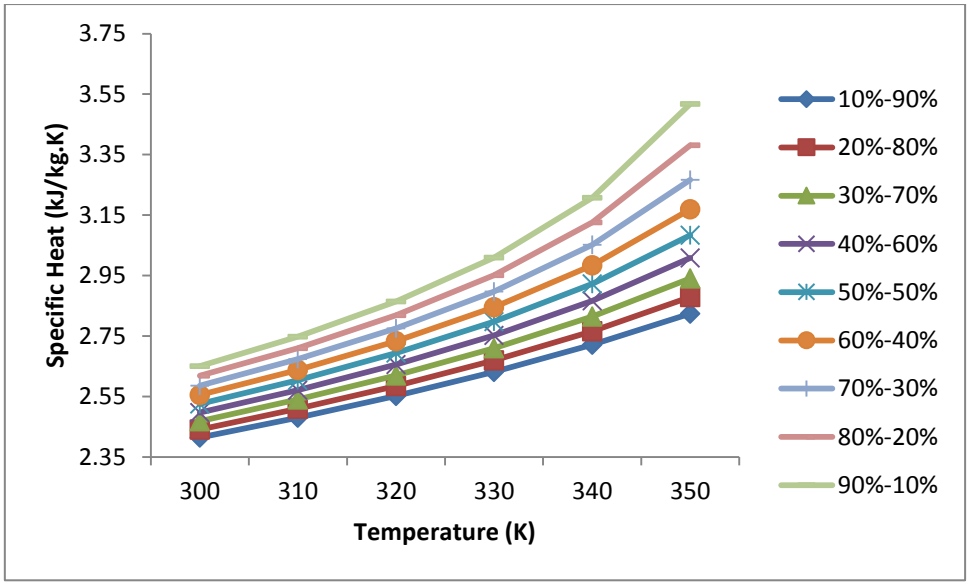

Figure 17 Specific heat as a function of Temperature at 4MPa

Figure 17 shows that specific heat is a function of temperature at a pressure of 4MPa. It is observed that as the specific heat increases with increase in temperature range from 300-350K of different compositions.

At Pressure 5MPa

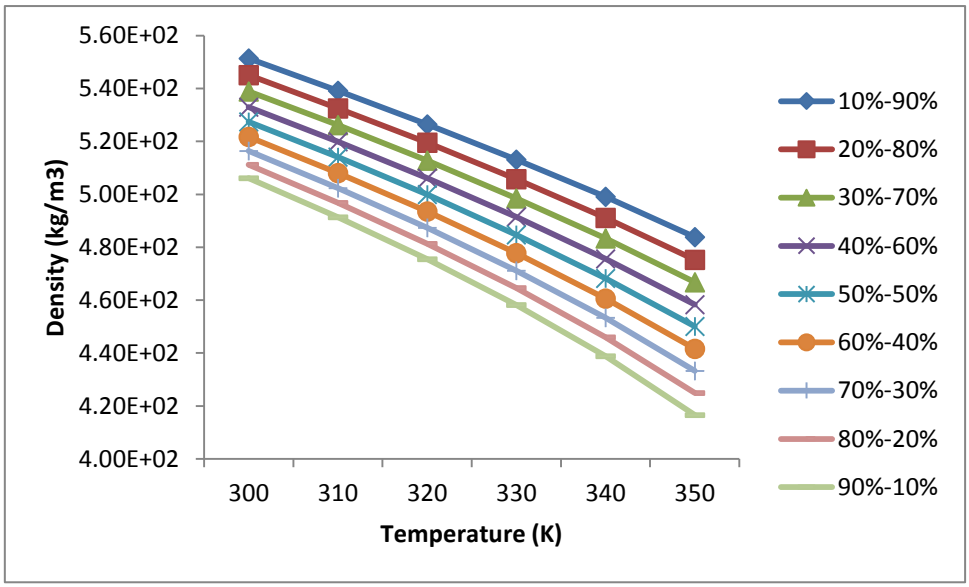

Figure 18 Density as a function of Temperature at 5MPa

Figure 18 shows that density is a function of temperature at constant pressure. It is observed that density decreases with increase in temperature range 300-350K for a mixed refrigerant at different compositions.

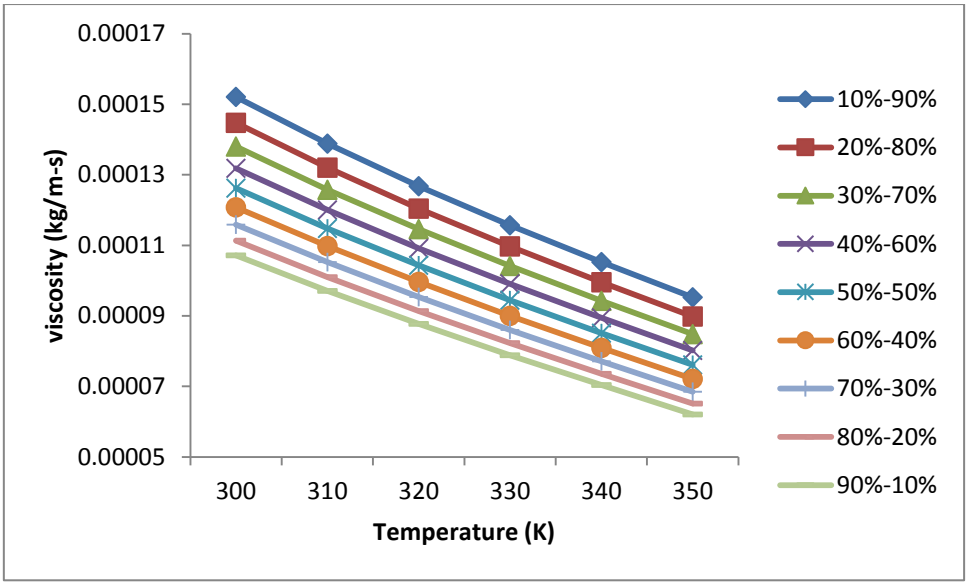

Figure 19 Viscosity as a function of Temperature at 5MPa

Figure 19 represents that viscosity is a function temperature at pressure of 5MPa. It is observed that as the temperature increases viscosity decrease for a mixed refrigerant for all 9 cases.

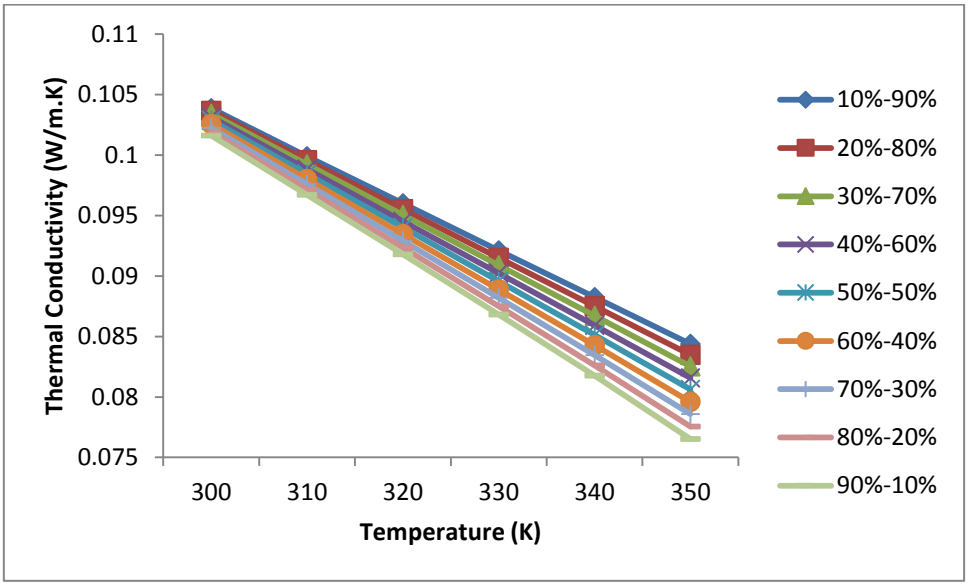

Figure 20 Thermal conductivity w.r.t temperature

Figure 20 reveals that thermal conductivity is a function of temperature at constant pressure. Meanwhile, it is observed that as the temperature increases thermal conductivity in a refrigerant mixture for all the above 9 compositions.

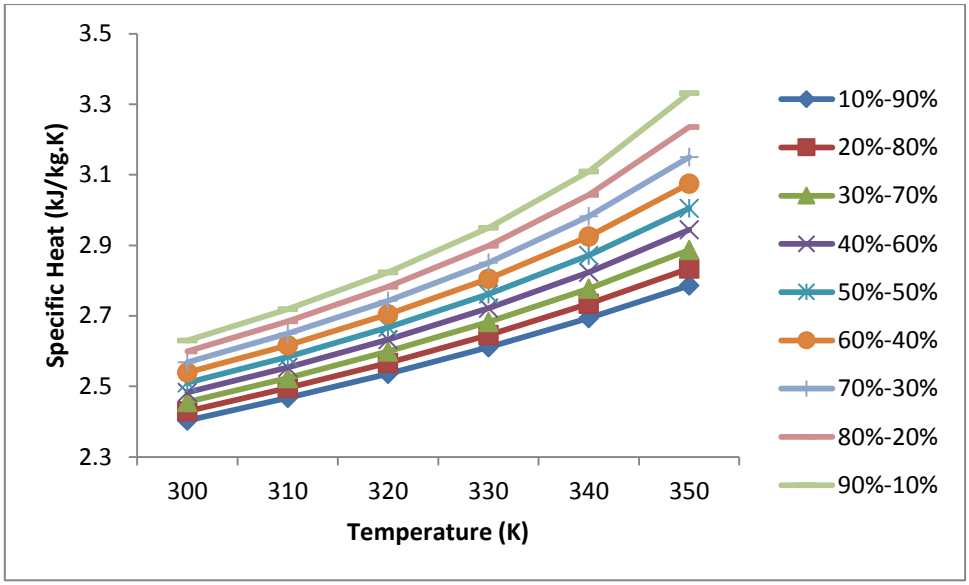

Figure 21 Specific Heat as a function of Temperature at 5MPa

Figure 21 shows that specific heat is a function of temperature at pressure constant. It is also observed that as the specific heat increases with an increase in the temperature for a mixed refrigerant of all 9 cases.

At Pressure 6MPa

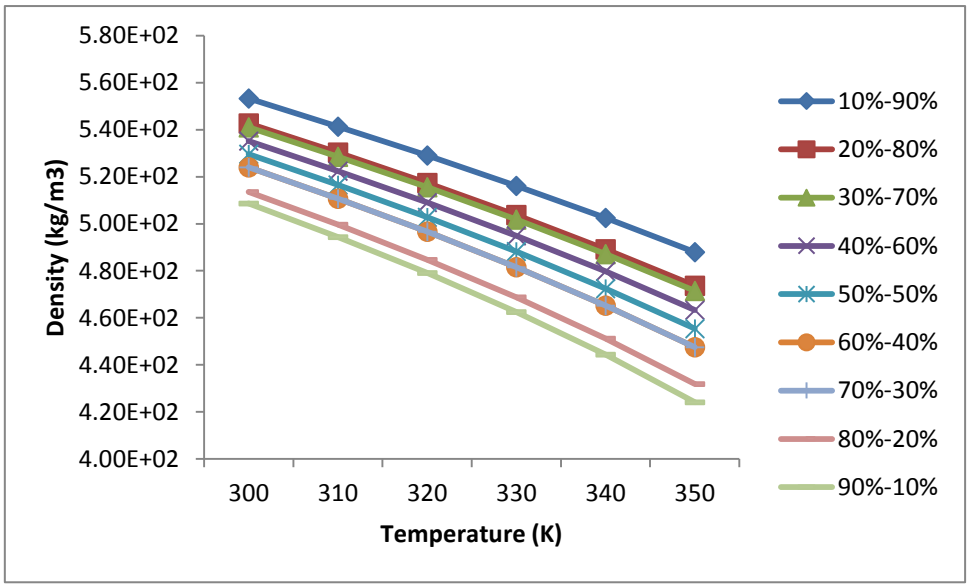

Figure 22 Density as a function of temperature at 6MPa

Figure 22 reveals that density is a function of temperature a constant temperature of 6MPa. It is also observed that as the temperature increases density decreases for a mixed refrigerant of all 9 cases.

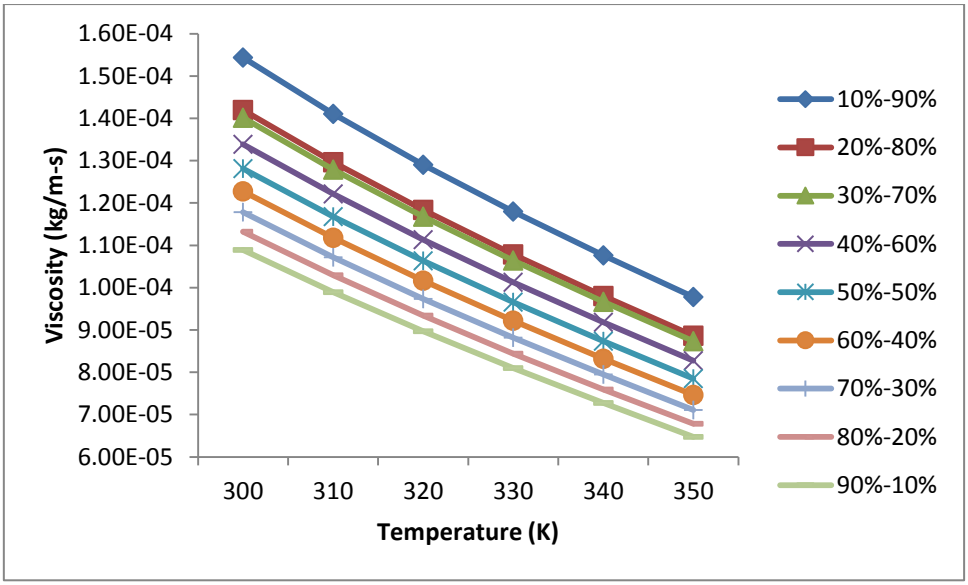

Figure 23 Viscosity as a function of Temperature at 6MPa

Figure 23 reveals that viscosity is a function of temperature at constant pressure 6MPa. Moreover, it is also observed that as the temperature increase from 300-350K viscosity decreases in a mixed refrigerant of all 9 cases.

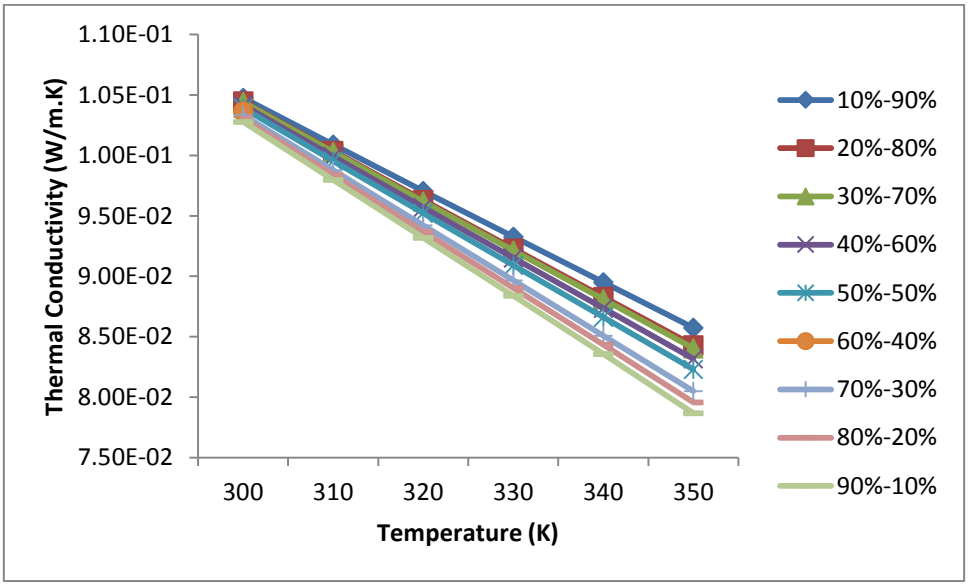

Figure 24 Thermal conductivity as a function of Temperature at 6MPa

Figure 24 Thermal conductivity as a function of temperature at a constant pressure of 6MPa. Meanwhile, it is observed that as the thermal conductivity decreases with increase in temperature of 300-350K at different compositions.

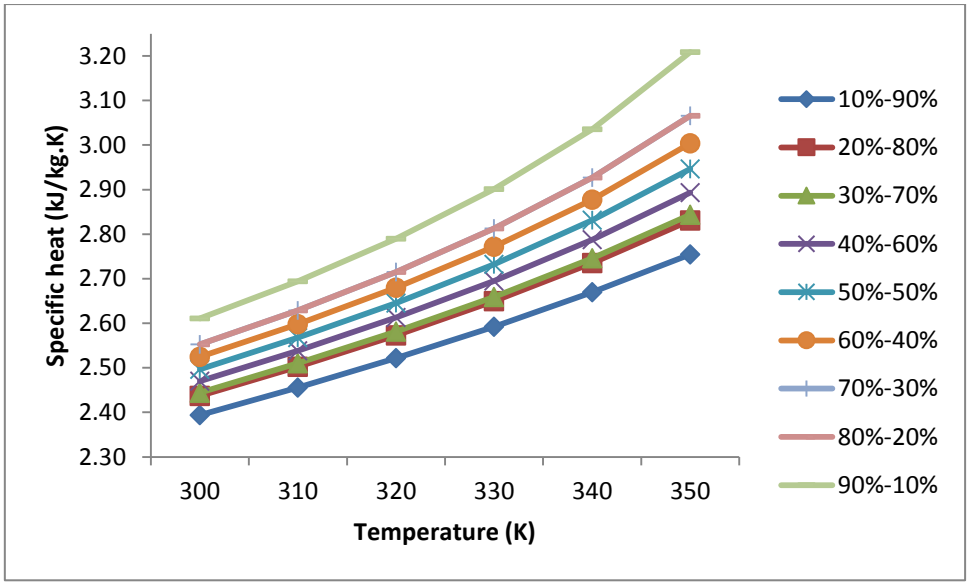

Figure 25 specific heat as a function of Temperature at 6MPa

Figure 25 reveals that specific heat is a function of temperature at constant pressure of 6Mpa. Moreover, it is observed that as the specific heat increases with increase in temperature at 300-350K for a mixed refrigerant of all 9 cases.

At Pressure 7MPa

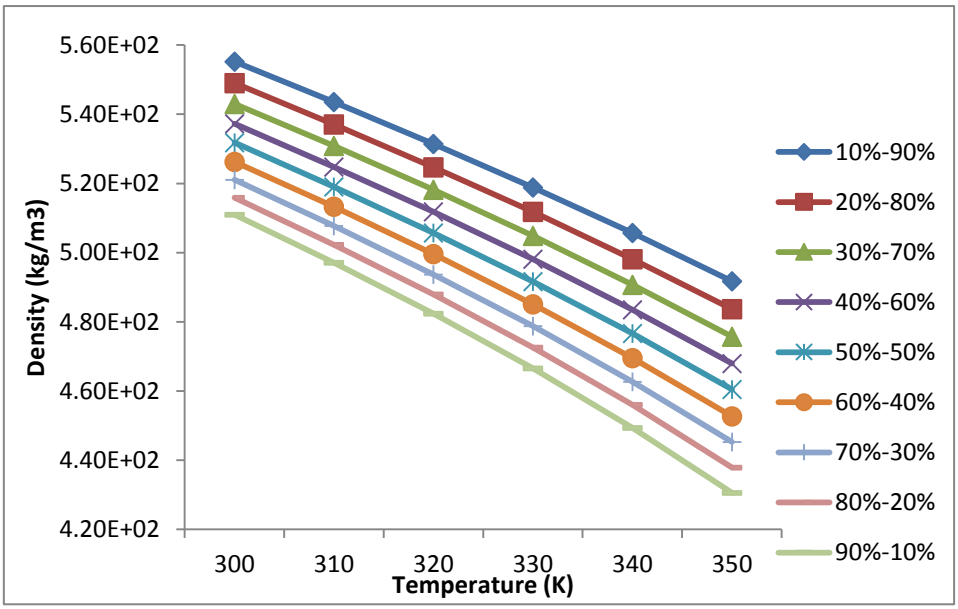

Figure 26 Density as a function of Temperature at 7MPa

Figure 26 represents that density decreases with increases in temperature at constant pressure. It is observed that as the density decreases with increase in temperature of 300-350K for a mixed refrigerant of all above 9 cases

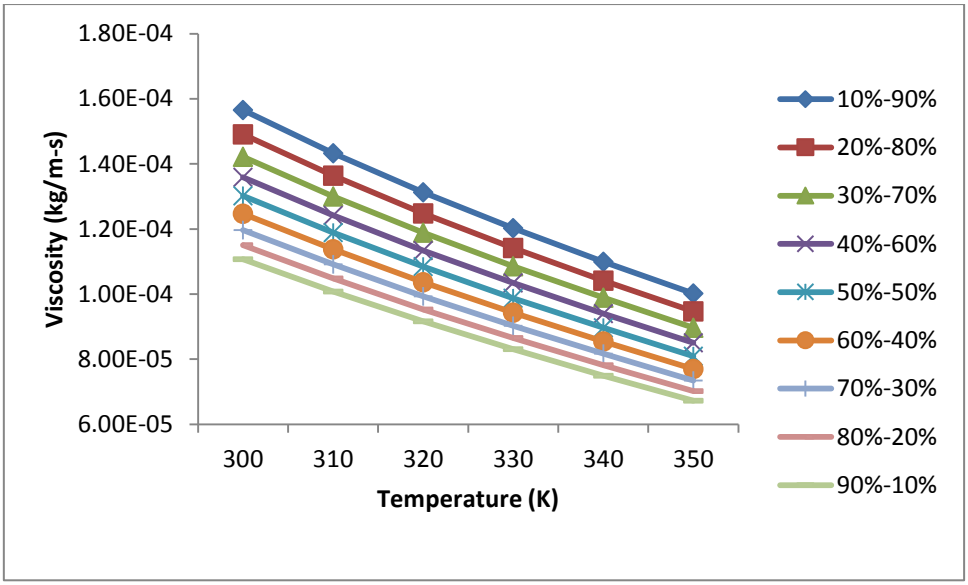

Figure 27 viscosity as a function of temperature at 7MPa

Figure 27 reveals that thermal conductivity is a function of temperature at constant pressure 7MPa. Moreover, it is observed that as the viscosity decreases with increase in temperature ranges from 300-350K for a mixed refrigerant.

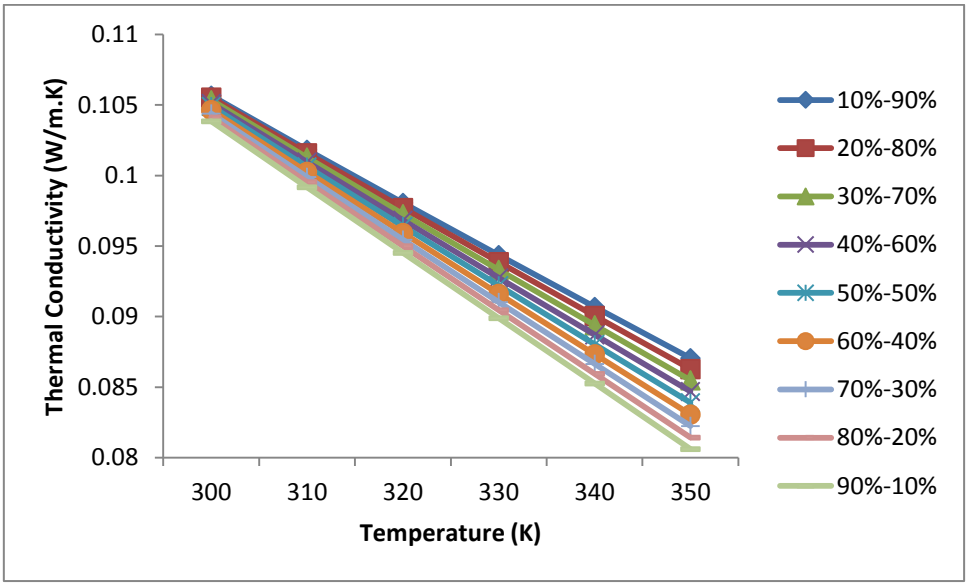

Figure 28 Thermal conductivity as a function of temperature at 7MPa

Figure 28 shows that thermal conductivity is a function of temperature at constant pressure of 7MPa. Moreover, it is observed that as thermal conductivity decrease with increase in temperature in a mixed refrigerant for all 9 cases.

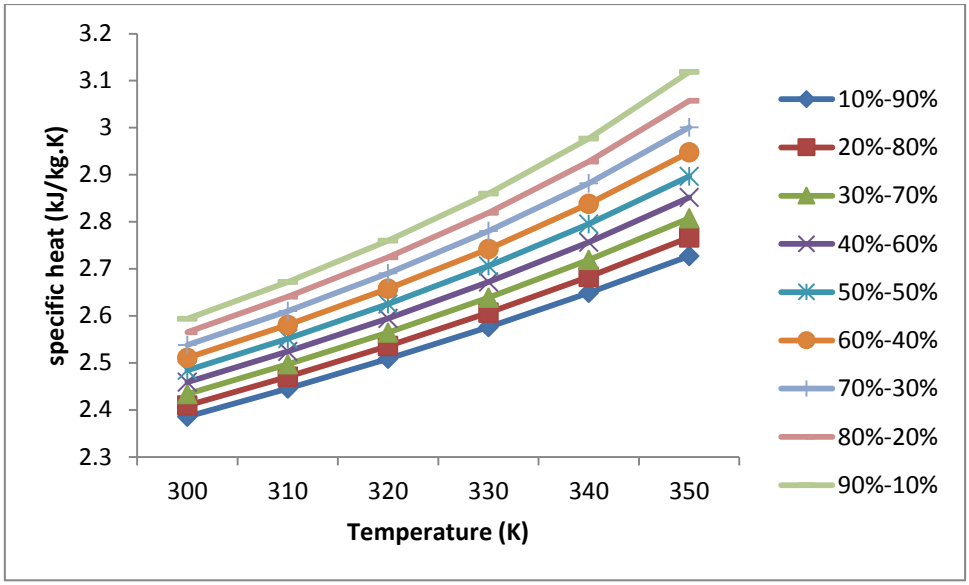

Figure 29 Specific Heat as a function of Temperature at 7MPa

Figure 29 represents specific heat as a function of temperature constant pressure 7MPa. Moreover, it is observed that as specific heat increases with increase in temperature in a mixed refrigerant for all 9 cases.

8.2 CFD Analysis of Mixed Refrigerant at Different Inlet Temperature

In the present research, pressure drop, heat transfer, Reynolds number and Nusselt number are calculated for a mixed refrigerant. The analysis are done on mixed refrigerants, results are evaluated at pressure 3MPa, and different inlet temperatures such as 300 to 330K with the effect of different mass flow rates 0.05 to 0.1 kg /s at different compositions. Moreover, it was observed that as the mass flow rate increase (kg/s) pressure drop, heat transfer, Reynolds number and Nusselt number increases at different compositions.

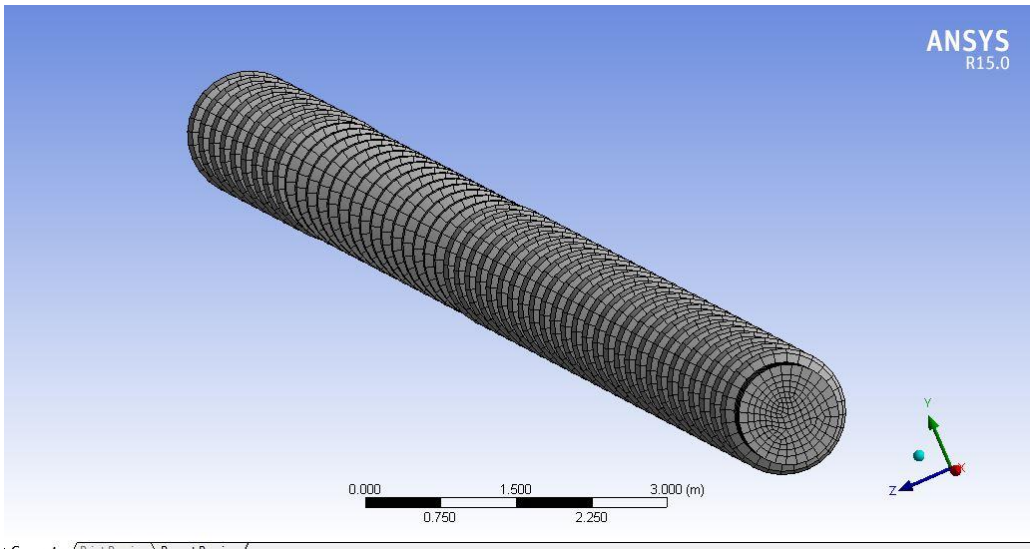

Figure 30 Mesh analysis of compressor

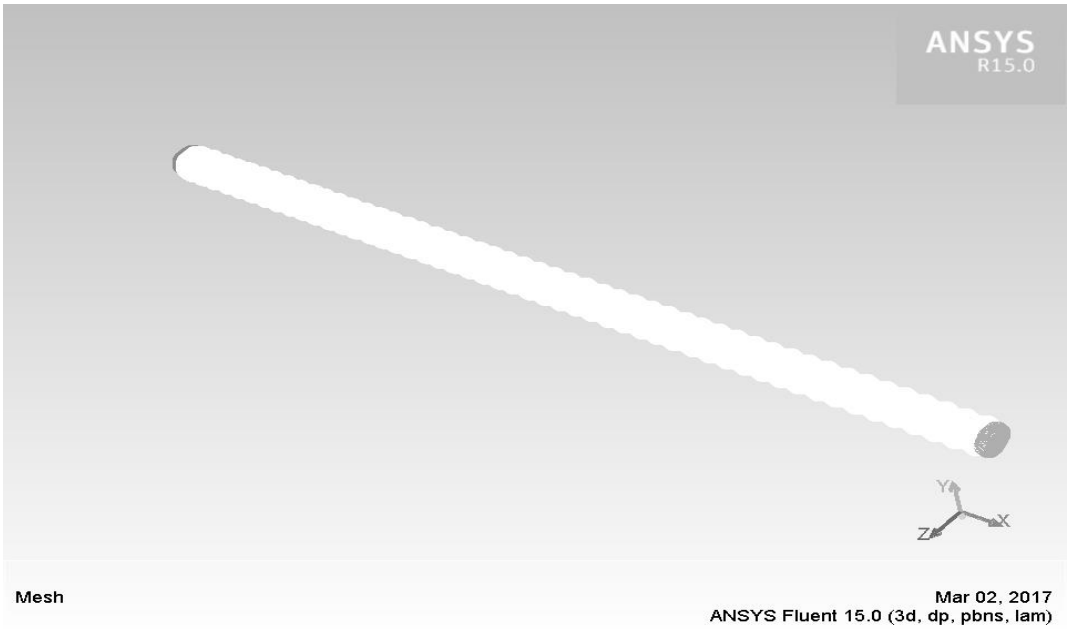

Figure 31 represents stimulated results for mixed refrigerant

Figure 31 represents mesh analysis of compressor pipe with dimension of length 1000m and diameter is 0.064m

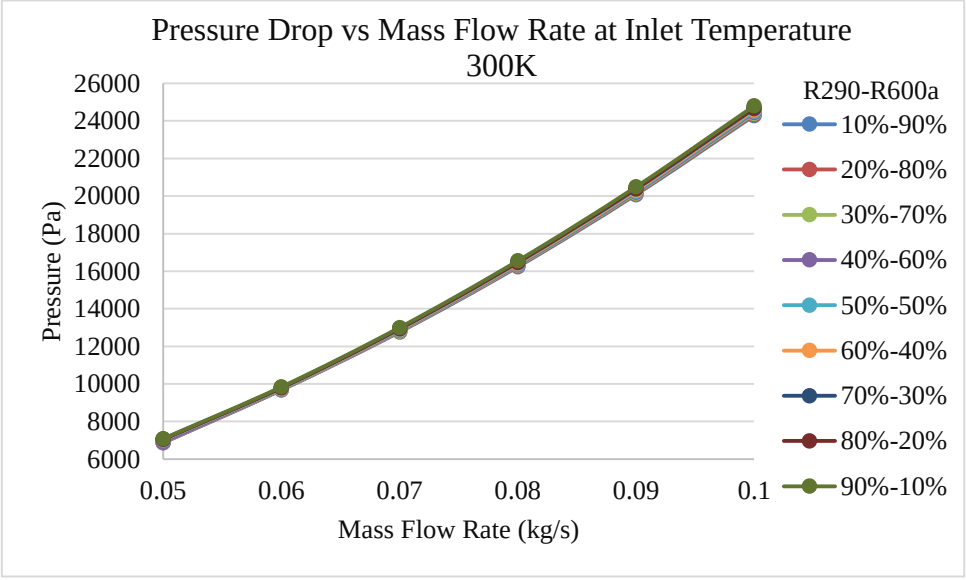

Figure 32 Pressure drop vs Mass flow rate at 300K

Figure 32 shows that variation of pressure drop with respect to different mass flow rate at 300K inlet temperature and different compositions of a mixed refrigerant. Moreover, it was observed that as the mass flow rate increases and pressure drop is increases exponentially.

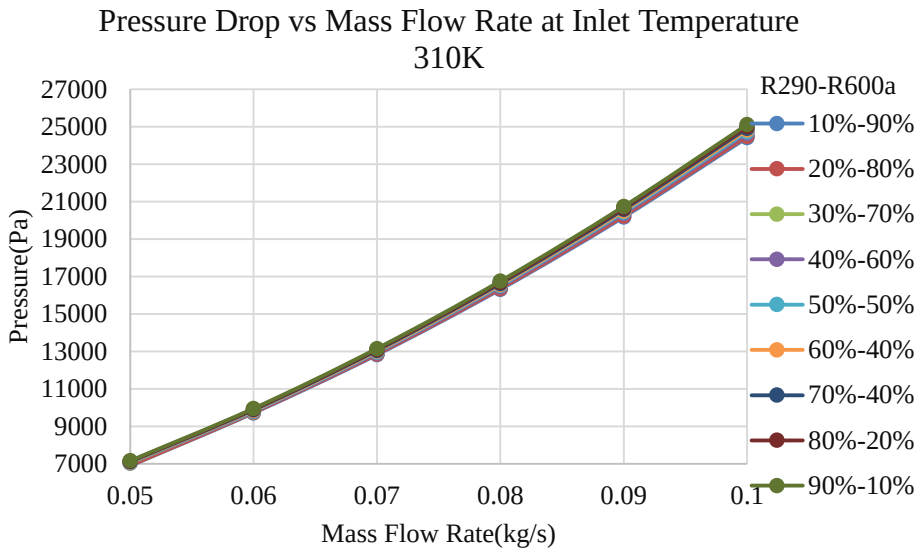

Figure 33 Pressure drop vs Mass flow rate at 310K

Figure 33 shows that variation of pressure drop with respect to different mass flow rate at 310K inlet temperature and different compositions of a mixed refrigerant. Moreover, it was observed that as the mass flow rate increases and pressure drop is increases exponentially.

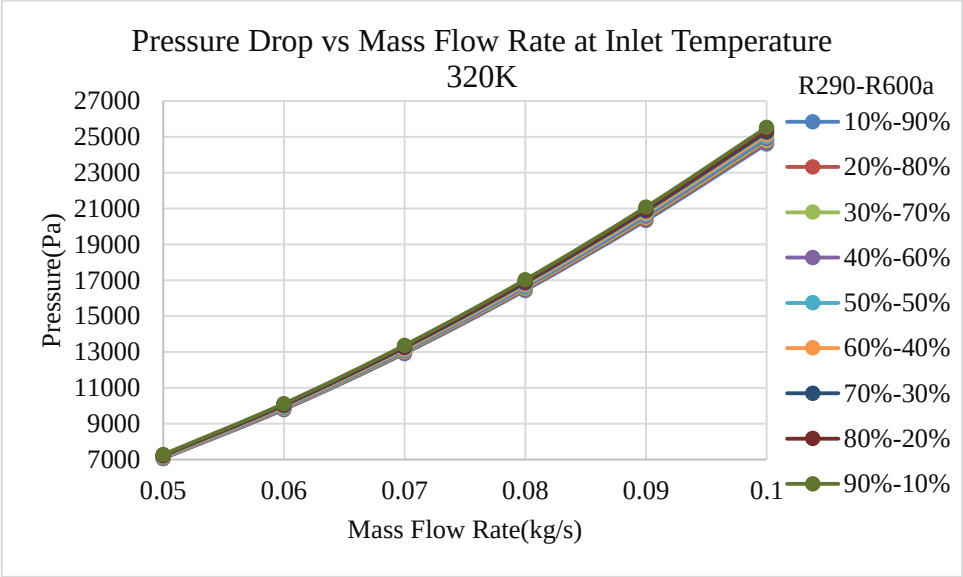

Figure 34 Pressure drop vs Mass flow rate at 320K

Figure 34 shows that variation of pressure drop with respect to different mass flow rate at 320K inlet temperature and different compositions of a mixed refrigerant. Moreover, it was observed that as the mass flow rate increases and pressure drop is increases exponentially.

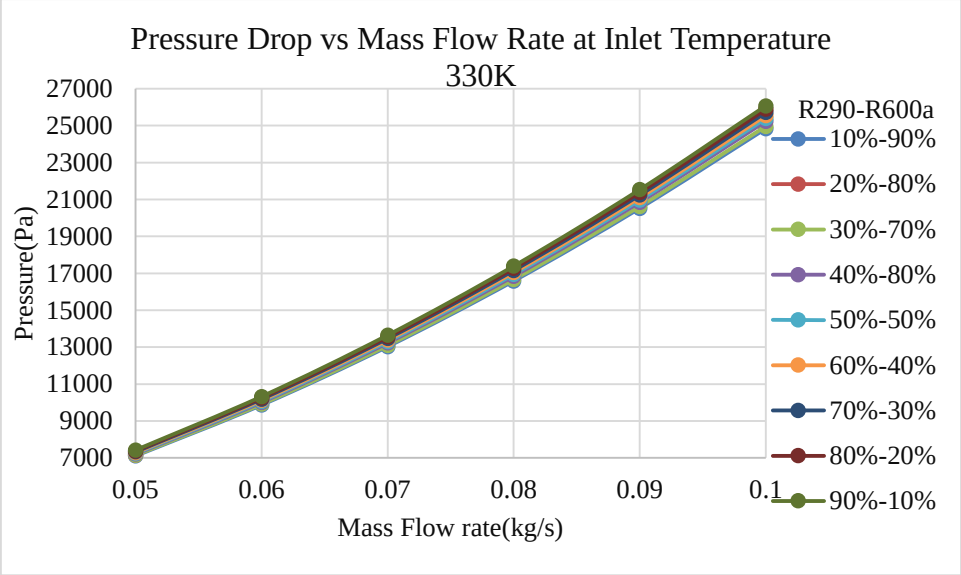

Figure 35 Pressure drop vs Mass flow rate at 330K

Figure 35 shows that variation of pressure drop with respect to different mass flow rate at 330K inlet temperature and different compositions of a mixed refrigerant. Moreover, it was observed, that as the mass flow rate increases and pressure drop is increases exponentially.

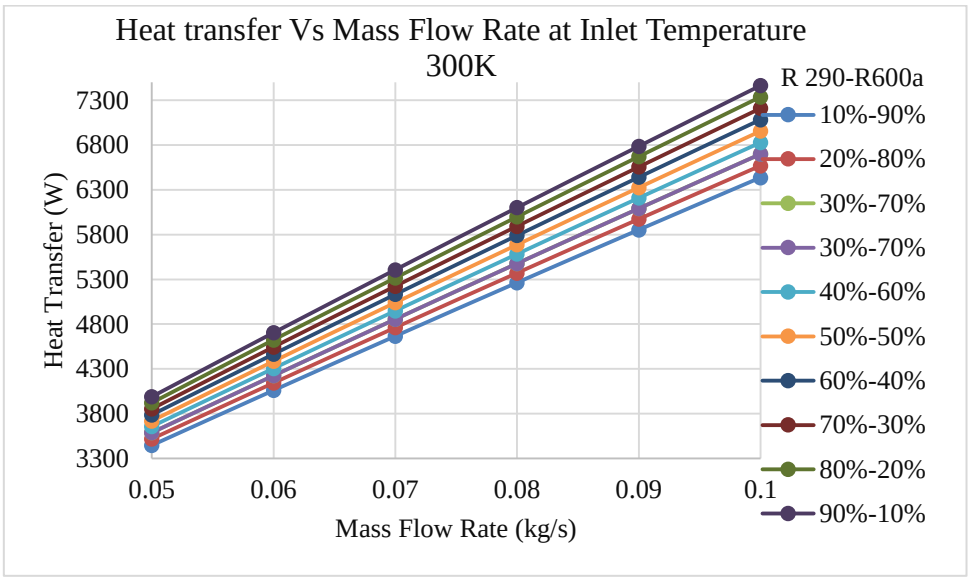

Figure 36 Heat transfer vs Mass flow rate at 300K

Figure 36 shows that variation of heat transfer rate with respect to different mass flow rate at 300K inlet temperature and different compositions of a mixed refrigerant. Moreover, it was observed that as the mass flow rate increases and pressure drop is increases linearly.

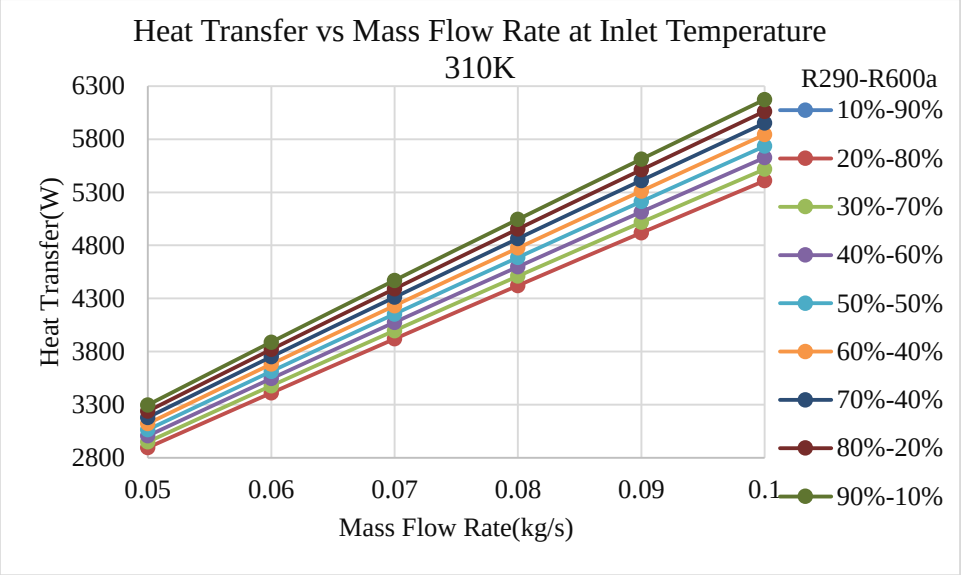

Figure 37 Heat transfer vs Mass flow rate at 310K

Figure 37 shows that variation of heat transfer rate with respect to different mass flow rate at 310K inlet temperature and different compositions of a mixed refrigerant. Moreover, it was observed, that as the mass flow rate increases and pressure drop is increases linearly

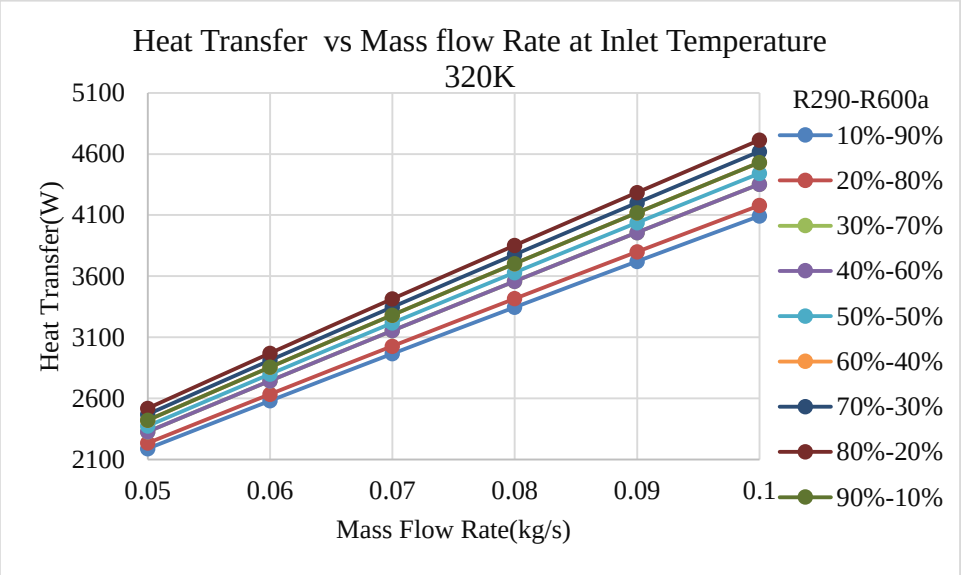

Figure 38 Heat transfer vs Mass flow rate at 320K

Figure 38 shows that variation of heat transfer rate with respect to different mass flow rate at 320K inlet temperature and different compositions of a mixed refrigerant. Moreover, it was observed, that as the mass flow rate increases and pressure drop is increases linearly

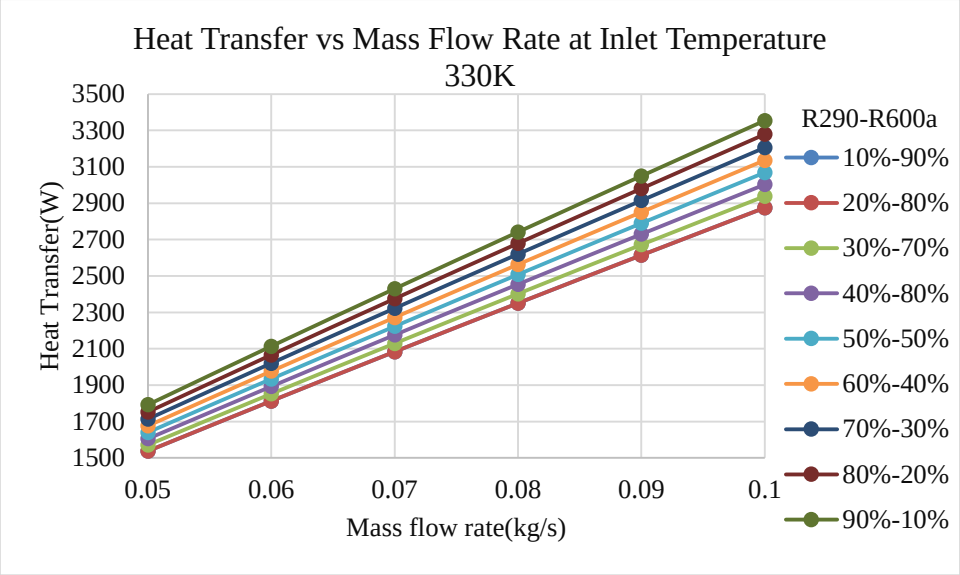

Figure 39 Heat transfer vs Mass flow rate at 330K

Figure 39 shows that variation of heat transfer rate with respect to different mass flow rate at 300K inlet temperature and different compositions of a mixed refrigerant. Moreover, it was observed, that as the mass flow rate increases and pressure drop is increases linearly

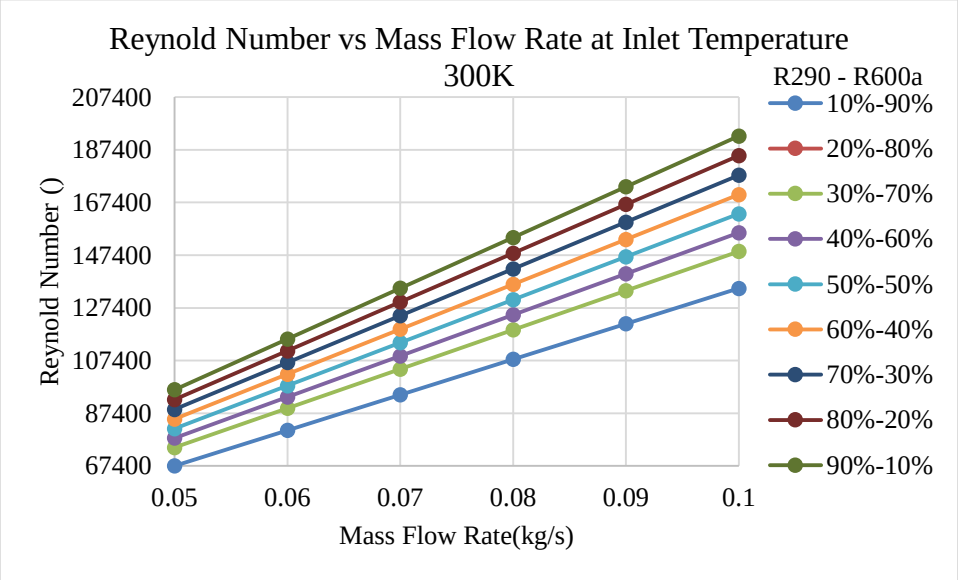

Figure 40 Reynold number vs Mass flow rate at 300K

Figure 40 shows that variation of Reynold number with respect to different mass flow rate at 300K inlet temperature and different compositions of a mixed refrigerant. Moreover, it was observed, that as the mass flow rate increases and pressure drop is increases linearly

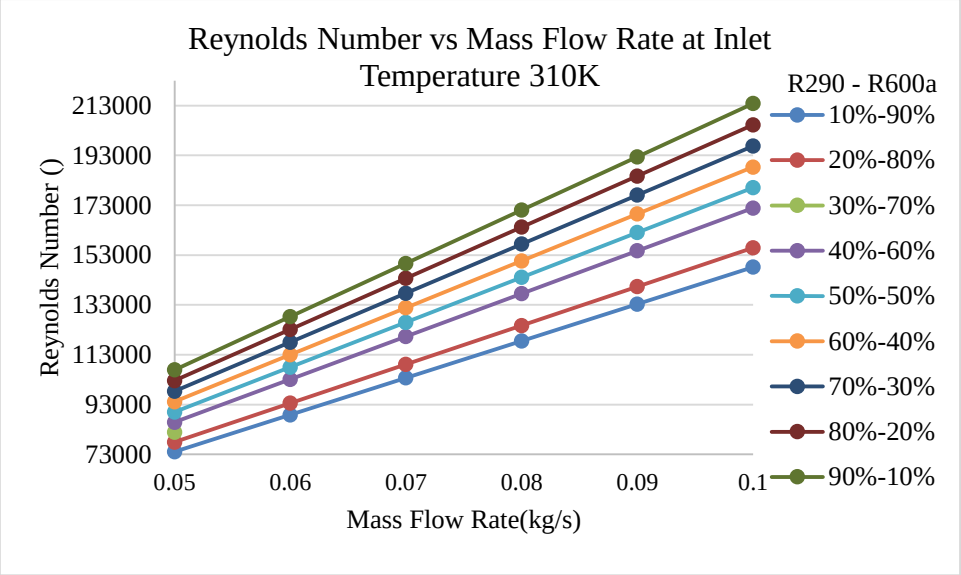

Figure 41 Reynold number vs Mass flow rate at 310K

Figure 41 shows that variation of Reynold number with respect to different mass flow rate at 310K inlet temperature and different compositions of a mixed refrigerant. Moreover, it was observed that as the mass flow rate increases and pressure drop is increases linearly

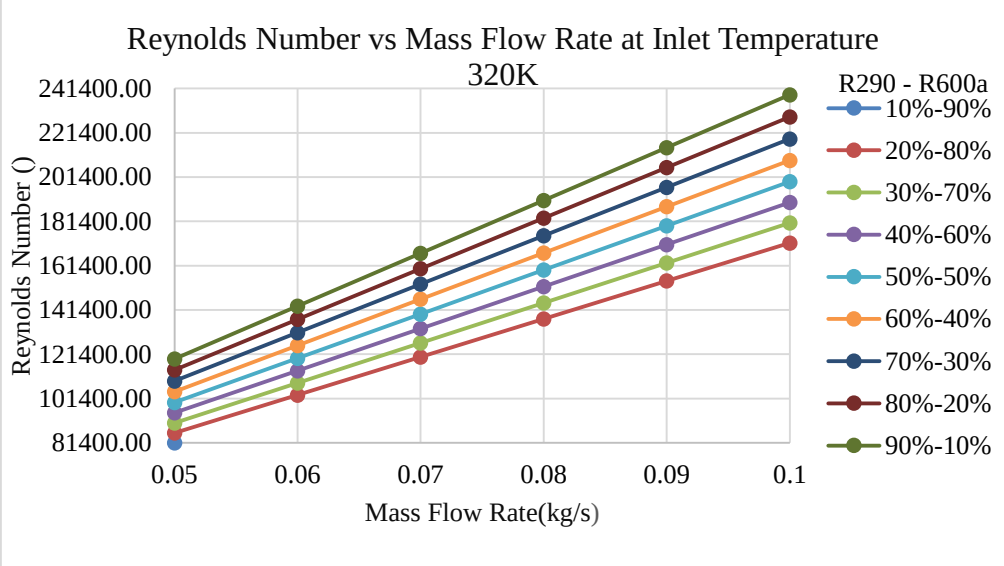

Figure 42 Reynold number vs Mass flow rate at 320K

Figure 42 shows that variation of Reynold number with respect to different mass flow rate at 320K inlet temperature and different compositions of a mixed refrigerant. Moreover, it was observed that as the mass flow rate increases and pressure drop is increases linearly

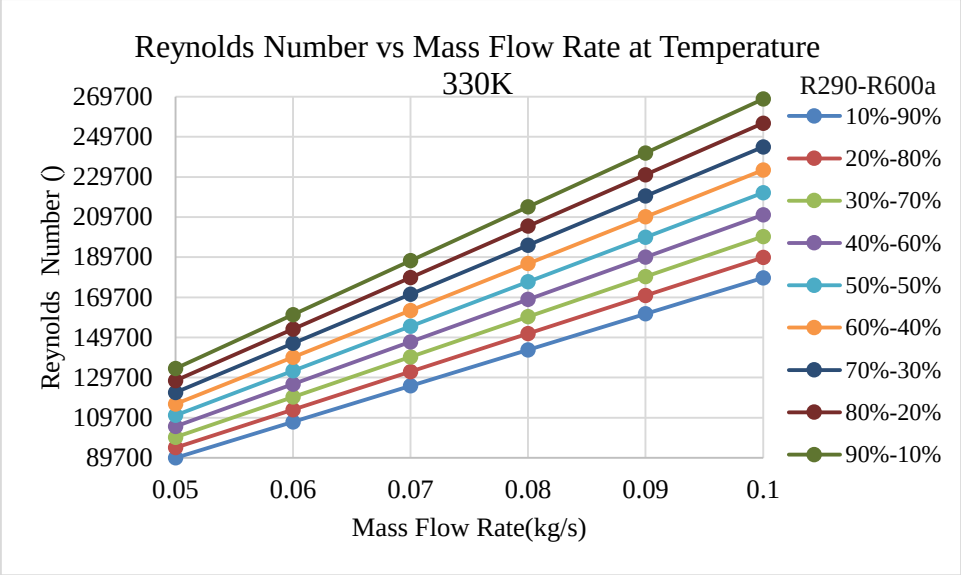

Figure 43 Reynold number vs Mass flow rate at 330K

Figure 43 shows that variation of Reynold number with respect to different mass flow rate at 330K inlet temperature and different compositions of a mixed refrigerant. Moreover, it was observed that as the mass flow rate increases and pressure drop is increases linearly

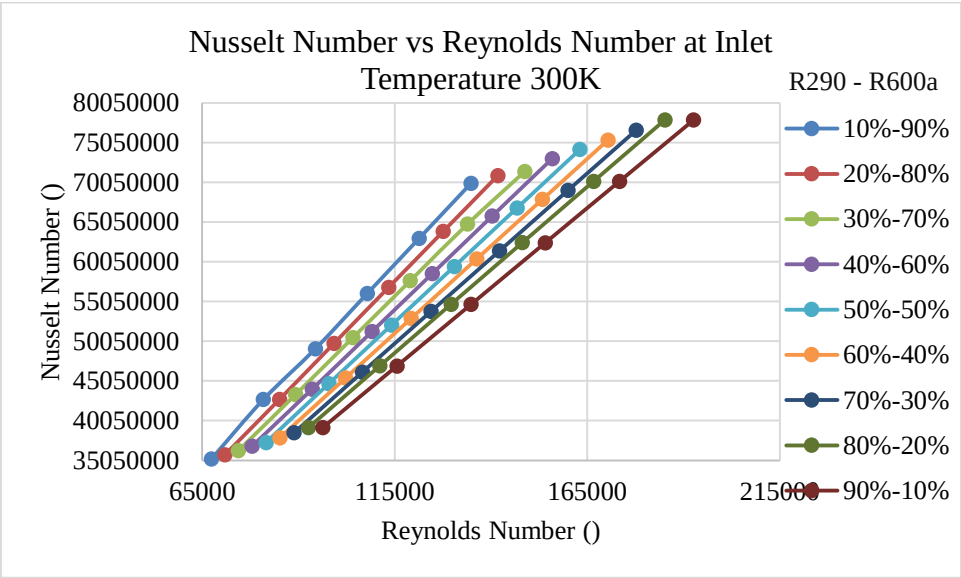

Figure 44Nusselt number vs Reynolds number at 300K

Figure 44 shows that variation of Nusselt number with respect to Reynolds number at 300K inlet temperature and different compositions of a mixed refrigerant. Moreover, it was observed that as the mass flow rate increases and pressure drop is increases linearly

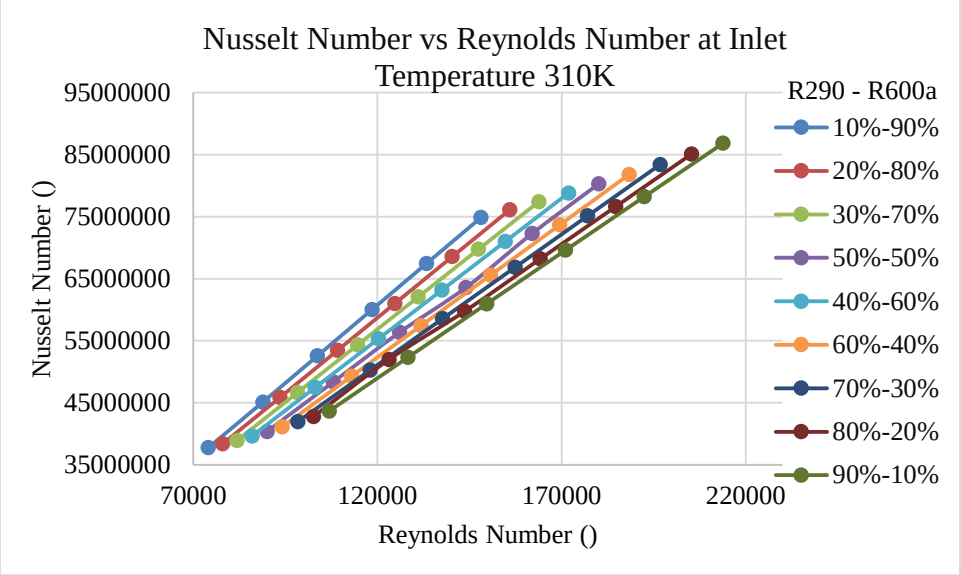

Figure 45 Nusselt number vs Reynolds number at 310K

Figure 45 shows that variation of Nusselt number with respect to Reynolds number at 310K inlet temperature and different compositions of a mixed refrigerant. Moreover, it was observed that as the mass flow rate increases and pressure drop is increases linearly

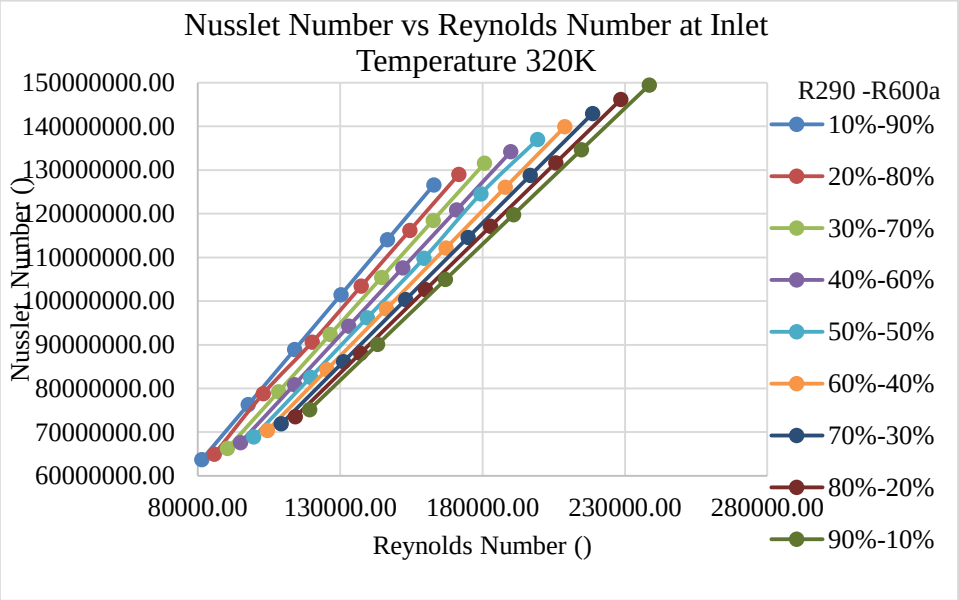

Figure 46 Nusselt number vs Reynolds number at 320K

Figure 46 shows that variation of Nusselt number with respect to Reynolds number at 320K inlet temperature and different compositions of a mixed refrigerant. Moreover, it was observed that as the mass flow rate increases and pressure drop is increases linearly

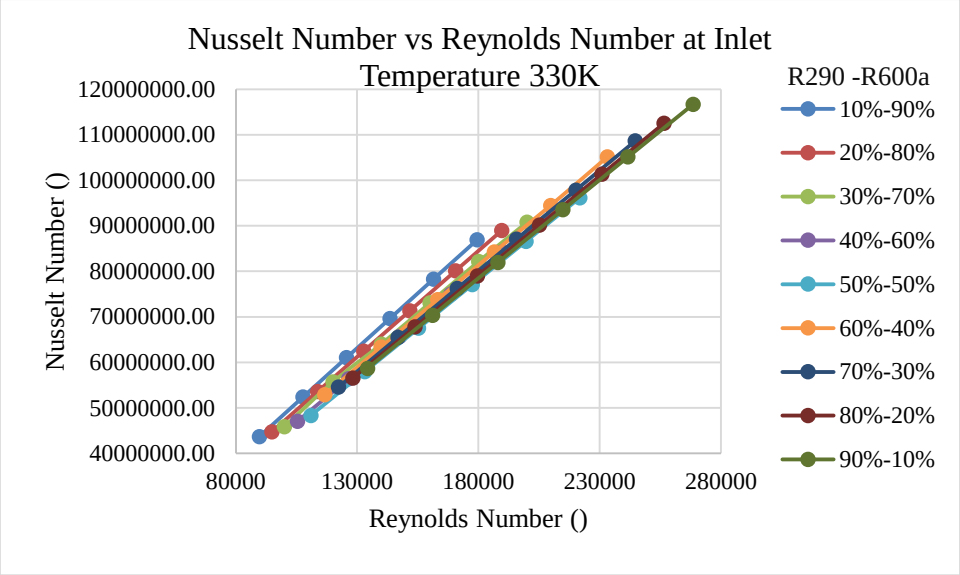

Figure 47 Nusselt number vs Reynolds number at 330K

Figure 47 shows that variation of Nusselt number with respect to Reynolds number at 330K inlet temperature and different compositions of a mixed refrigerant. Moreover, it was observed that as the mass flow rate increases and pressure drop is increases linearly

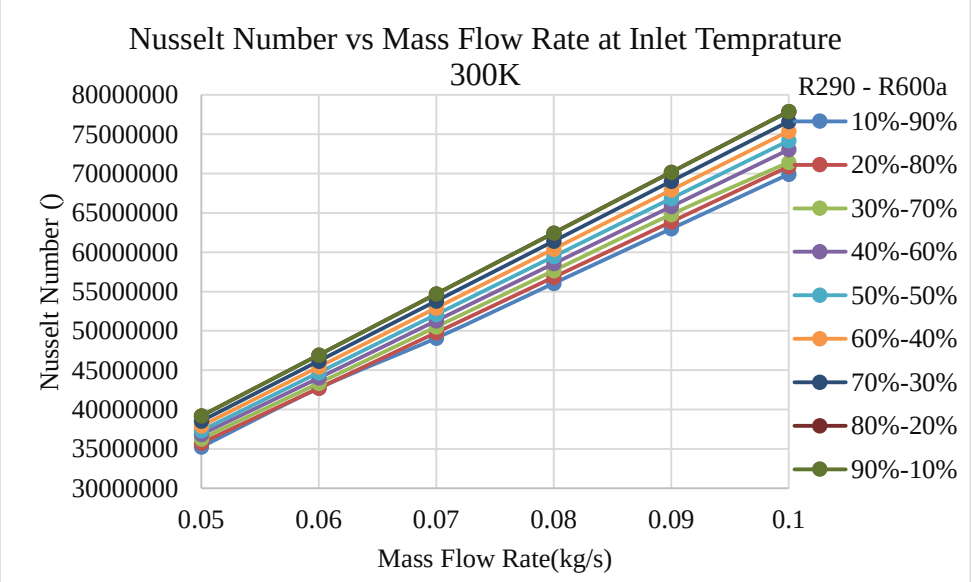

Figure 48 Nusselt number vs Mass flow rate at 300K

Figure 48 shows that variation of Nusselt number with respect to Mass flow rate at 300K inlet temperature and different compositions of a mixed refrigerant. Moreover, it was observed, that as the mass flow rate increases and pressure drop is increases linearly

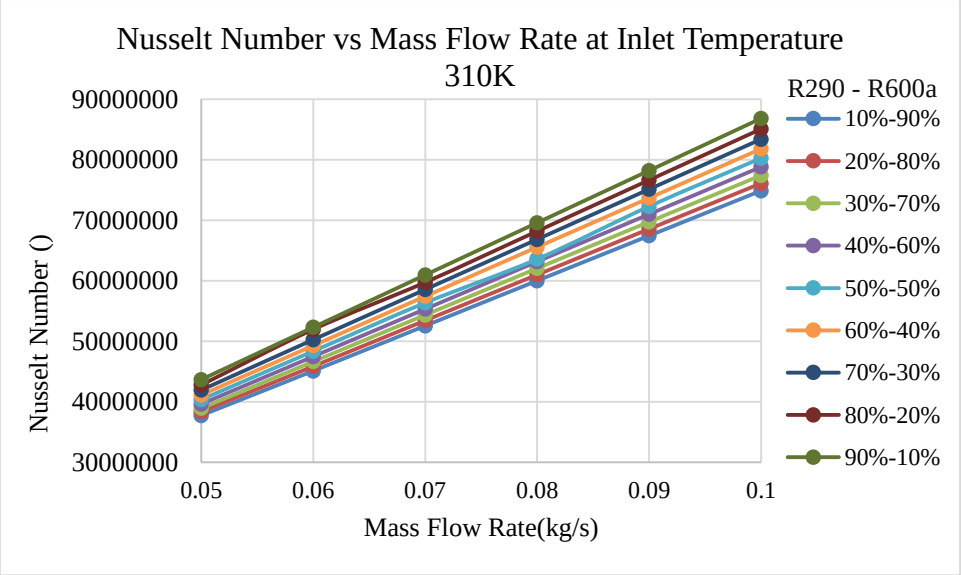

Figure 49 Nusselt number vs Mass flow rate at 310K

Figure 49 shows that variation of Nusselt number with respect to Mass flow rate at 310K inlet temperature and different compositions of a mixed refrigerant. Moreover, it was observed that as the mass flow rate increases and pressure drop is increases linearly

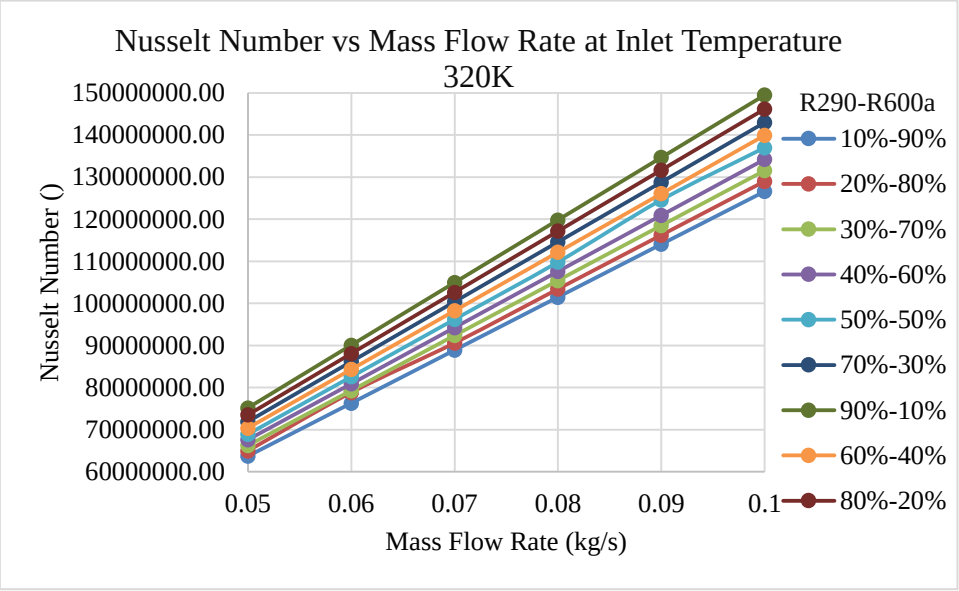

Figure 50 Nusselt number vs Mass flow rate at 320K

Figure 50 shows that variation of Nusselt number with respect to Mass flow rate at 320K inlet temperature and different compositions of a mixed refrigerant. Moreover, it was observed, that as the mass flow rate increases and pressure drop is increases linearly

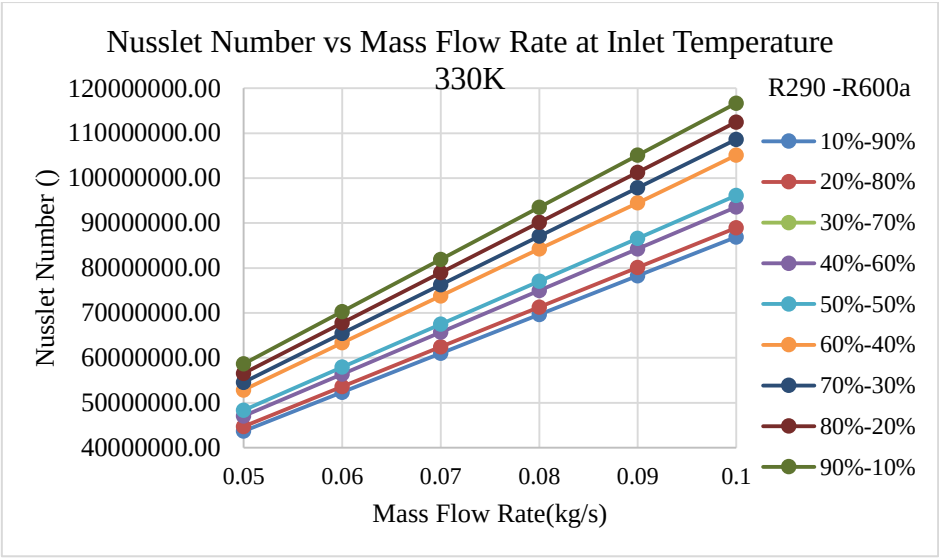

Figure 51 Nusselt number vs Mass flow rate at 330K

Figure 51 shows that variation of Nusselt number with respect to Mass flow rate at 330K inlet temperature and different compositions of a mixed refrigerant. Moreover, it was observed that as the mass flow rate increases and pressure drop is increases linearly

8.3 Thermophysical Properties of Mixed refrigerant with addition of CuO Nano-Particle at pressure 3MPa

- **Effective Thermal Conductivity**

At Pressure 3MPa

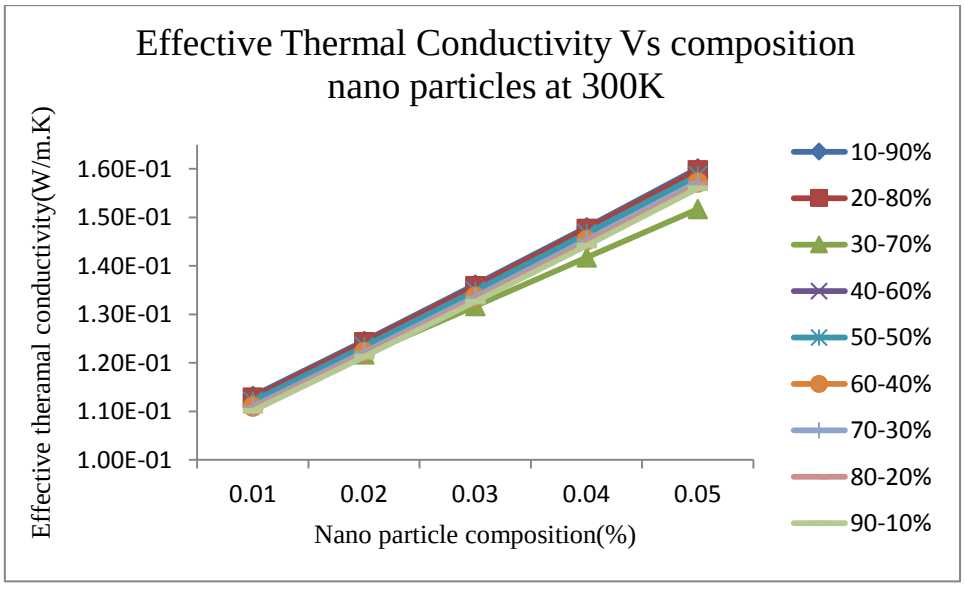

Figure 52 Effective Thermal conductivity w.r.t Volume concentration of nanoparticles

Figure 52 shows the variation of the effective thermal conductivity as a function of volume concentration of Nano-particles. It can be seen that the volume concentration of Nano particles there is an increase in the effective thermal conductivity of the mixed refrigerant for all 9 cases.

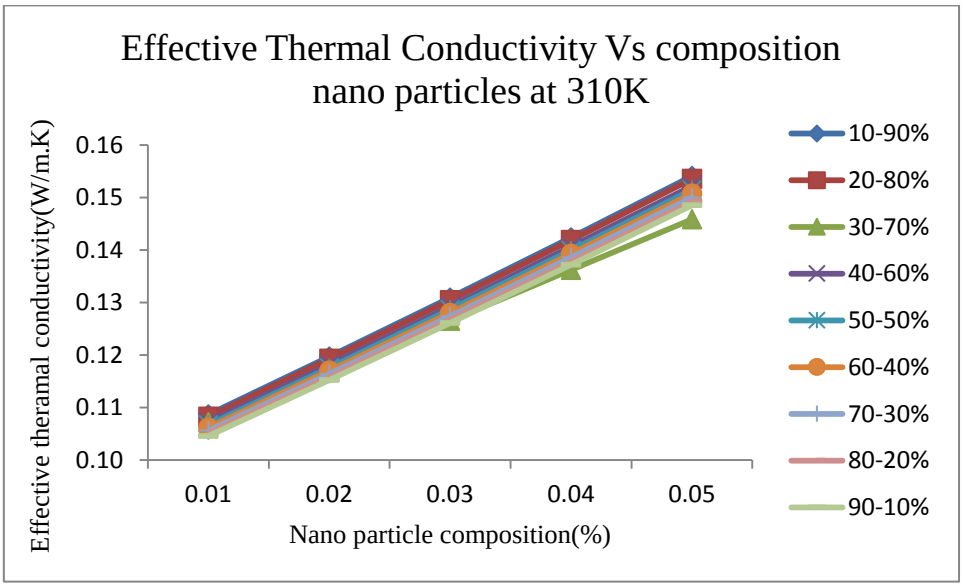

Figure 53 Effective Thermal conductivities w.r.t Volume concentration of nanoparticles

Figure 53 shows the variation of the effective thermal conductivity as a function of volume concentration of Nano-particles. It can be observed that as the volume concentration of Nano particles there is an increase in the effective thermal conductivity of the mixed refrigerant for all 9 cases at constant temperature.

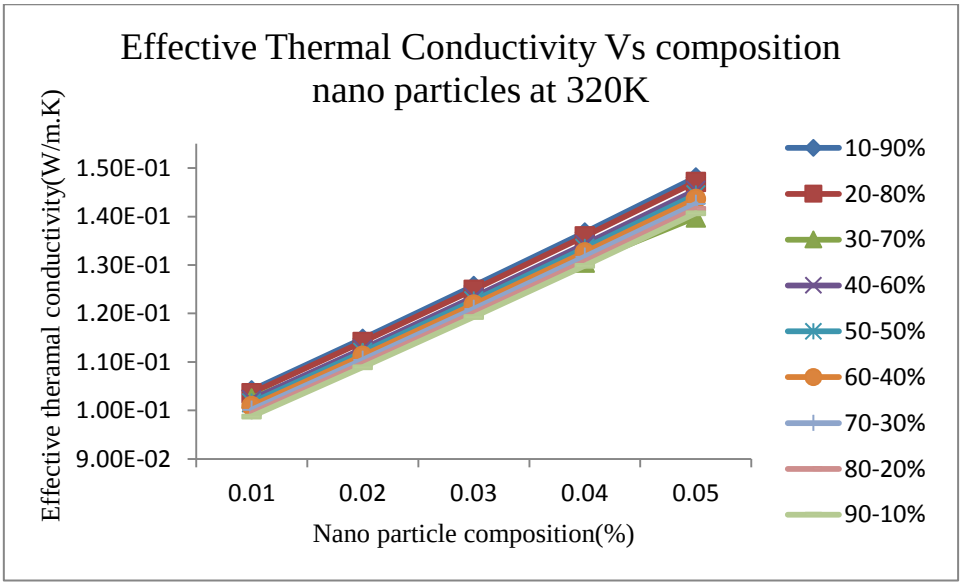

Figure 54 Effective Thermal conductivities vs Volume concentration of nanoparticles

Figure 54 reveals that the comparison of the effective thermal conductivity with volumetric concentration of nanoparticle at constant temperature. It can be observed that with the increase in volume concentration of nanoparticles there is an increase effective thermal conductivity.

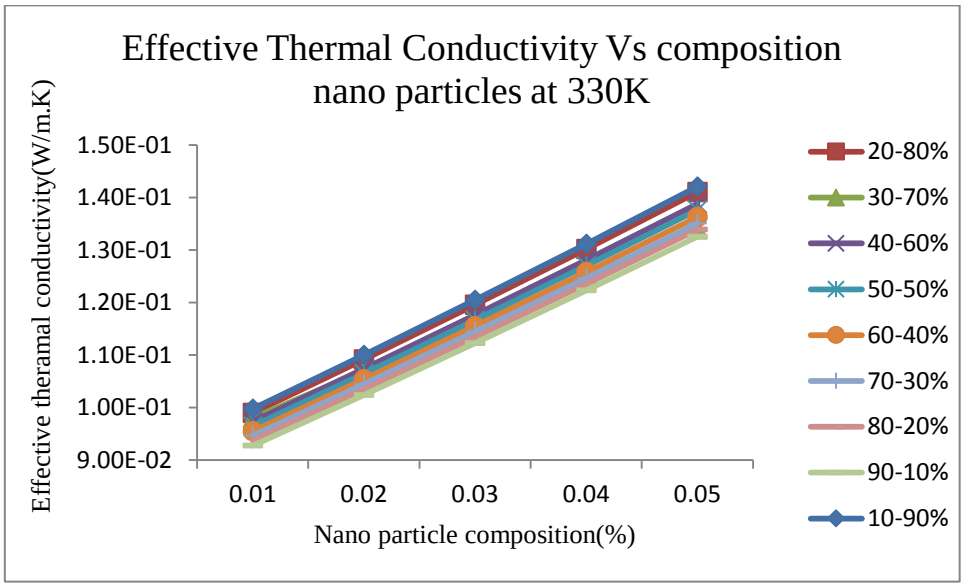

Figure 55 Effective Thermal conductivities vs Volume concentration of nanoparticles

Figure 55 represents that effective thermal conductivity as a function of volume concentration of the nanoparticle. It reveals that the volume concentration of nanoparticle increases, there is an increase effective thermal conductivity for a mixed refrigerant of all the 9 cases

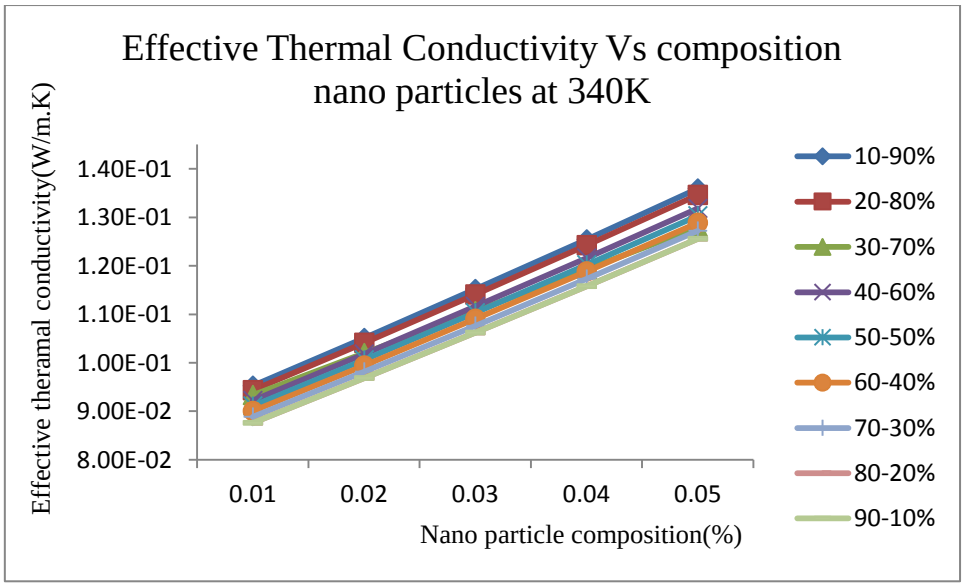

Figure 56 Effective Thermal conductivities w.r.t Volume concentration of nanoparticles

Figure 56 reveals that the volume concentration is a function of the effective thermal conductivity. It is observed that the effective thermal conductivity increases with increase in volume concentration of the nanoparticle at constant temperature for a mixed refrigerant for all compositions.

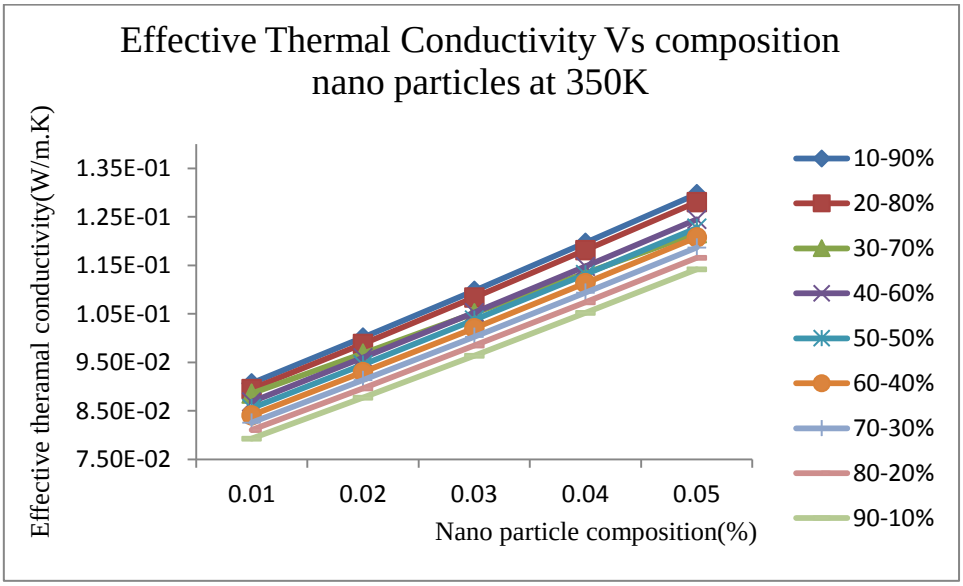

Figure 57 Effective Thermal conductivities w.r.t volume concentration of nanoparticles

Figure 57 shows that at constant temperature variation of effective thermal conductivity w.r.t volume concentration of nanoparticle. Moreover, it is observed that as the volume concentration increases effective thermal conductivity is also increases for all 9 cases.

- **Effective Viscosity**

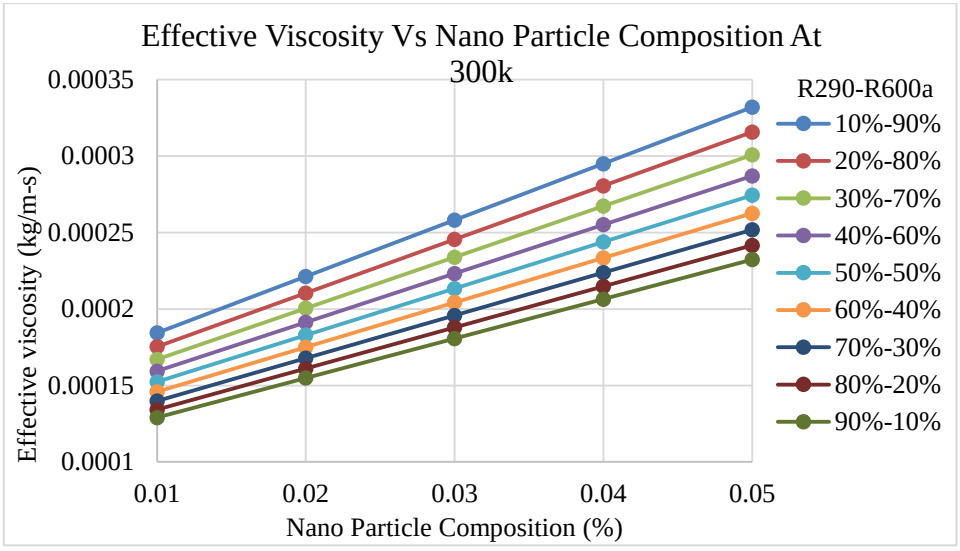

Figure 58 Effective viscosity w.r.t volume concentration of nanoparticles

Figure 58 shows the variation of the effective viscosity as a function of volume concentration of Nano-particles. It can be seen that the volume concentration of Nano particles there is an increase in the effective thermal conductivity of the mixed refrigerant for all 9 cases.

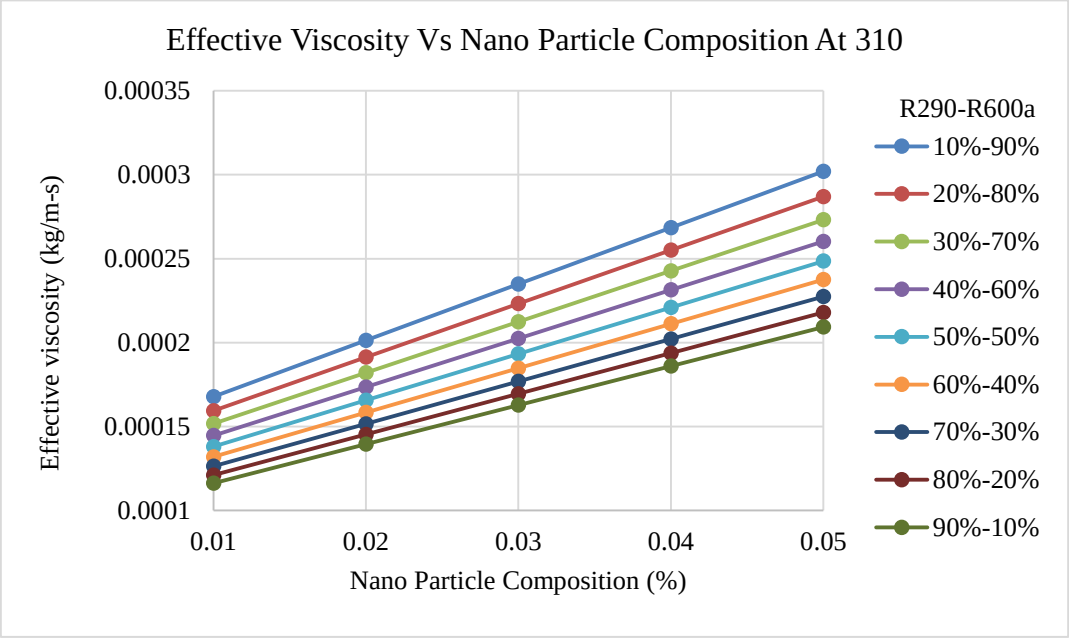

Figure 59 Effective viscosity w.r.t volume concentration of nanoparticles.

Figure 59 represents that effective viscosity as a function of volume concentration of the nanoparticle. It reveals that the volume concentration of nanoparticle increases, there is an increase effective thermal conductivity for a mixed refrigerant of all the 9 cases

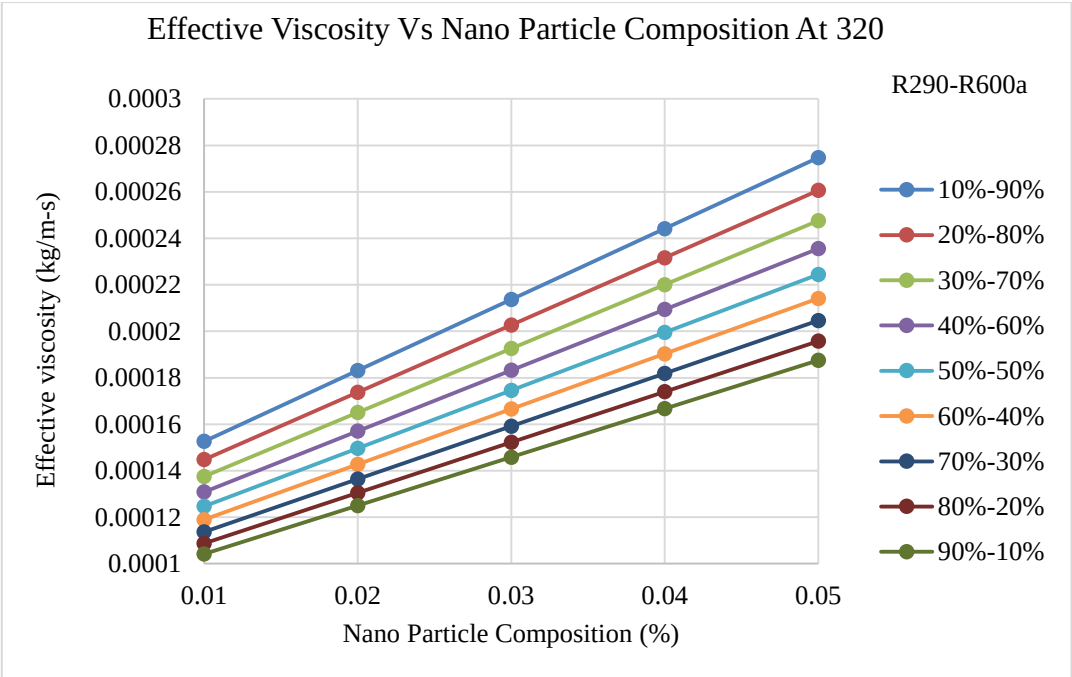

Figure 60 Effective viscosity w.r.t volume concentration of nanoparticles.

Figure 60 represents that effective viscosity as a function of volume concentration of the nanoparticle. It reveals that the volume concentration of nanoparticle increases, there is an increase effective thermal conductivity for a mixed refrigerant of all the 9 cases

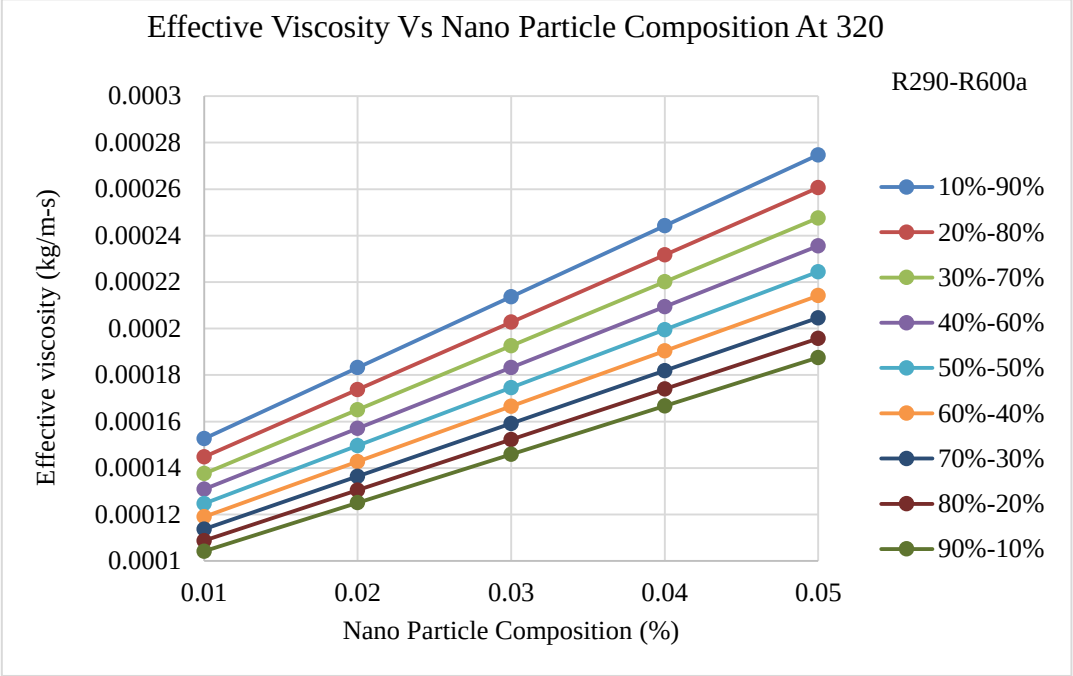

Figure 61 Effective viscosity w.r.t volume concentration of nanoparticles.

Figure 61 reveals that the volume concentration is a function of the effective viscosity. It is observed that the effective thermal conductivity increases with increase in volume concentration of the nanoparticle at constant temperature for a mixed refrigerant for all compositions.

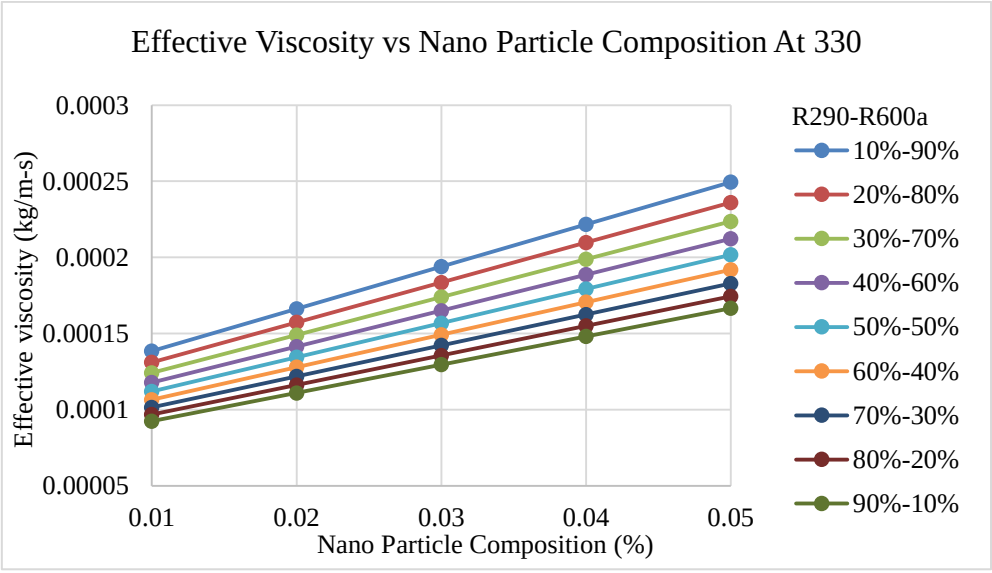

Figure 62 Effective viscosity w.r.t volume concentration of nanoparticles.

Figure 62 shows that at constant temperature variation of effective viscosity w.r.t volume concentration of nanoparticle. Moreover, it is observed that as the volume concentration increases effective thermal conductivity is also increases for all 9 cases.

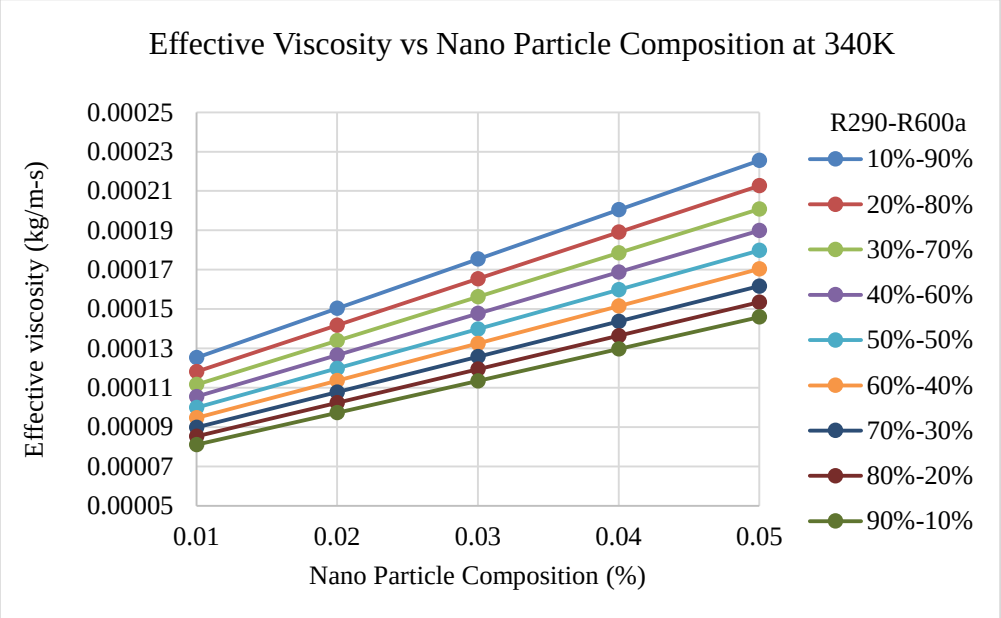

Figure 63 Effective viscosity w.r.t volume concentration of nanoparticles.

Figure 63 shows the variation of the effective viscosity as a function of volume concentration of Nano-particles. It can be observed that as the volume concentration of Nano particles there is an increase in the effective viscosity of the mixed refrigerant for all 9 cases at constant temperature.

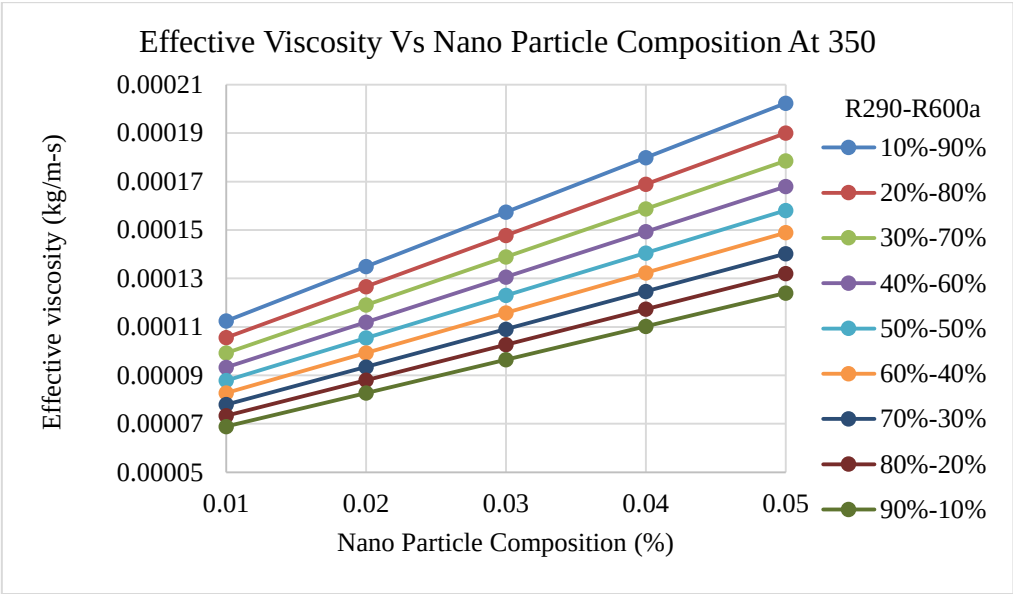

Figure 64 Effective viscosity w.r.t volume concentration of nanoparticles.

Figure 64 shows the variation of the effective viscosity as a function of volume concentration of Nano-particles. It can be observed that as the volume concentration of Nano particles there is an increase in the effective viscosity of the mixed refrigerant for all 9 cases at constant temperature.

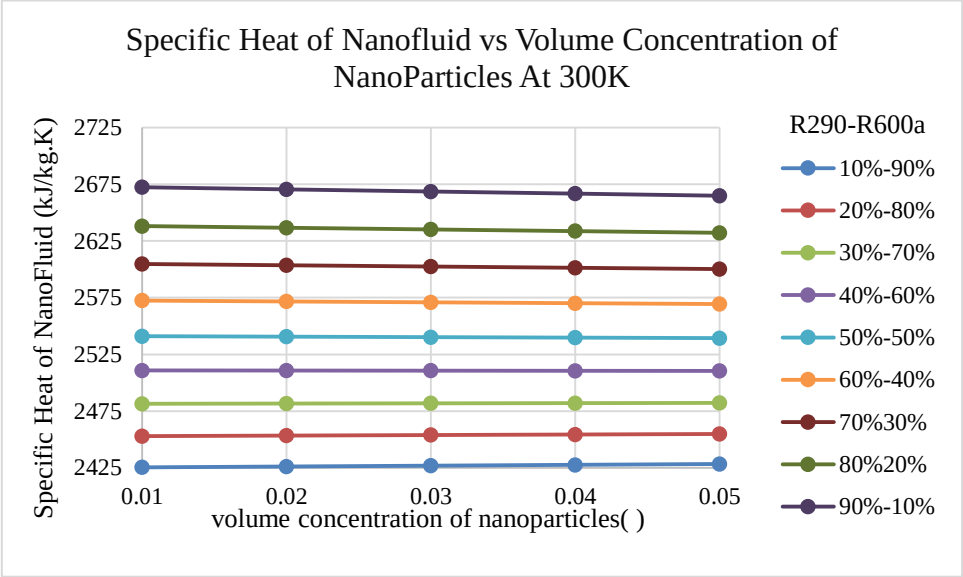

Figure 65 Effective specific heat w.r.t volume concentration of nanoparticles.

Figure 65 shows the variation of effective specific heat as a function volume concentration of Nano-particle at pressure 3MPa. Moreover, it is also observed that as the effective specific heat decrease with increase in volume concentration of Nano-Particle at pressure 3MPa for a mixed refrigeration at different compositions at 300K

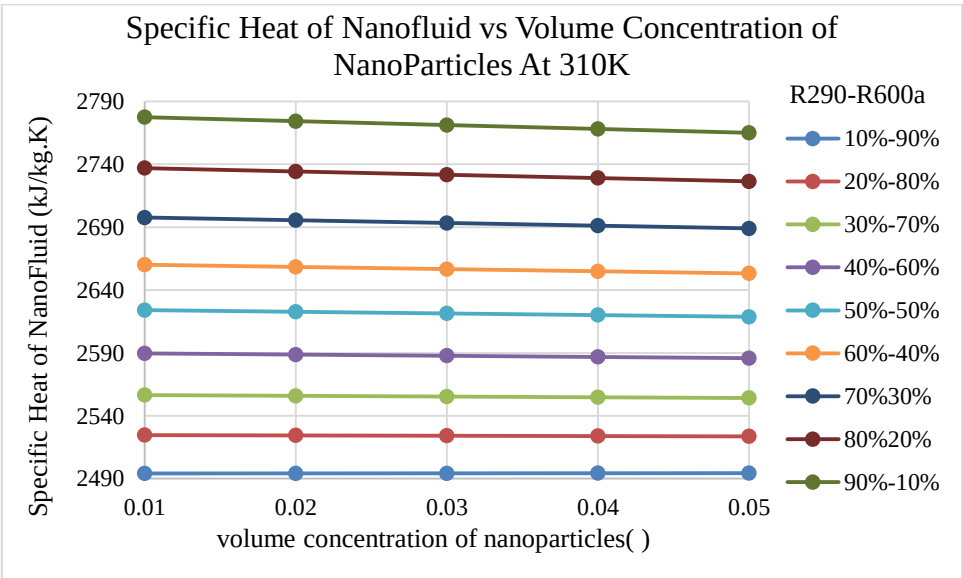

Figure 66 Effective specific heat w.r.t volume concentration of nanoparticles.

Figure 66 shows the variation of effective specific heat as a function volume concentration of Nano-particle at pressure 3MPa. Moreover, it is also observed that as the effective specific heat decrease with increase in volume concentration of Nano-Particle at pressure 3MPa for a mixed refrigeration at different compositions

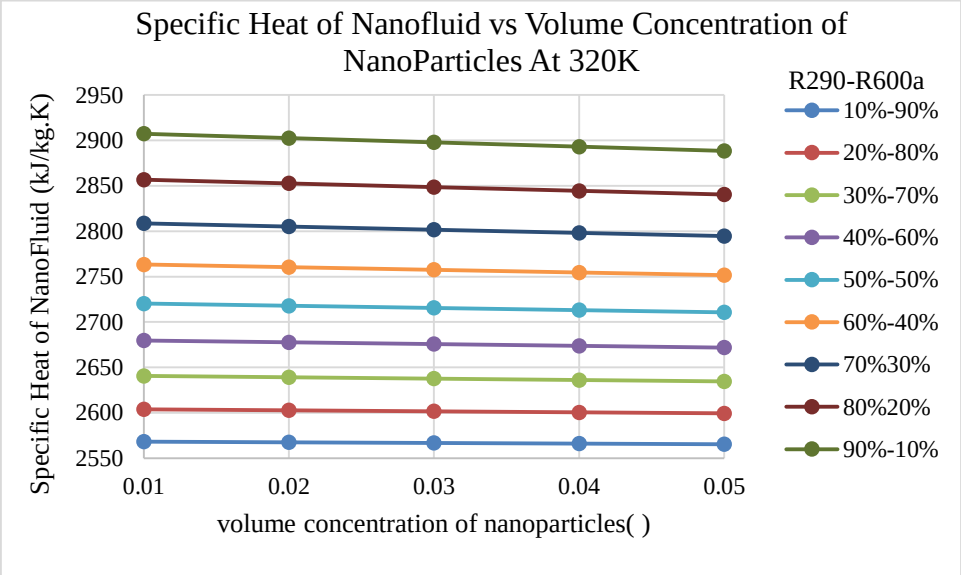

Figure 67 Effective specific heat w.r.t volume concentration of nanoparticles.

Figure 67 shows the variation of effective specific heat as a function volume concentration of Nano-particle at pressure 3MPa. Moreover, it is also observed that as the effective specific heat decrease with increase in volume concentration of Nano-Particle at pressure 3MPa for a mixed refrigeration at different compositions

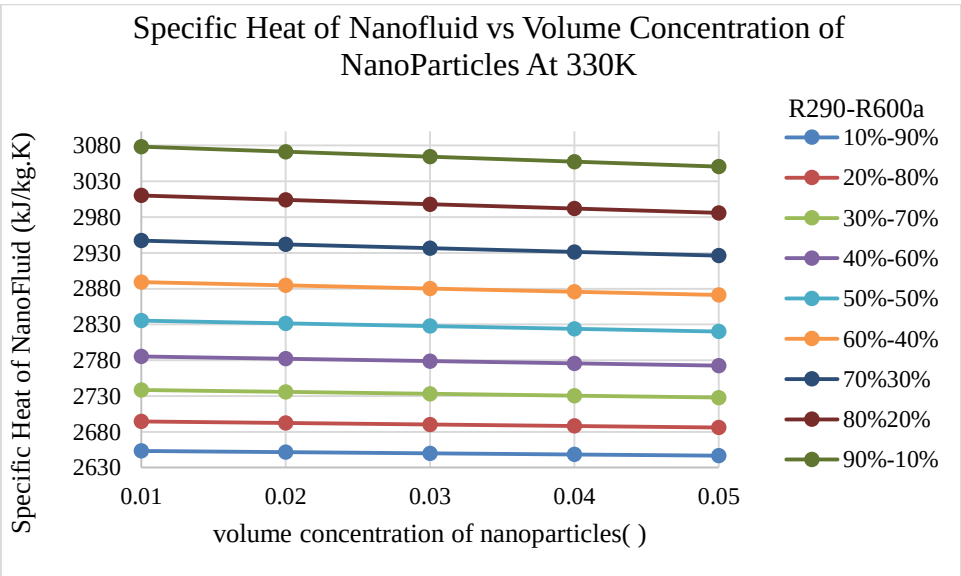

Figure 68 Effective specific heat w.r.t volume concentration of nanoparticles.

Figure 68 shows the variation of effective specific heat as a function volume concentration of Nano-particle at pressure 3MPa. Moreover, it is also observed that as the effective specific heat decreases linearly with increase in volume concentration of Nano-Particle at pressure 3MPa for a mixed refrigeration at different compositions

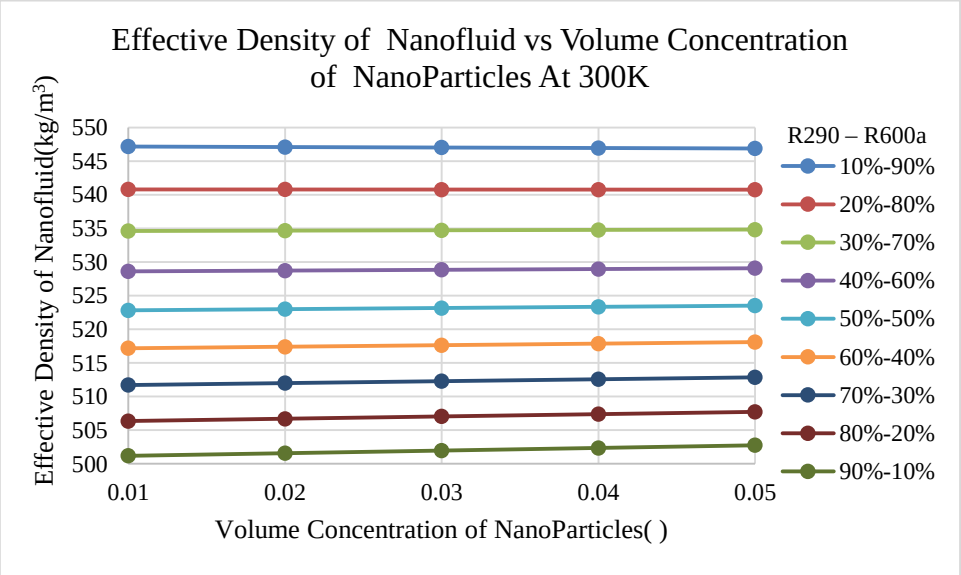

Figure 69 Effective density w.r.t volume concentration of nanoparticles.

Figure 69 shows the variation of effective density as a function volume concentration of Nano-particle at pressure 3MPa. Moreover, it is also observed that as the effective density decreases linearly with increase in volume concentration of Nano-Particle at pressure 3MPa for a mixed refrigeration at different compositions for CuO Nano-Particle.

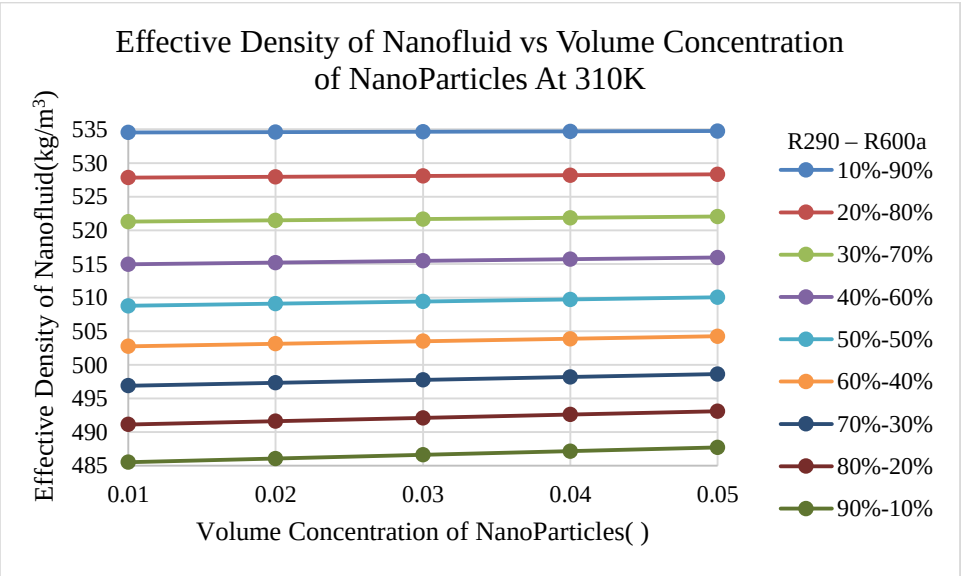

Figure 70 Effective density w.r.t volume concentration of nanoparticles.

Figure 70 shows the variation of effective density as a function volume concentration of Nano-particle at pressure 3MPa. Moreover, it is also observed that as the effective density decreases linearly with increase in volume concentration of Nano-Particle at pressure 3MPa for a mixed refrigeration at different compositions for CuO Nano-Particle.

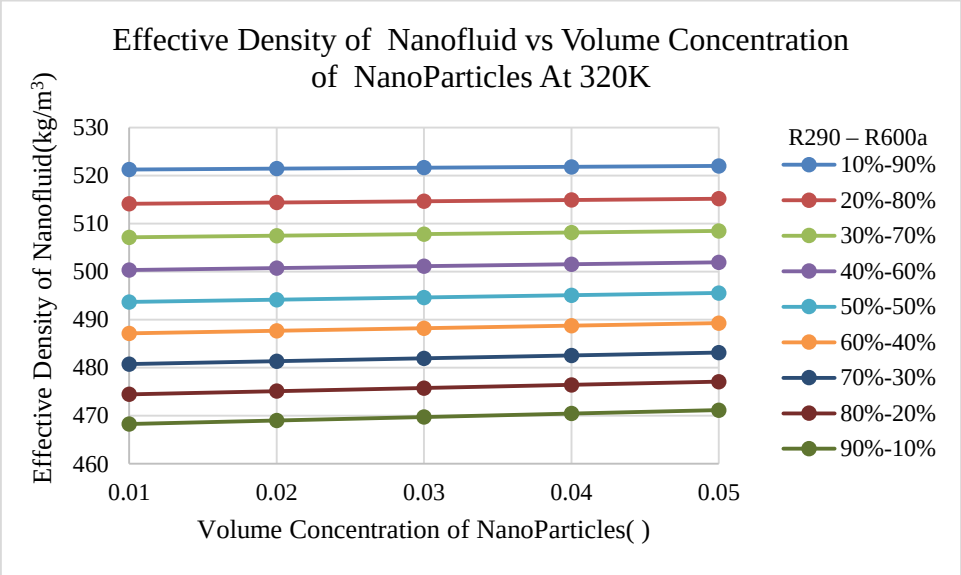

Figure 71 Effective density w.r.t volume concentration of nanoparticles.

Figure 71 shows the variation of effective density as a function volume concentration of Nano-particle at pressure 3MPa. Moreover, it is also observed that as the effective Density decreases linearly with increase in volume concentration of Nano-Particle at pressure 3MPa for a mixed refrigeration at different compositions for CuO Nano-Particle.

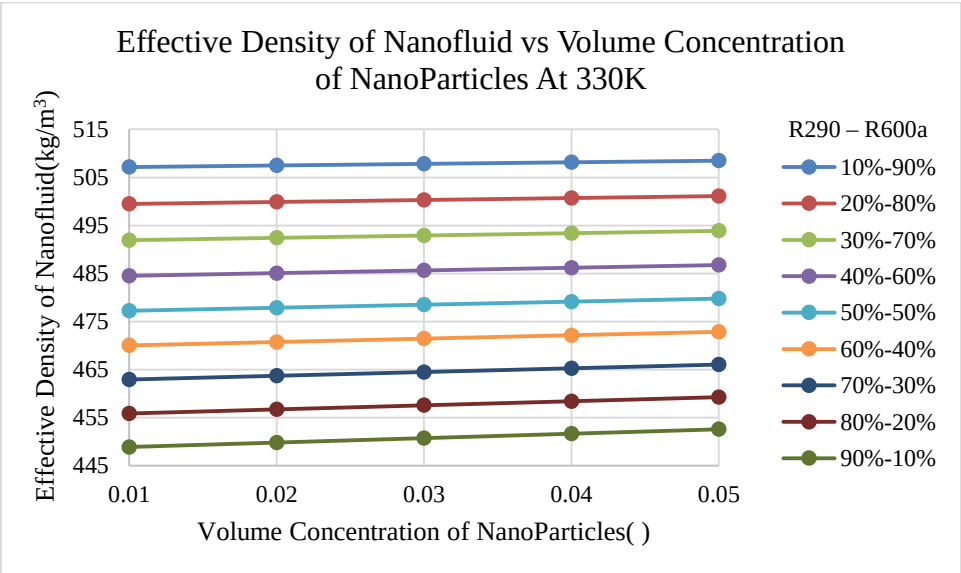

Figure 72 Effective density w.r.t volume concentration of nanoparticles.

Figure 72 shows the variation of effective density as a function volume concentration of Nano-particle at pressure 3MPa. Moreover, it is also observed that as the effective density decrease linearly with increase in volume concentration of Nano-Particle at pressure 3MPa for a mixed refrigeration at different compositions for CuO Nano-Particle.

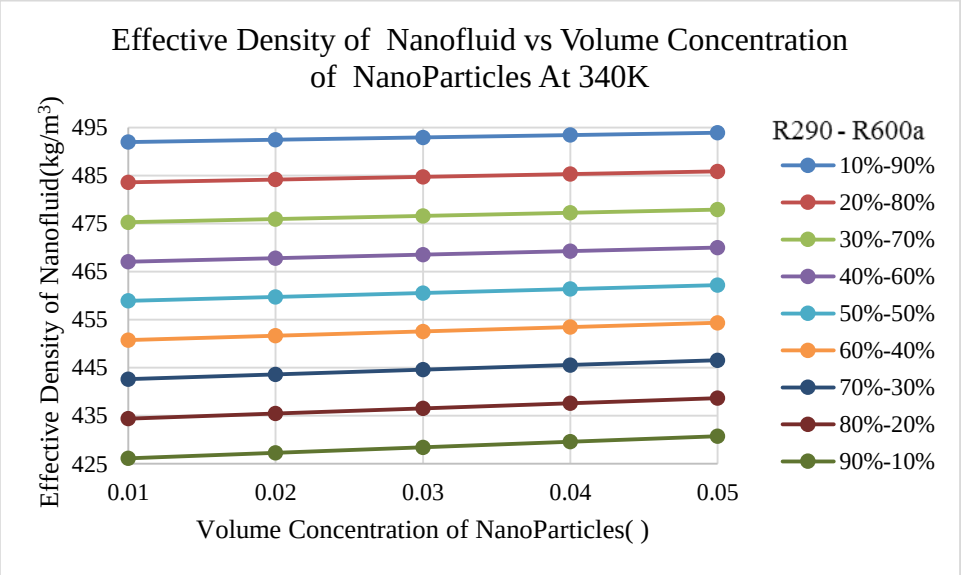

Figure 73 Effective density w.r.t volume concentration of nanoparticles

Figure 73 shows the variation of effective density as a function volume concentration of Nano-particle at pressure 3MPa. Moreover, it is also observed that as the effective density decrease linearly with increase in volume concentration of Nano-Particle at pressure 3MPa for a mixed refrigeration at different compositions for CuO Nano-Particle.

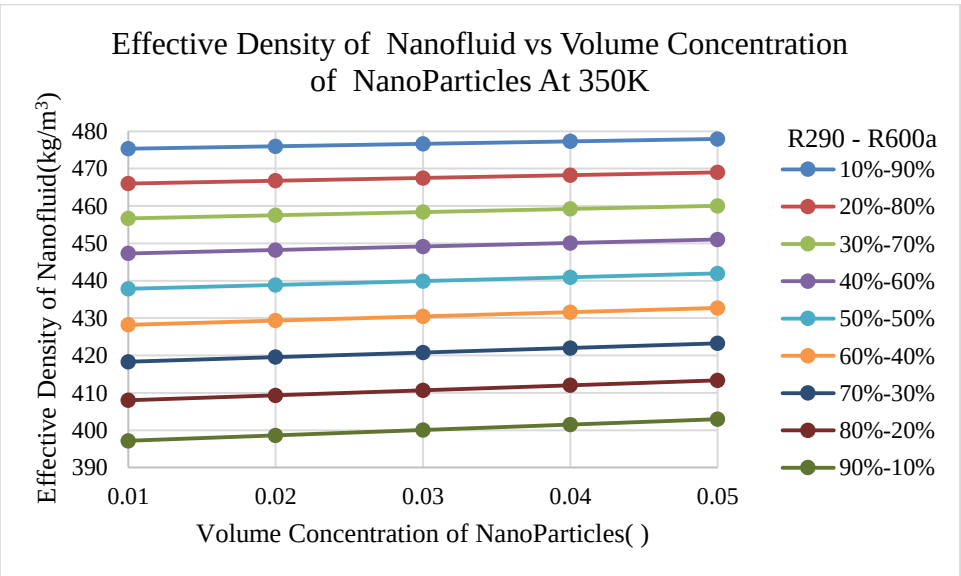

Figure 74 Effective density w.r.t volume concentration of nanoparticles

Figure 74 shows the variation of effective density as a function volume concentration of Nano-particle at pressure 3MPa. Moreover, it is also observed that as the effective density decrease linearly with increase in volume concentration of Nano-Particle at pressure 3MPa for a mixed refrigeration at different compositions for CuO Nano-Particle.

8.4 CFD Analysis of Mixed Refrigerant with addition of CuO Nano-article at Pressure 3MPa

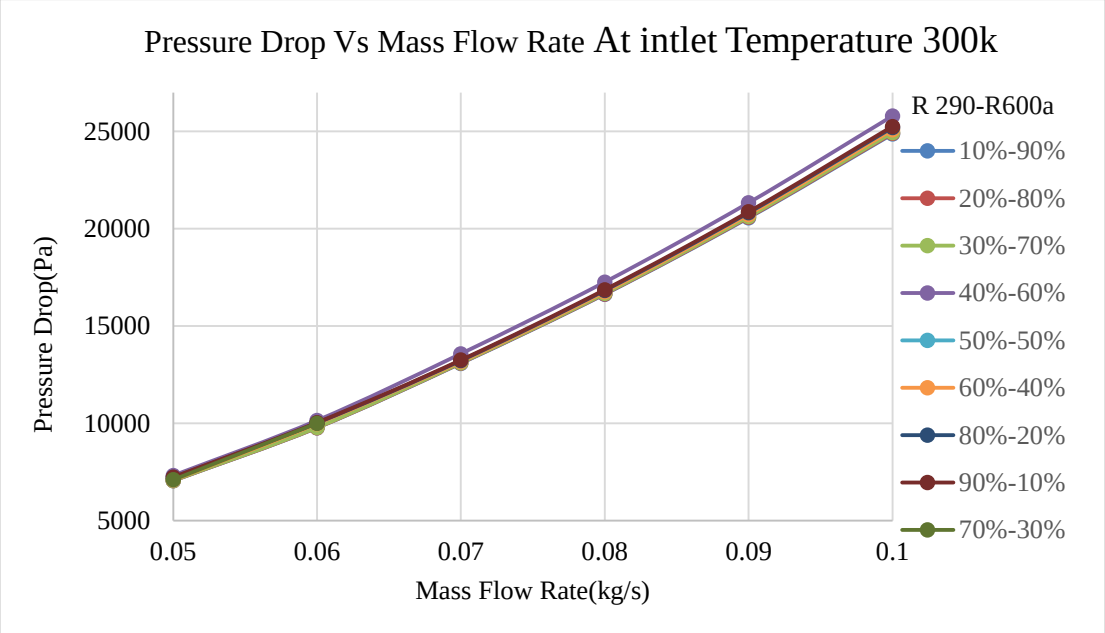

Figure 75 Pressure Drop vs Mass flow rate CuO Nano-Particle at 300K

Figure 75 shows that variation of pressure drop with respect to different mass flow rate at 300K inlet temperature and different compositions of a mixed refrigerant. Moreover, it was observed that as the mass flow rate increases and pressure drop is increases exponentially for CuO Nano-particle.

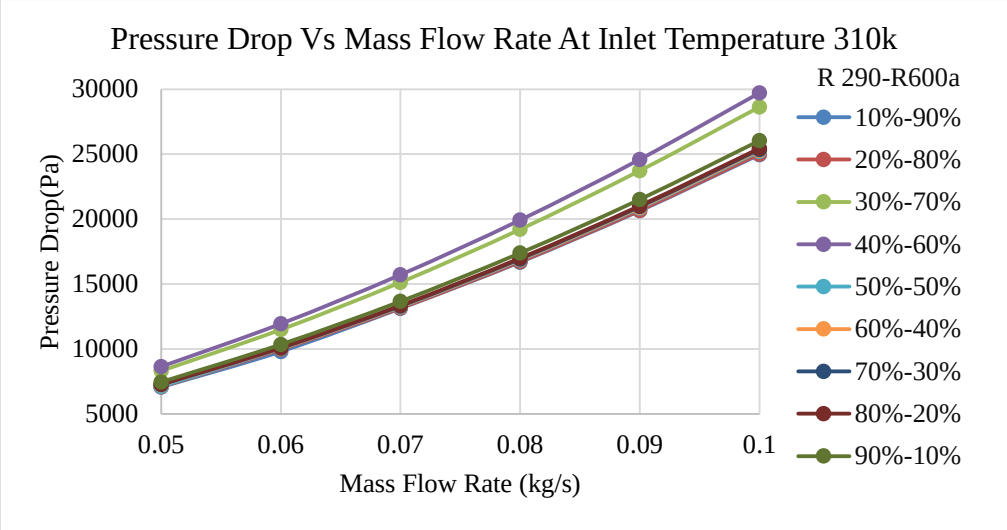

Figure 76 Pressure Drop vs Mass flow rate CuO Nano-Particle at 310K

Figure 76 shows that variation of pressure drop with respect to different mass flow rate at 310K inlet temperature and different compositions of a mixed refrigerant. Moreover, it was observed that as the mass flow rate increases and pressure drop is increases exponentially for CuO Nano-particle.

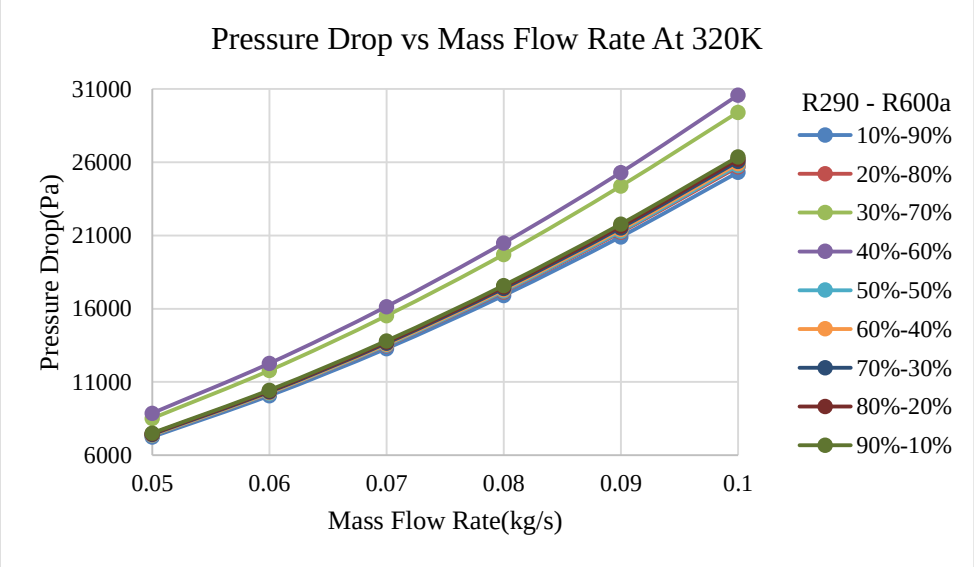

Figure 77 Pressure Drop vs Mass flow rate CuO Nano-Particle at 320K

Figure 77 shows that variation of pressure drop with respect to different mass flow rate at 320K inlet temperature and different compositions of a mixed refrigerant. Moreover, it was observed that as the mass flow rate increases and pressure drop is increases exponentially for CuO Nano-particle.

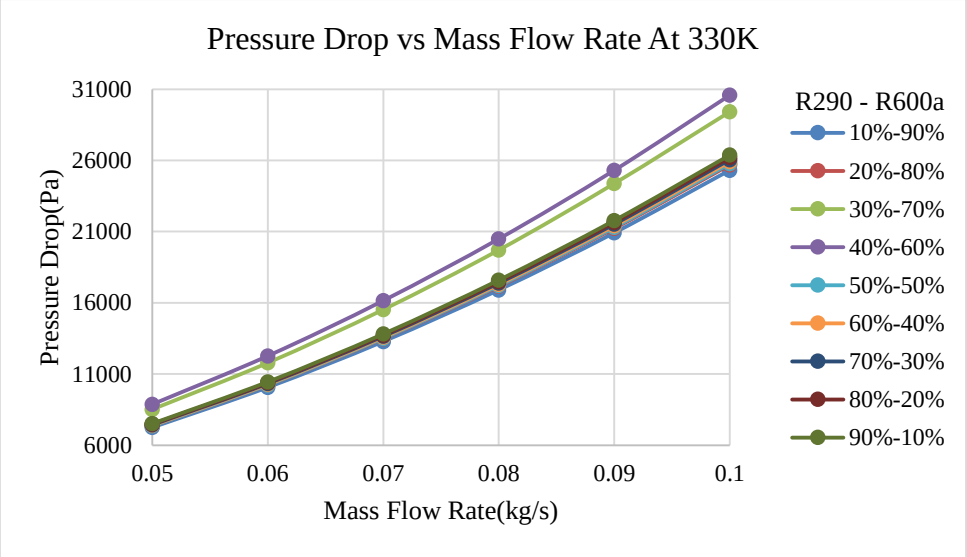

Figure 78 Pressure Drop vs Mass flow rate CuO Nano-Particle at 330K

Figure 78 shows that variation of pressure drop with respect to different mass flow rate at 330K inlet temperature and different compositions of a mixed refrigerant. Moreover, it was observed that as the mass flow rate increases and pressure drop is increases exponentially for CuO Nano-particle.

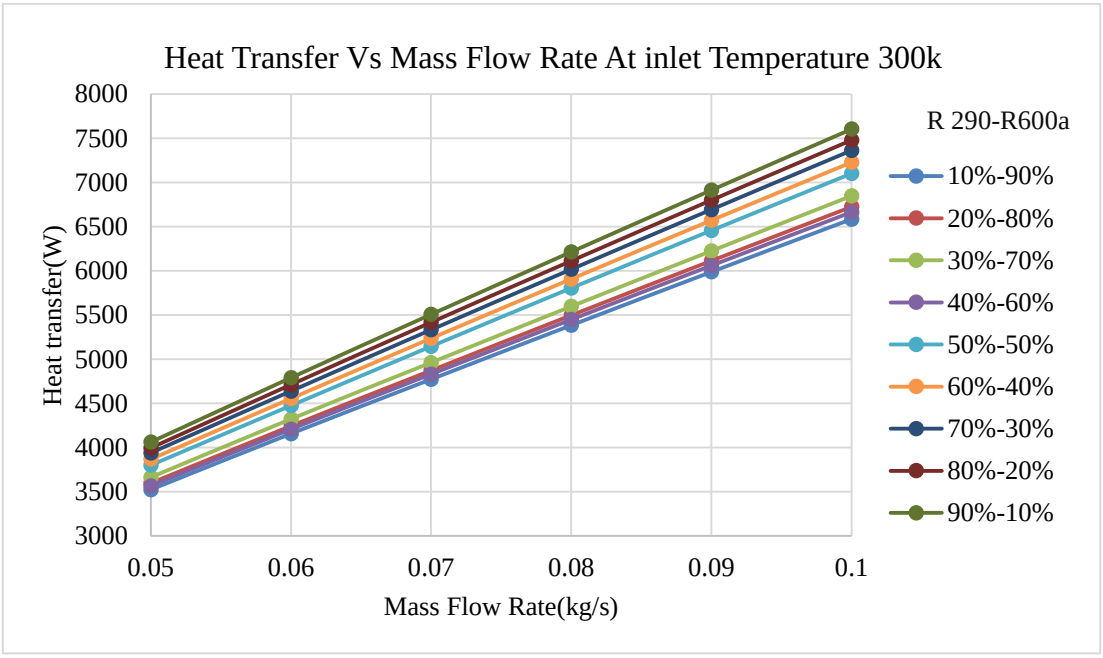

Figure 79 Heat transfer rate vs Mass flow rate CuO Nano-Particle at 300K

Figure 79 shows that variation of heat transfer rate with respect to different mass flow rate at 300K inlet temperature and different compositions of a mixed refrigerant. Moreover, it was

observed that as the mass flow rate increases and heat transfer rate is also increase linearly for CuO Nano-particle.

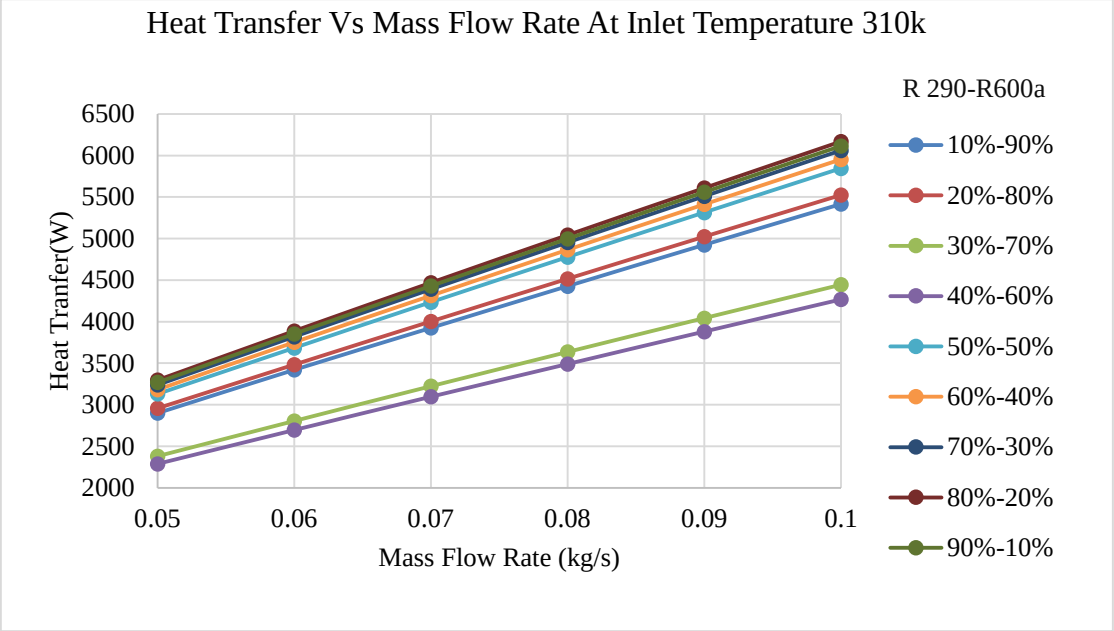

Figure 80 Heat transfer rate vs Mass flow Rate CuO Nano-Particle at 310K

Figure 80 shows that variation of heat transfer rate with respect to different mass flow rate at 310K inlet temperature and different compositions of a mixed refrigerant. Moreover, it was observed that as the mass flow rate increases and heat transfer rate linearly for CuO Nano-particle.

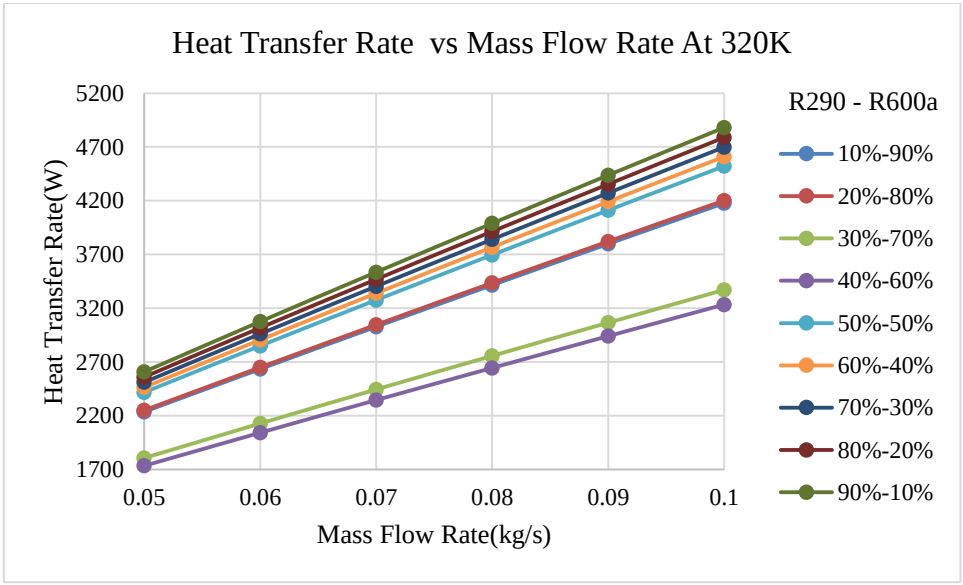

Figure 81 Heat transfer rate vs mass flow rate of CuO Nano-Particle at 320K

Figure 81 Figure 82shows that variation of heat transfer rate with respect to different mass flow rate at 320K inlet temperature and different compositions of a mixed refrigerant. Moreover, it was observed that as the mass flow rate increases and heat transfer rate is also increases linearly for CuO Nano-particle.

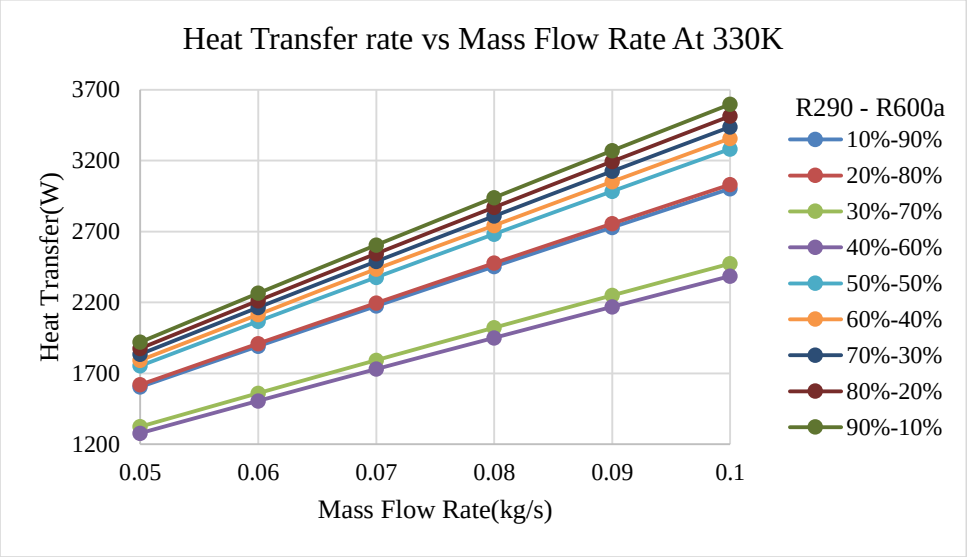

Figure 82 Heat transfer rate vs Mass flow rate CuO Nano-Particle at 330K

Figure 82 shows that variation of heat transfer rate with respect to different mass flow rate at 330K inlet temperature and different compositions of a mixed refrigerant. Moreover, it was observed that as the mass flow rate increases and heat transfer rate is increases linearly for CuO Nano-particle.

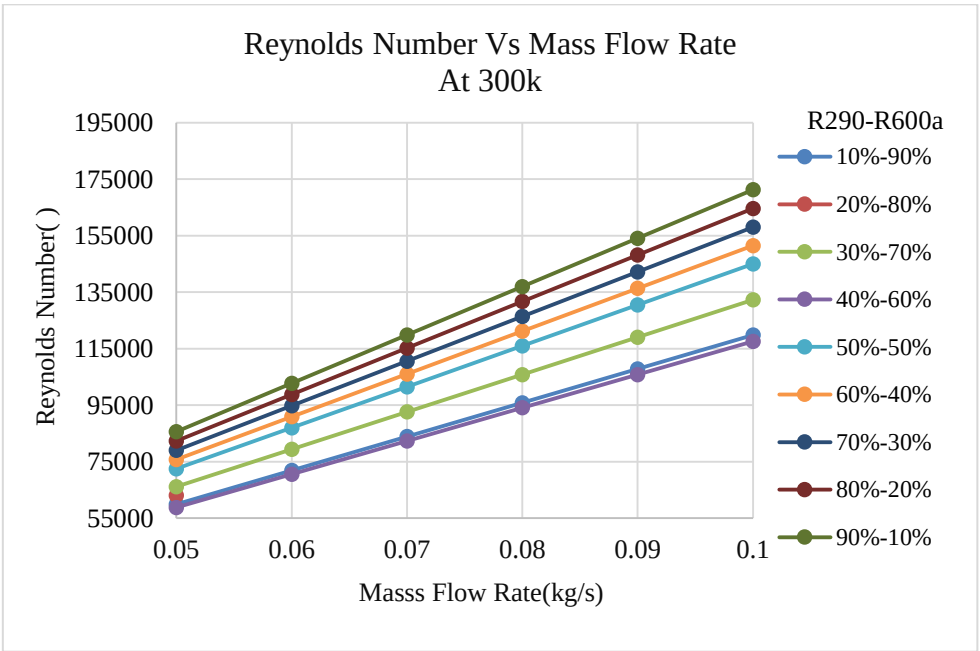

Figure 83 Reynolds Number vs Mass flow rate CuO Nano-Particle at 300K

Figure 83 shows that variation of pressure drop with respect to different mass flow rate at 300K inlet temperature and different compositions of a mixed refrigerant. Moreover, it was observed that as the mass flow rate increases and Reynolds Number is also increases linearly for CuO Nano-particle.

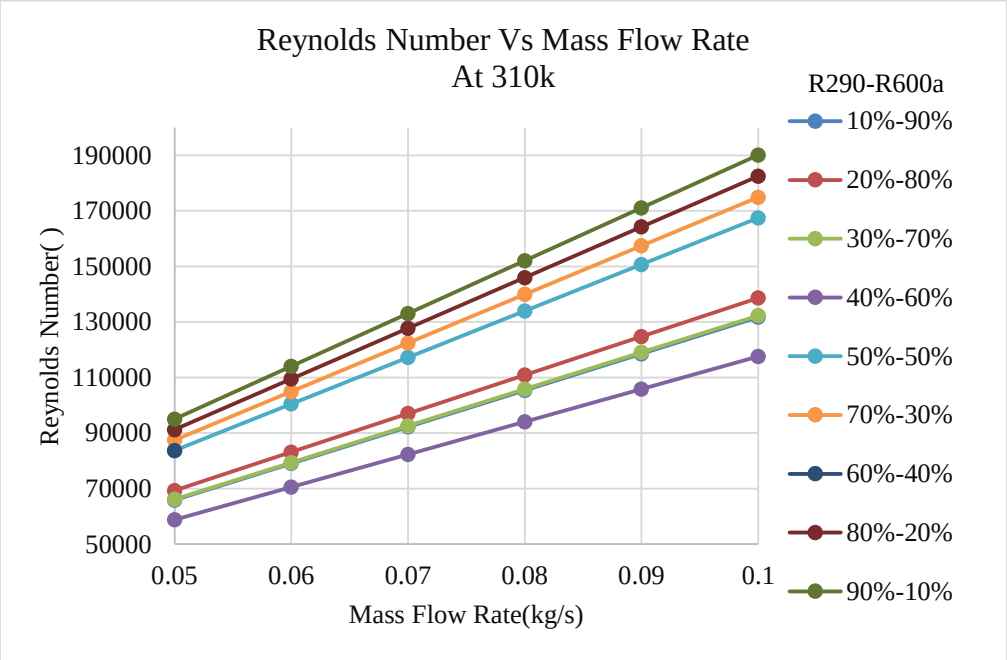

Figure 84 Reynolds Number vs Mass flow rate CuO Nano-Particle at 310K

Figure 84 shows that variation of Reynolds Number with respect to different mass flow rate at 310K inlet temperature and different compositions of a mixed refrigerant. Moreover, it was observed that as the mass flow rate increases and Reynolds Numbers is also increases linearly for CuO Nano-particle.

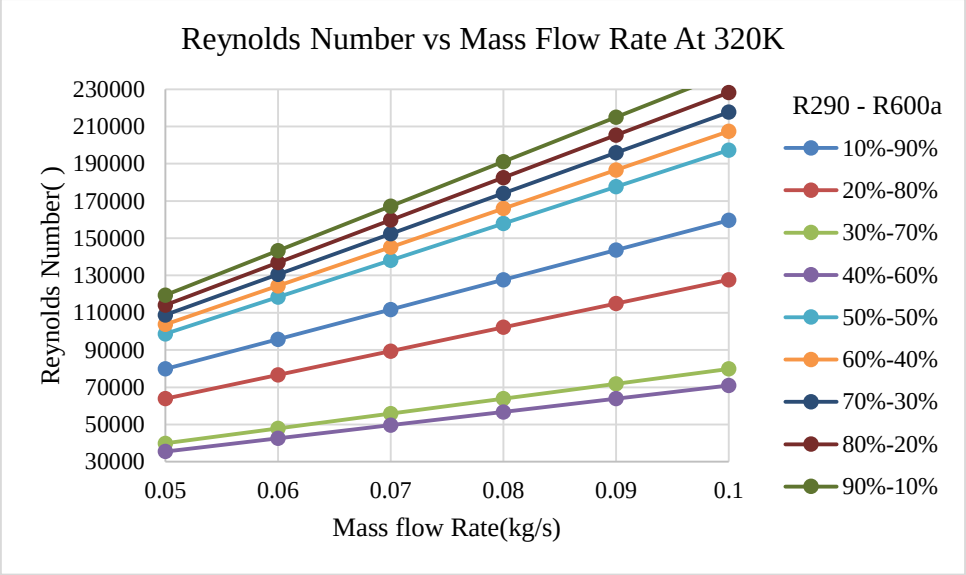

Figure 85 Reynolds Number vs Mass flow rate CuO Nano-Particle at 320K

Figure 85 shows that variation of Reynolds Number with respect to different mass flow rate at 320K inlet temperature and different compositions of a mixed refrigerant. Moreover, it was observed that as the mass flow rate increases and Reynolds Numbers is also increases linearly for CuO Nano-particle.

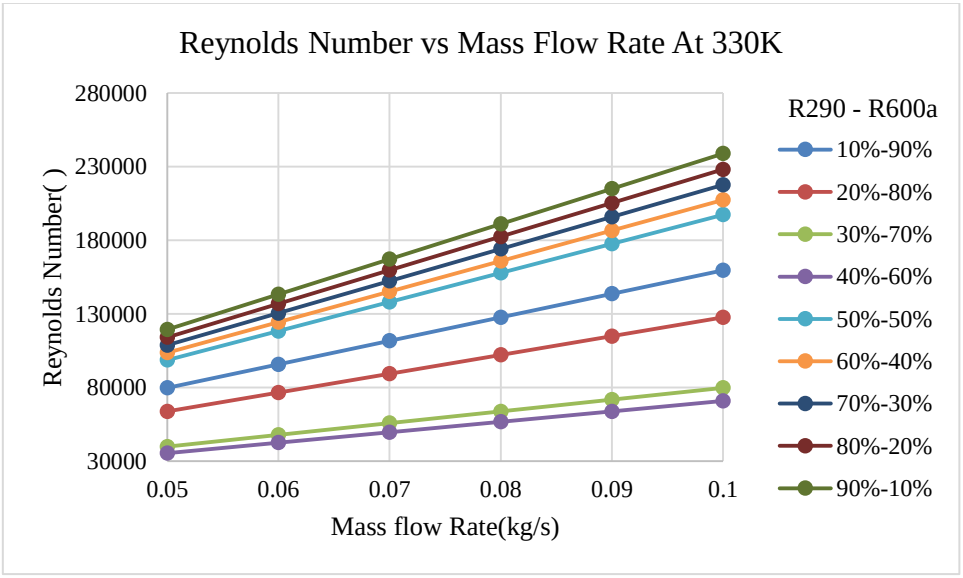

Figure 86 Reynolds Number vs Mass flow rate CuO Nano-Particle at 330K

Figure 86 shows that variation of Reynolds Number with respect to different mass flow rate at 330K inlet temperature and different compositions of a mixed refrigerant. Moreover, it was observed that as the mass flow rate increases and Reynolds Numbers is also increases linearly for CuO Nano-particle.

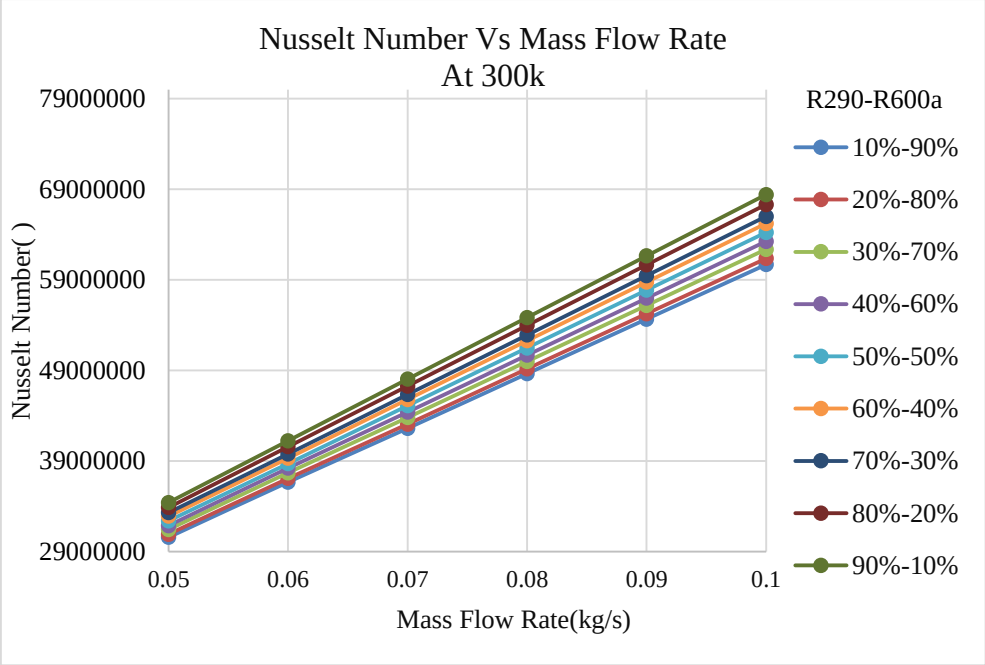

Figure 87 Nusselt Number vs Mass flow rate CuO Nano-Particle at 300K

Figure 87 shows that variation of Nusselt Number with respect to different mass flow rate at 300K inlet temperature and different compositions of a mixed refrigerant. Moreover, it was observed that as the mass flow rate increases and Nusselt Numbers is also increases linearly for CuO Nano-particle at pressure 3MPa.

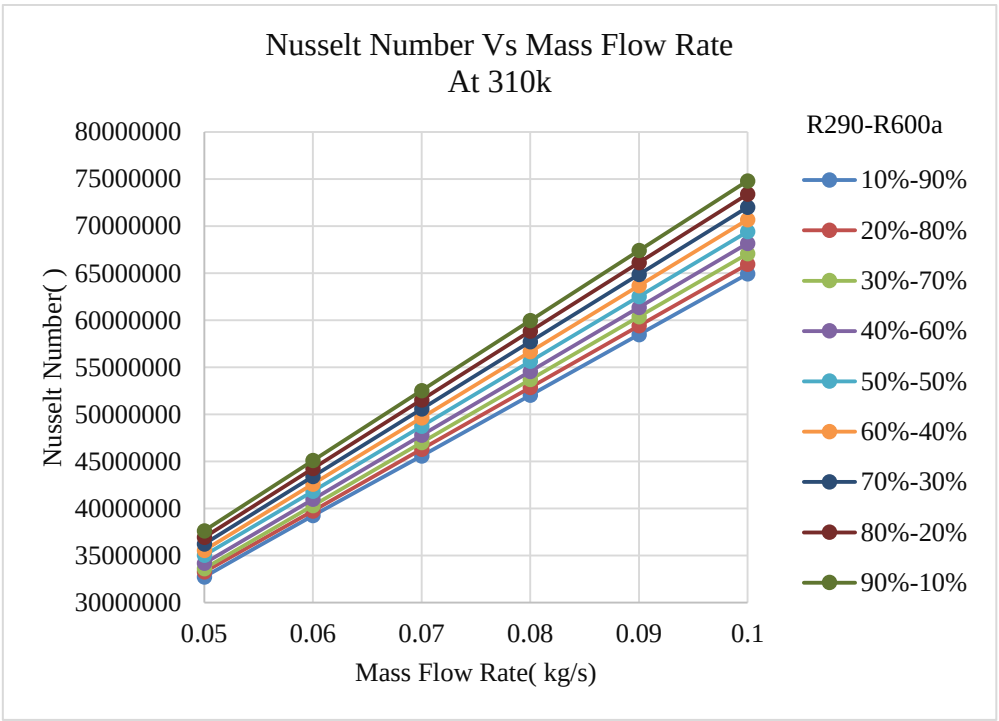

Figure 88 Nusselt Number vs Mass flow rate CuO Nano-Particle at 310K

Figure 88 shows that variation of Nusselt Number with respect to different mass flow rate at 310K inlet temperature and different compositions of a mixed refrigerant. Moreover, it was observed that as the mass flow rate increases and Nusselt Numbers is also increases linearly for CuO Nano-particle at pressure 3MPa.

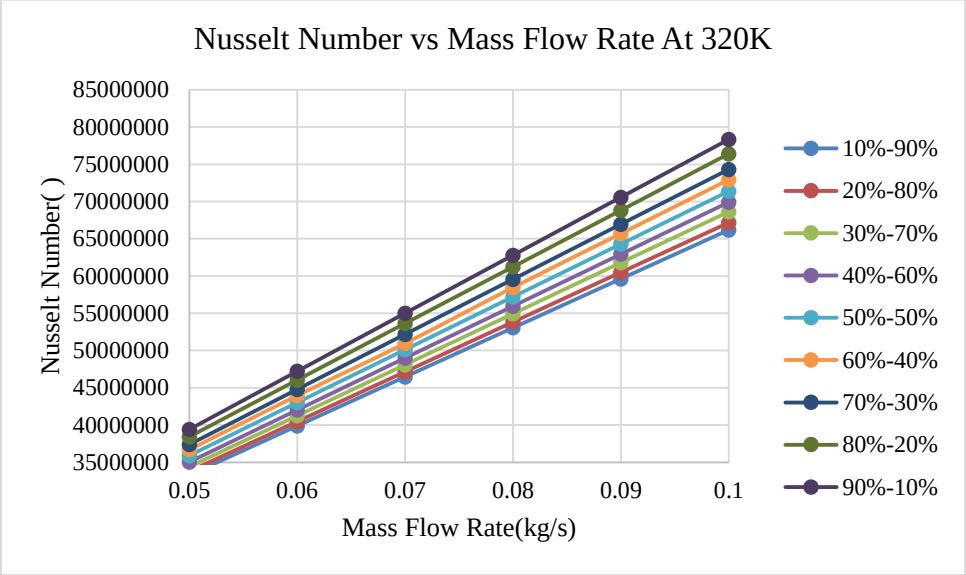

Figure 89 Nusselt Number vs Mass flow rate CuO Nano-Particle at 320K

Figure 89 shows that variation of Nusselt Number with respect to different mass flow rate at 320K inlet temperature and different compositions of a mixed refrigerant. Moreover, it was observed that as the mass flow rate increases and Nusselt Numbers is also increases linearly for CuO Nano-particle at pressure 3MPa.

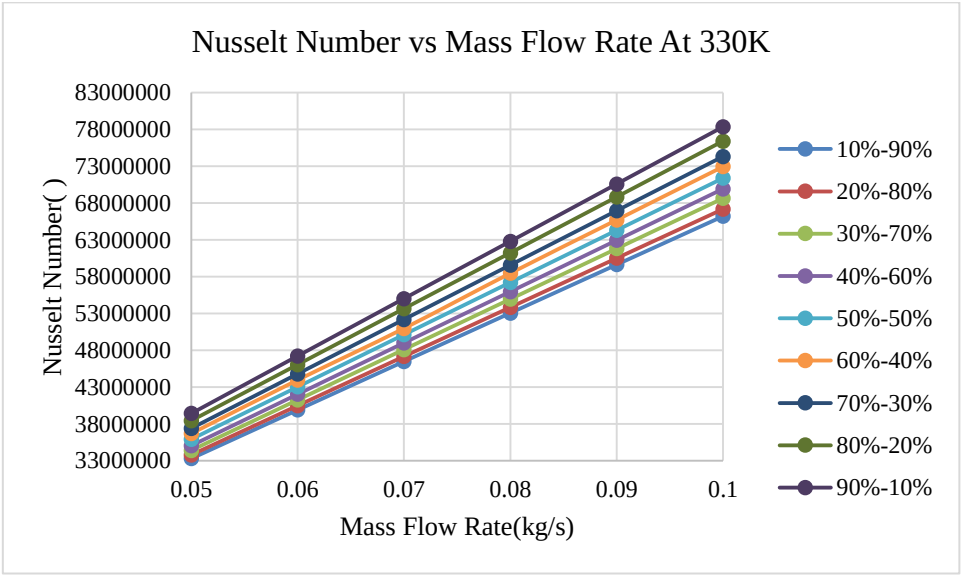

Figure 90 Nusselt Number vs Mass flow rate CuO Nano-Particle at 330K

Figure 90 shows that variation of Nusselt Number with respect to different mass flow rate at 330K inlet temperature and different compositions of a mixed refrigerant. Moreover, it was observed that as the mass flow rate increases and Nusselt Numbers is also increases linearly for CuO Nano-particle at pressure 3MPa.

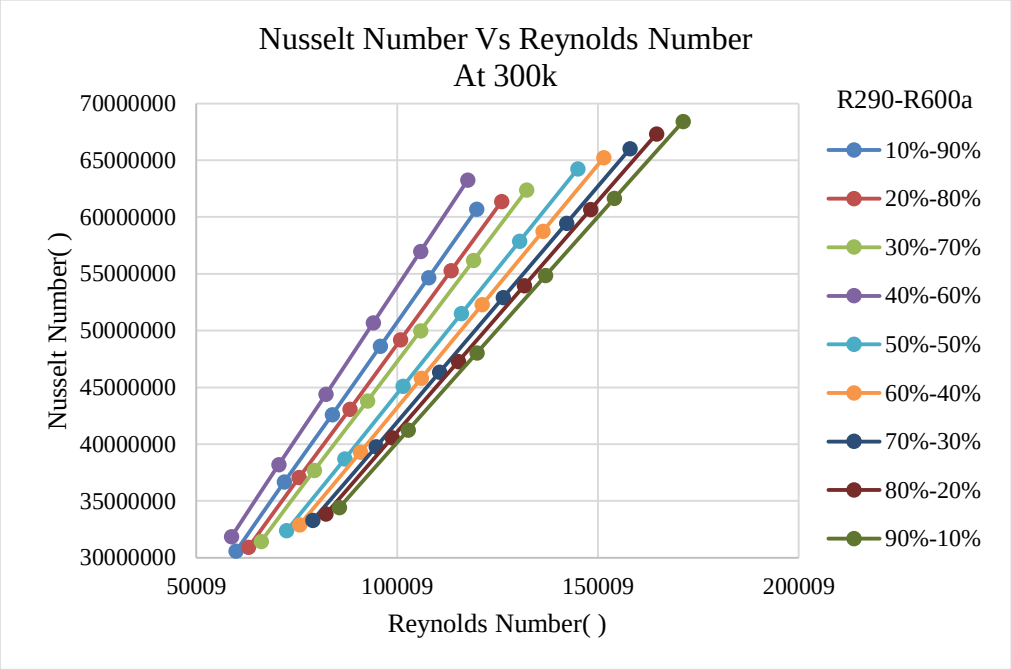

Figure 91 Nusselt Number vs Reynolds number rate CuO Nano-Particle at 300K

Figure 91 shows that variation of Nusselt Number with respect to Reynolds Number rate at 300K inlet temperature and different compositions of a mixed refrigerant. Moreover, it was observed that as the Reynolds Number increases and Nusselt Numbers is also increases linearly for CuO Nano-particle at pressure 3MPa.

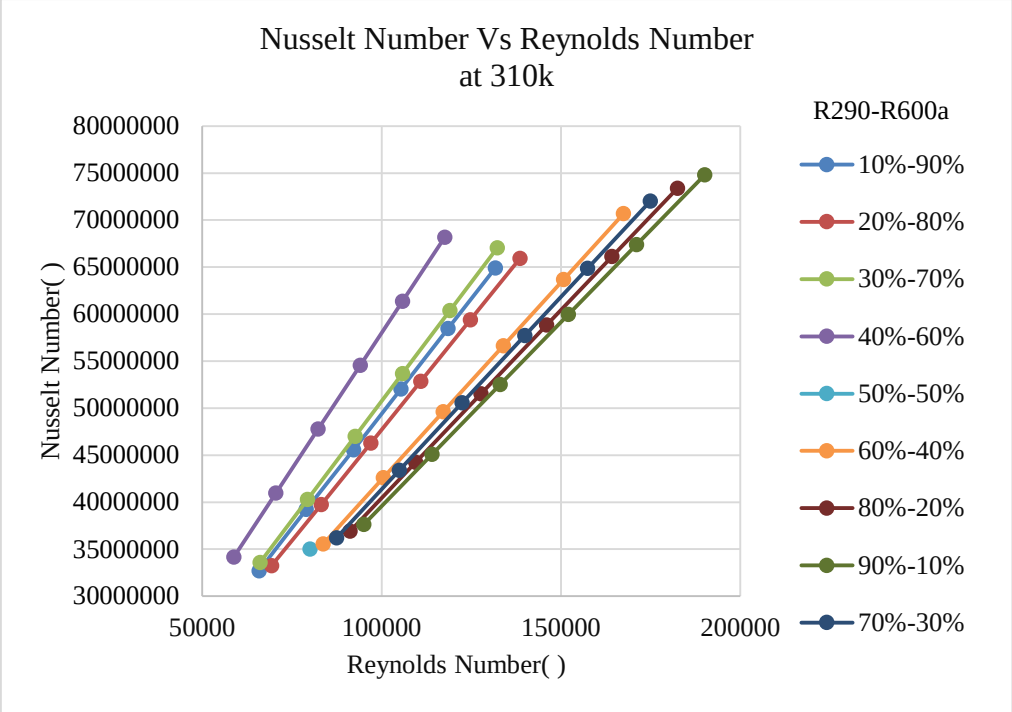

Figure 92 Nusselt Number vs Reynolds number rate CuO Nano-Particle at 310K

.Figure 92 shows that variation of Nusselt Number with respect to Reynolds Number rate at 310K inlet temperature and different compositions of a mixed refrigerant. Moreover, it was observed that as the Reynolds Number increases and Nusselt Numbers is also increases linearly for CuO Nano-particle at pressure 3MPa

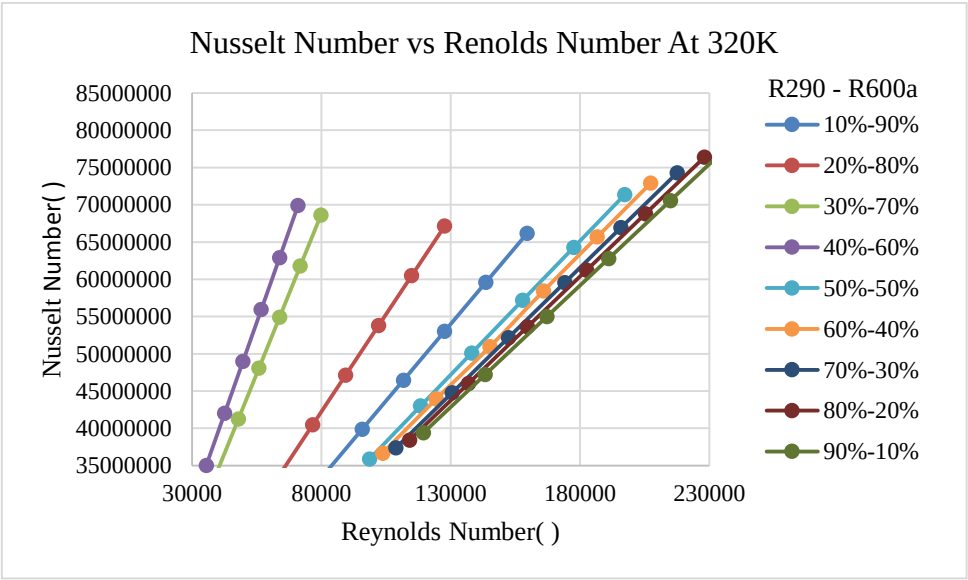

Figure 93 Nusselt Number vs Reynolds number rate CuO Nano-Particle at 320K

Figure 93 shows that variation of Nusselt Number with respect to Reynolds Number rate at 320K inlet temperature and different compositions of a mixed refrigerant. Moreover, it was observed that as the Reynolds Number increases and Nusselt Numbers is also increases linearly for CuO Nano-particle at pressure 3MPa

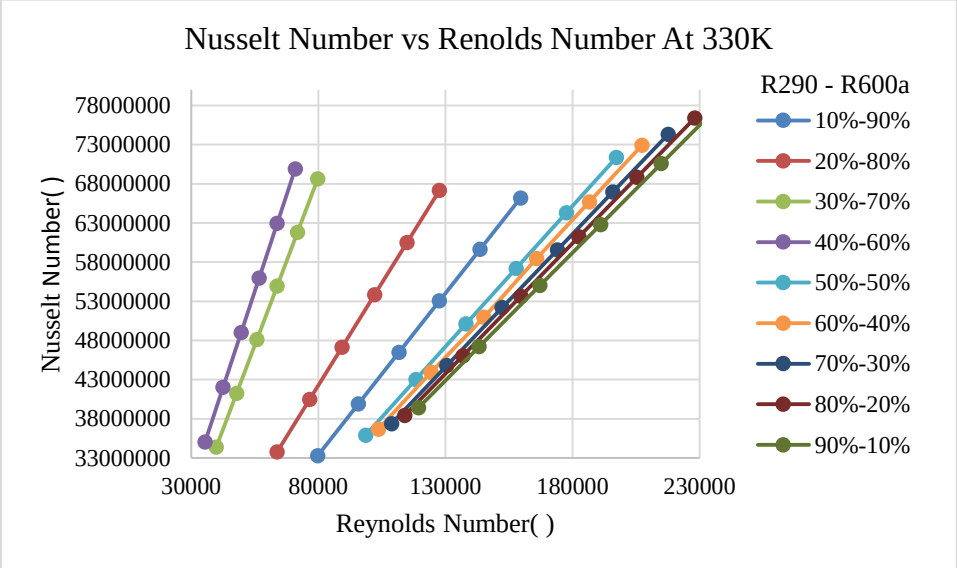

Figure 94 Nusselt Number vs Reynolds number rate CuO Nano-Particle at 300K

Figure 94 shows that variation of Nusselt Number with respect to Reynolds Number rate at 330K inlet temperature and different compositions of a mixed refrigerant. Moreover, it was observed that as the Reynolds Number increases and Nusselt Numbers is also increases linearly for CuO Nano-particle at pressure 3MPa.

9 Summary and Conclusions

The purpose this research work was carried out in National Institute of Standard Technology (NIST®) for inspecting the thermophysical properties of Propane (R290) and ISO-butane (R600a) at a temperature of 300-350K and pressure of 3MPa to 7MPa. In addition, results are calculated for density, viscosity, thermal conductivity and Specific heat.

From the previous chapter we concluded that

- Thermal conductivity of a refrigerant mixture at different compositions decreased with increase in temperature.
- Density of a refrigerant mixture at different compositions decreased with increase in temperature.
- Viscosity of a refrigerant mixture at different compositions decreased with increase in temperature.
- Specific Heat of a refrigerant mixture at different compositions decreased with increase in temperature.
- Effective thermal conductivity of mixed refrigerant with addition of CuO Nano-particles increased at pressure 3MPa
- Effective viscosity of mixed refrigerant with addition of CuO Nano-particles increased at pressure 3MPa
- Effective density of mixed refrigerant with addition of CuO Nano-particles decreased at pressure 3MPa
- Effective specific heat of mixed refrigerant with addition of CuO Nano-particles may be decreased at pressure 3MPa
- Pressure drop of a mixed refrigerant with and without addition of CuO Nanoparticles increased exponentially at different inlet temperatures (300-330K) at pressure 3MPa
- Heat transfer rate of a mixed refrigerant with and without addition of CuO Nanoparticles increased linearly at different inlet temperatures (300-330K) at pressure 3MPa
- Reynolds number of a mixed refrigerant with and without addition of CuO Nanoparticles increased linearly at different inlet temperatures (300-330K) at pressure 3MPa
- Nusselt number of a mixed refrigerant with and without addition of CuO Nanoparticles increased linearly at different inlet temperatures (300-330K) at pressure 3MPa

References

[1] N. B. Christiansen, “Refrigeration - an introduction to the basics,” *Hist. Cool. Syst.*, vol. vol.6, no. 3, pp. 1–18, 2007.

[2] Y. Hou, Z. Zhang, and J. Zhang, “Significantly enhanced impulse breakdown performances of propylene carbonate modified by TiO2 nano-particles,” *Chem. Phys. Lett.*, vol. 662, pp. 192–195, 2016.

[3] A. Zyoud *et al.*, “Natural dye-sensitized ZnO nano-particles as photo-catalysts in complete degradation of E. coli bacteria and their organic content,” *J. Photochem. Photobiol. A Chem.*, vol. 328, pp. 207–216, 2016.

[4] M. K. Abdolbaqi *et al.*, “An experimental determination of thermal conductivity and viscosity of BioGlycol/water based TiO2 nanofluids,” *Int. Commun. Heat Mass Transf.*, vol. 77, pp. 22–32, 2016.

[5] M. K. Abdolbaqi *et al.*, “Experimental investigation and development of new correlation for thermal conductivity and viscosity of BioGlycol/water based SiO<inf>2</inf> nanofluids,” *Int. Commun. Heat Mass Transf.*, vol. 77, pp. 1–10, 2016.

[6] N. S. Akbar, N. Kazmi, D. Tripathi, and N. A. Mir, “Study of heat transfer on physiological driven movement with CNT nanofluids and variable viscosity,” *Comput. Methods Programs Biomed.*, vol. 136, pp. 21–29, 2016.

[7] H. W. Chiam, W. H. Azmi, N. A. Usri, R. Mamat, and N. M. Adam, “Thermal conductivity and viscosity of Al2O3 nanofluids for different based ratio of water and ethylene glycol mixture,” *Exp. Therm. Fluid Sci.*, 2016.

[8] Babita, S. K. Sharma, and S. M. Gupta, “Preparation and evaluation of stable nanofluids for heat transfer application: A review,” *Exp. Therm. Fluid Sci.*, vol. 79, pp. 202–212, 2016.

[9] K. Anoop, R. Sadr, R. Yrac, and M. Amani, “High-pressure rheology of alumina-silicone oil nanofluids,” *Powder Technol.*, vol. 301, pp. 1025–1031, 2016.

[10] A. Aminian, “Predicting the effective thermal conductivity of nanofluids for intensification of heat transfer using artificial neural network,” *Powder Technol.*, vol.

301, pp. 288–309, 2016.

[11] M. K. K. Abdolbaqi *et al.*, “Experimental investigation on stability and thermal conductivity of diathermic oil based TiO2 nanofluids,” *Int. Commun. Heat Mass Transf.*, vol. 77, no. 4, pp. 13–23, 2016.

[12] W. H. Azmi, K. V Sharma, P. K. Sarma, R. Mamat, S. Anuar, and V. D. Rao, “Experimental determination of turbulent forced convection heat transfer and friction factor with SiO 2 nanofluid,” *Exp. Therm. FLUID Sci.*, pp. 1–9, 2013.

[13] C. Anushree and J. Philip, “Assessment of long term stability of aqueous nanofluids using different experimental techniques,” *J. Mol. Liq.*, vol. 222, pp. 350–358, 2016.

[14] R. Deepak Selvakumar and S. Dhinakaran, “A multi-level homogenization model for thermal conductivity of nanofluids based on particle size distribution (PSD) analysis,” *Powder Technol.*, vol. 301, pp. 310–317, 2016.

[15] M. Du and G. H. Tang, “Plasmonic nanofluids based on gold nanorods/nanoellipsoids/nanosheets for solar energy harvesting,” *Sol. Energy*, vol. 137, pp. 393–400, 2016.

[16] J. R. Eggers and S. Kabelac, “Nanofluids revisited,” *Appl. Therm. Eng.*, vol. 106, pp. 1114–1126, 2016.

[17] T. Hayat, S. Qayyum, M. Imtiaz, and A. Alsaedi, “Comparative study of silver and copper water nanofluids with mixed convection and nonlinear thermal radiation,” *Int. J. Heat Mass Transf.*, vol. 102, pp. 723–732, 2016.

[18] S. M. Hosseini and M. M. Alavianmehr, “New version of Tammann-Tait equation: Application to nanofluids,” *J. Mol. Liq.*, vol. 220, pp. 404–408, 2016.

[19] M. Raja, R. Vijayan, P. Dineshkumar, and M. Venkatesan, “Review on nanofluids characterization, heat transfer characteristics and applications,” *Renew. Sustain. Energy Rev.*, vol. 64, pp. 163–173, 2016.

[20] N. Zhao, S. Li, and J. Yang, “A review on nano fl uids : Data-driven modeling of thermalphysical properties and the application in automotive radiator,” *Renew. Sustain. Energy Rev.*, vol. 66, pp. 596–616, 2016.

[21] B. Wei, C. Zou, and X. Li, “Experimental investigation on stability and thermal conductivity of diathermic oil based TiO2 nanofluids,” *Int. J. Heat Mass Transf.*, vol. 104, pp. 537–543, 2017.

[22] H. Togun, “Effect of laminar separation fl ow and nano fl uids on heat transfer augmentation with passive techniques : A review ☆,” *Int. Commun. Heat Mass Transf.*, vol. 77, pp. 9–14, 2016.

[23] E. A. Taborda, C. A. Franco, S. H. Lopera, V. Alvarado, and F. B. Cortés, “Effect of nanoparticles / nanofluids on the rheology of heavy crude oil and its mobility on porous media at reservoir conditions,” *Fuel*, vol. 184, pp. 222–232, 2016.

[24] K. S. Suganthi, V. L. Vinodhan, and K. S. Rajan, *ZnO – Propylene Glycol – Water Nanofluids with Improved Properties for Potential Applications in Renewable Energy and Thermal Management*. Elsevier B.V., 2016.

[25] S. Singh, K. Sharma, K. Lal, and N. M. Tripathi, “To Study the Behaviour of Nanorefrigerant in Vapour Compression Cycle- a Review,” no. January 2016, pp. 648–652, 2015.

[26] N. A. C. Sidik, I. M. Adamu, M. M. Jamil, G. H. R. Kefayati, R. Mamat, and G. Najafi, “Recent progress on hybrid nanofluids in heat transfer applications: A comprehensive review,” *Int. Commun. Heat Mass Transf.*, vol. 78, pp. 68–79, 2016.

[27] R. Shu, Y. Gan, H. Lv, and D. Tan, “Preparation and rheological behavior of ethylene glycol-based TiO2 nanofluids,” *Colloids Surfaces A Physicochem. Eng. Asp.*, vol. 509, pp. 86–90, 2016.

[28] M. Sardarabadi and M. Passandideh-Fard, “Experimental and numerical study of metal-oxides/water nanofluids as coolant in photovoltaic thermal systems (PVT),” *Sol. Energy Mater. Sol. Cells*, vol. 157, pp. 533–542, 2016.

[29] B. Dawidowicz and J. T. Cieśliński, “Heat transfer and pressure drop during flow boiling of pure refrigerants and refrigerant/oil mixtures in tube with porous coating,” *Int. J. Heat Mass Transf.*, vol. 55, no. 9–10, pp. 2549–2558, 2012.

[30] M. Y. Wen and C. Y. Ho, “Condensation heat-transfer and pressure drop characteristics of refrigerant R-290/R-600a-oil mixtures in serpentine small-diameter U-tubes,” *Appl.*

Therm. Eng., vol. 29, no. 11–12, pp. 2460–2467, 2009.

[31] A. Cavallini, D. Del Col, and L. Rossetto, "Heat transfer and pressure drop of natural refrigerants in minichannels (low charge equipment)," *Int. J. Refrig.*, vol. 36, no. 2, pp. 287–300, 2013.

[32] A. S. Dalkilic, "Condensation pressure drop characteristics of various refrigerants in a horizontal smooth tube," *Int. Commun. Heat Mass Transf.*, vol. 38, no. 4, pp. 504–512, 2011.

[33] J. Huang, T. J. Sheer, and M. Bailey-Mcewan, "Heat transfer and pressure drop in plate heat exchanger refrigerant evaporators," *Int. J. Refrig.*, vol. 35, no. 2, pp. 325–335, 2012.

[34] X. Huang, G. Ding, H. Hu, Y. Zhu, Y. Gao, and B. Deng, "Flow condensation pressure drop characteristics of R410A - Oil mixture inside small diameter horizontal microfin tubes," *Int. J. Refrig.*, vol. 33, no. 7, pp. 1356–1369, 2010.

[35] G. A. Longo, "Heat transfer and pressure drop during HFC refrigerant saturated vapour condensation inside a brazed plate heat exchanger," *Int. J. Heat Mass Transf.*, vol. 53, no. 5–6, pp. 1079–1087, 2010.

[36] Y. Zou and P. S. Hrnjak, "Single-phase and two-phase flow pressure drop in the vertical header of microchannel heat exchanger," *Int. J. Refrig.*, vol. 44, pp. 12–22, 2014.

[37] S. M. Sami and B. Song, "Heat transfer and pressure drop characteristics of HFC quaternary refrigerant mixtures inside horizontal enhanced surface tubing," *Appl. Therm. Eng.*, vol. 16, no. 6, pp. 461–473, 1996.

[38] R. Cao, Y. Qi, and R. Chen, "pVTx properties of binary R1234ze(E)/R600a system," *J. Chem. Thermodyn.*, vol. 111, pp. 191–198, 2017.

[39] C. S. Choudhari and S. N. Sapali, "Performance Investigation of Natural Refrigerant R290 as a Substitute to R22 in Refrigeration Systems," *Energy Procedia*, vol. 109, no. November 2016, pp. 346–352, 2017.

[40] G. He, F. Liu, D. Cai, and J. Jiang, "Experimental investigation on flow boiling heat transfer performance of a new near azeotropic refrigerant mixture R290/R32 in

horizontal tubes," *Int. J. Heat Mass Transf.*, vol. 102, pp. 561–573, 2016.

[41] W. Zhang, Z. Yang, X. Zhang, D. Lv, and N. Jiang, "Experimental research on the explosion characteristics in the indoor and outdoor units of a split air conditioner using the R290 refrigerant," *Int. J. Refrig.*, vol. 67, pp. 408–417, 2016.

[42] Q. Chen, J. Yu, and G. Yan, "Performance analysis of a modified zeotropic mixture (R290/R600) refrigeration cycle with internal subcooler for freezer applications," *Appl. Therm. Eng.*, vol. 108, pp. 172–180, 2016.

[43] J. Wu, J. Lin, Z. Zhang, Z. Chen, J. Xie, and J. Lu, "Experimental investigation on cold startup characteristics of a rotary compressor in the R290 air-conditioning system under cooling condition," *Int. J. Refrig.*, vol. 65, pp. 209–217, 2016.

[44] T. S. Pilla, P. K. G. Sunkari, S. L. Padmanabhuni, S. S. Nair, and R. S. Dondapati, "Experimental Evaluation Mechanical Performance of the Compressor with Mixed Refrigerants R-290 and R-600a," *Energy Procedia*, vol. 109, pp. 113–121, 2017.

[45] H. Huang and J. R. Thome, "An experimental study on flow boiling pressure drop in multi-microchannel evaporators with different refrigerants," *Exp. Therm. Fluid Sci.*, vol. 80, pp. 391–407, 2017.

[46] D. Yang, B. Sun, H. Li, and X. Fan, "Experimental study on the heat transfer and flow characteristics of nanorefrigerants inside a corrugated tube," *Int. J. Refrig.*, vol. 56, pp. 213–223, 2015.

[47] Q. Liu, A. Shen, and Y. Duan, "Parametric optimization and performance analyses of geothermal organic Rankine cycles using R600a/R601a mixtures as working fluids," *Appl. Energy*, vol. 148, pp. 410–420, 2015.

[48] M. Y. Wen, K. J. Jang, and C. Y. Ho, "The characteristics of boiling heat transfer and pressure drop of R-600a in a circular tube with porous inserts," *Appl. Therm. Eng.*, vol. 64, no. 1–2, pp. 348–357, 2014.